

Intrinsic and extrinsic factors affecting cortical development

Ole Johanns

Universitätsklinikum Hamburg-Eppendorf
Zentrum für Molekulare Neurobiologie Hamburg
Nachwuchsgruppe Neuronale Entwicklung

Fachbereich Chemie

An der Universität Hamburg eingereichte Dissertation

2023

Gutachter der schriftlichen Prüfung:

Prof. Dr. rer. nat. Hartmut Schlüter

Prof. Dr. rer. nat. Matthias Kneussel

Mitglieder der Prüfungskommission:

PD Dr. rer. nat. habil. Markus Perbandt

Jun.-Prof. Dr. med. Esther Diekhof

Dr. Froylan Calderon de Anda

Datum der Disputation: 15.09.2023

Druckfreigabe: 21.09.2023

Diese Dissertation wurde am Zentrum für Molekulare Neurobiologie (ZMNH) des Universitätsklinikum Eppendorf (UKE) der Universität Hamburg (UHH) in der Arbeitsgruppe für Neuronale Entwicklung unter der Leitung des Nachwuchsgruppenleiter Dr. Froylan Calderon de Anda vom 1.11.2017 bis zum 12.06.2023 durchgeführt. Die Betreuung dieser Dissertation wurde von Prof. Dr. Hartmut Schlüter, Prof. Dr. Matthias Kneussel und Dr. Froylan Calderon de Anda übernommen.

1 Publications

Results 10.1, Figure 4, Figure 5, Supplementary Figure 1 and Supplementary Figure 2 of this thesis are based on the following publication:

Scharrenberg, R., Richter, M., **Johanns, O.** *et al.* TAOK2 rescues autism-linked developmental deficits in a 16p11.2 microdeletion mouse model. *Mol Psychiatry* (2022). <https://doi.org/10.1038/s41380-022-01785-3>

2 Table of contents

1	Publications	i
2	Table of contents.....	i
3	Table of figures	v
4	Abbreviations	1
5	Zusammenfassung.....	2
6	Summary.....	3
7	Introduction.....	4
7.1	Neuronal development and Immune system.....	4
	Neuronal development	4
	7.1.1.1 Gross brain development	4
	7.1.1.2 Murine vs human brain	5
	7.1.1.3 Neuronal cell development	5
	7.1.1.4 Cortical development	5
	Embryonal immune system development	7
	7.1.1.5 General immune system development	7
	7.1.1.6 Placenta	7
	7.1.1.7 Blood Brain barrier	7
	7.1.1.8 Early border associated Macrophages and Microglia infiltration	8
	7.1.1.9 Later Astroglia and Oligodendrocyte development	8
	Maternal immune system and maternal immune activation	9
	7.1.1.10 Maternal immune status during pregnancy	9
	7.1.1.11 Maternal immune response to viruses	9
	7.1.1.12 Maternal immune response to bacteria.....	9
	7.1.1.13 Maternal vaccination during pregnancy.....	10
	7.1.1.14 Virus / Bacterium / Toxin reaching embryo vs Maternal immune reaction affecting embryo	10
	7.1.1.15 Offspring's immune reaction to maternal immune activation and infection	10
	Autism spectrum disorders affecting the immune system	10
	7.1.1.16 Immune dysfunctions in patients with ASD	10

Autism spectrum disorders in clinic and research	11
7.1.1.17 Clinical description of ASD.....	11
7.1.1.18 Neurological implications in ASD.....	11
7.1.1.19 ASD symptoms in research models	11
7.2 Intrinsic factors predisposing ASD.....	12
Patient based mutations	12
7.2.1.1 Genetic causes for ASD.....	12
7.2.1.2 16p11.2 mutation.....	12
7.2.1.3 TAOK2 mutation	12
Model based mutations	13
7.2.1.4 16p11.2 mutation.....	13
7.2.1.5 Taok2 mutation	13
7.2.1.6 Other genetic mutations	13
7.3 Extrinsic factors predisposing ASD	14
Human / Patient appearances.....	14
7.3.1.1 Viral infection	14
7.3.1.2 Bacterial infection.....	14
7.3.1.3 Autoimmune disorders in mothers and ASD in offspring	14
7.3.1.4 Toxins.....	15
Models for extrinsic factors.....	15
7.3.1.5 Influenza infection.....	15
7.3.1.6 ZIKA infection	15
7.3.1.7 Maternal immune activation (Poly(I:C) and LPS)	15
7.3.1.8 Interleukins.....	16
7.3.1.9 Other factors	16
7.3.1.10 In situ treatment.....	16
8 Hypotheses.....	17
9 Methods	19
9.1 Contribution	19
9.2 Preparation.....	19
Solutions.....	19
9.2.1.1 Slicing and fixation.....	19
9.2.1.2 Staining.....	19
9.2.1.3 Immune treatment.....	20
Animal work.....	20
9.2.1.4 Mouse Models.....	20

9.2.1.5	In Utero Electroporation	20
9.2.1.6	Maternal immune activation	20
9.2.1.7	Preparation of murine organs	20
9.2.1.8	Identification of transfected hemisphere	20
9.2.1.9	Cryosectioning	21
9.2.1.10	Preparation of acute slice cultures	21
9.2.1.11	Treatment of slices	21
Imaging	21
9.2.1.12	Mounting	21
9.2.1.13	Live imaging	21
9.2.1.14	Imaging fixed tissue	22
9.3	Analysis	22
Microglia	22
9.3.1.1	Microglia fixed tissue	22
9.3.1.2	Microglia time lapses	22
Neurons	23
9.3.1.3	Neurons fixed tissue	23
9.3.1.4	Neurons live imaging	23
10	Results	25
10.1	Neuronal migration and autism spectrum disorder related genetic variations	25
	The effect of ASD-related human variants of TAOK2 on neuronal migration	25
	The effect of mutations in the ASD susceptible region 16p11.2 on neuronal migration	25
10.1.1.1	Figure 4: Human variants of TAOK2 α affect neuronal migration in mice	26
10.1.1.2	Figure 5: Neuronal migration is impaired in Het 16p11.2 deletion and recovered by TAOK2. 27	27
10.2	Neuronal migration and immune perturbations in situ	27
	The effect of LPS and Poly(I:C) treatment in situ on neuronal positioning	27
10.2.1.1	Figure 6: Immune treatment affecting the position of neurons after migration. .	30
	The effect of LPS and Poly(I:C) treatment in situ on neuronal migration and bipolarity	30
10.2.1.2	Figure 7: Migration of neuronal populations in live imaging.	31
	The effect of LPS and Poly(I:C) treatment in situ on single neuron velocity	33
10.2.1.3	Figure 8: Single neuron velocity and mode of migration.	34
10.3	Neuronal migration and maternal immune activation	35
	The effect of maternal immune activation on neuronal migration	35
10.3.1.1	Figure 9: Cortical layering after maternal immune activation.	38
11	Discussion	39

11.1	Genetic intrinsic factor	39
11.2	Infection related external factors in neuronal migration.....	39
	Immune activation in acute slices	40
11.2.1.1	Neuronal migration in the somatosensory cortex as observed in situ	40
11.2.1.2	Behavior of microglia post treatment with Poly(I:C) and LPS in situ.....	41
	Maternal immune activation.....	42
11.3	Limitations of this study	43
11.4	Alternative models	44
	Genetic markers for microglia and neurons.....	44
	Acute slices.....	45
11.5	Alternative analysis methods	45
	Parameters Microglia Tracking.....	45
	Microglia morphology	46
11.6	Follow up experiments.....	46
12	Supplementary figures	47
12.1.1.1	Supplementary Figure 1: Neuronal migration by slice after transfection with human variants of TAOK.....	47
12.1.1.2	Supplementary Figure 2: Neuronal migration in 16p11.2 het mice by slice after transfection with human variants of TAOK.	48
12.1.1.3	Supplementary Figure 3: Morphology and localization of Microglia	50
12.1.1.4	Supplementary Figure 4: Position and migration velocity of Microglia.	52
12.1.1.5	Supplementary Figure 5: Relative position of microglia and neurons	52
12.1.1.6	Supplementary Figure 6: Migration of Poly(I:C) treated neurons.....	53
12.1.1.7	Supplementary Figure 7: Migration of LPS treated neurons in Experiment 16 and 22.	54
12.1.1.8	Supplementary Figure 8: Migration of LPS treated neurons in Experiment 23 and 24.	55
12.1.1.9	Supplementary Figure 9: Migration of neuronal populations in live imaging.....	56
12.1.1.10	Supplementary Figure 10: Single neuron velocity and mode of migration.....	58
12.1.1.11	Supplementary Figure 11: Microglia velocity after LPS and Poly(I:C) treatment in situ.	59
12.1.1.12	Supplementary Figure 12: Cortical layering after maternal immune activation...	59
12.1.1.13	Supplementary Figure 13: Frequency distribution of Ctip2 positive neurons.	61
12.1.1.14	Supplementary Figure 14: Frequency distribution of Satb2 positive neurons.....	62
13	Literature.....	63
14	Appendix Material.....	76
14.1	Equipment	76

14.2	Material	76
14.3	Software and Plugins	77
14.4	DNA.....	77
14.5	GHS classification	77
14.6	RStudio Script	78
	Data import and distance calculations from ImageJ point selection tool.....	78
	Scaling and uncoding of data in maternal immune activation.....	80
	Depiction of data in histograms and differential histograms.....	81
	Velocity of single neurons with coordinates from ImageJ tracking	83
15	Acknowledgement.....	86
16	Eidesstattliche Versicherung	86

3 Table of figures

Figure 1:	Neuronal differentiation in the developing cortex.	6
Figure 2:	Schematic representation of human TAOK2 isoforms with patient derived mutations. (Richter et al., 2018, fig. 4).....	13
Figure 3:	Acute cortical slice cultures.....	17
Figure 4:	Human variants of TAOK2 α affect neuronal migration in mice. (Scharrenberg et al., 2022)	26
Figure 5:	Neuronal migration is impaired in Het 16p11.2 deletion and recovered by TAOK2.	27
Figure 6:	Immune treatment affecting the position of neurons after migration.....	29
Figure 7:	Migration of neuronal populations in live imaging.	32
Figure 8:	Single neuron velocity and mode of migration.	34
Figure 9:	Cortical layering after maternal immune activation.	37

Supplementary Figure 1:	Neuronal migration by slice after transfection with human variants of TAOK.	47
Supplementary Figure 2:	Neuronal migration in 16p11.2 het mice by slice after transfection with human variants of TAOK.....	48
Supplementary Figure 3:	Morphology and localization of Microglia.....	49
Supplementary Figure 4:	Position and migration velocity of Microglia.....	51
Supplementary Figure 5:	Relative position of microglia and neurons.	52
Supplementary Figure 6:	Migration of Poly(I:C) treated neurons.....	53
Supplementary Figure 7:	Migration of LPS treated neurons in Experiment 16 and 22.	54
Supplementary Figure 8:	Migration of LPS treated neurons in Experiment 23 and 24.	55
Supplementary Figure 9:	Migration of neuronal populations in live imaging.	56
Supplementary Figure 10:	Single neuron velocity and mode of migration.	58
Supplementary Figure 11:	Microglia velocity after LPS and Poly(I:C) treatment in situ.	59
Supplementary Figure 12:	Cortical layering after maternal immune activation.	60
Supplementary Figure 13:	Frequency distribution of Ctip2 positive neurons.	61
Supplementary Figure 14:	Frequency distribution of Satb2 positive neurons.	62

4 Abbreviations

ASD: Autism spectrum disorder

BAM: Border associated macrophages

B-cell: bone marrow derived lymphocytes

Breg: regulatory B-cells

Ctip2: COUP-TF-interacting protein 2

DNA: desoxyribonucleic acid

E15-E17: embryonal day 15 to 17, age of the embryos

ERK / Erk1/2: extracellular signal-regulated kinase

Fmrp: Fragile x mental retardation protein

IL-6: Interleukin 6

IUE: *in utero* electroporation

LAP: Linear Assignment Problem

LoG: Laplacian of Gaussian

LPS: Lipopolysaccharid

MG: Microglia

mTORc1: mammalian target of rapamycin complex 1

NDD: Neuronal developmental disorder

NK-cells: natural killer cells

OPC: Oligodendrocyte progenitor cell

PAMP: pathogen-associated molecular pattern

PBS: Phosphate buffered solution

PFA: Paraformaldehyde

Poly(I:C): polyinosinic-polycytidylic acid

PRR: pattern recognition receptor

Satb2: Special AT-rich sequence-binding protein 2

TAOK2: Thousand and one amino acid kinase 2

T-cell: Thymus derived lymphocytes

Treg: regulatory T-cells

TNF- α : Tumor necrosis factor alpha

5 Zusammenfassung

Im Rahmen dieser Dissertation beschreibe ich Beeinträchtigungen der neuronalen Migration, ausgelöst durch intrinsische genetische oder extrinsische immunologische Faktoren. Als intrinsische genetische Faktoren habe ich den Einfluss von Varianten des Autismus-Risiko Genes TAOK2 (Tausend und eine Aminosäure Kinase) aus Patienten und einer heterozygoten Ausprägung der 16p11.2 Gen Region im Mäusegehirn untersucht. Ich habe herausgefunden, dass Mutationen aus Autismus-Patienten in TAOK2 α , aber nicht in TAOK2 β zu einer verminderten neuronalen Migration im Neokortex der Maus führen. Weiterhin habe ich herausgefunden, dass die beeinträchtigte neuronale Migration im heterozygoten 16p11.2 Maus Modell durch den Wildtyp TAOK2 α , aber nicht durch die in einem Autismus-Patienten vorkommende Variante TAOK2 α A135P behoben werden kann. Als immunologische Faktoren habe ich den Einfluss einer direkten Immunaktivierung von Mäusegehirnen *in situ* durch die Behandlung mit Lipopolysaccharid (LPS) und Polyinosinic-Polycytidilischer Säure (Poly(I:C)) und der indirekten Immunaktivierung der Mutter während der Schwangerschaft durch die Injektion von Poly(I:C) oder die Infektion mit Grippe (H1N1) untersucht. Durch Analysen an kortikalen Schnittkulturen (transfiziert an E15, Schnittkulturen an E17) habe ich herausgefunden, dass eine Behandlung *in situ* mit Poly(I:C), aber nicht mit LPS, zu einer Verminderung der neuronalen radialen Migration führt, gemessen an der Position der Neuronen nach Abschluss des Experimentes (E19). Die Analyse der Migration aller Neuronen in Video-Analysen hat ergeben, dass nach einer Behandlung mit LPS die mediane Migration aller Neuronen reduziert ist, während nach einer Poly(I:C)-Behandlung nur die Migration der bipolaren Neuronen reduziert ist. Weiterhin habe ich eine Verringerung des Anteils bipolarer Neuronen ausschließlich nach der Behandlung mit LPS beobachtet. Die Geschwindigkeit der Migration einzelner bipolarer Neuronen wurde weder durch die Behandlung mit LPS noch mit Poly(I:C) beeinflusst. Ich habe die Aktivierung von Mikroglia, einer Klasse von Immunzellen im Gehirn, anhand ihrer Morphologie in fixierten Schnittkulturen und anhand ihrer Migrationsgeschwindigkeit in Video-Analysen untersucht. Der Anteil an verzweigten (ramified) Mikroglia war nach einer Behandlung mit LPS signifikant reduziert. Die Geschwindigkeit der Migration von Mikroglia war nach einer Behandlung mit LPS signifikant erhöht. Abschließend habe ich zeigen können, dass in der Maus eine Immunaktivierung des Muttertieres durch eine Grippeinfektion (H1N1) oder eine Poly(I:C)-Injektion zu einem frühen Zeitpunkt der Schwangerschaft in den Nachkommen zum Zeitpunkt E17 zu einer Verschiebung der Position von Ctip2- und Satb2- positiven Neuronen in Richtung Ventrikel führt. Meine Ergebnisse zeigen, dass die neuronale Migration durch klinisch relevante Mutationen in Autismus-Risikogenen und durch den Autismus-Risikofaktor Immunaktivierung in der Schwangerschaft beeinträchtigt werden kann. Diese Ergebnisse betonen, dass die neuronale Migration als Teil der neuronalen Entwicklung möglicherweise auch zur Entwicklung einer Autismus-Spektrum-Störung mit beitragen kann.

6 Summary

In this thesis I describe impairments in neuronal migration induced by intrinsic genetic and extrinsic immune system related factors. As an intrinsic genetic factor, I studied the impact of human variants of autism spectrum disorders (ASD-) risk genes Thousand-and-One-Amino-Acid-Kinase-2 (TAOK2) and 16p11.2 in the murine brain. I found that human variants of TAOK2 α but not TAOK2 β lead to a reduction in neuronal migration and that in a model of 16p11.2 heterozygous deletion TAOK2 α but not the human variant TAOK α A135P was able to rescue migration impairments. Regarding immune system related extrinsic factors, I discovered that a treatment with polyinosinic-polycytidilic acid (Poly(I:C)), but not lipopolysaccharide (LPS) treatment impairs the resting point of neuronal migration in a model of acute slice culture of E15-E17 *in utero* electroporated murine brains. Analyses of the migration in live imaging revealed a reduced median distance of migration for LPS treated neurons in general and for Poly(I:C) treated bipolar neurons. I was further able to show a reduction in the bipolar fraction of neurons after LPS treatment, which was not accompanied by a change of single bipolar neuron velocity in either LPS or Poly(I:C) treatment. I assessed the activation of microglia under the influence of different treatments by their morphology in fixed slices and the velocity of their migration in live imaging. Immune activation via LPS leads to a reduced fraction of ramified microglia and to an increase in the velocity compared to microglia in untreated control slices. Finally, I was able to show the impact of a maternal immune activation by maternal H1N1 infection and Poly(I:C) injection on neuronal migration with a positioning of cortical layer neurons positive for Ctip2 and Satb2 more distal to the marginal zone compared to neurons of PBS injected mother's offspring. This highlights that neuronal migration is a component of neuronal development which can be affected by patient-derived mutations in risk genes or maternal immune activation as an autism risk factor and might thereby further contribute to the development of autism spectrum disorders.

7 Introduction

For this thesis I studied the contribution of certain internal and external factors on neuronal migration involved in known pathologies regarding the development of autism spectrum disorders. In my introduction I want to provide a brief background about the development of neurons, the brain and the two main components of the immune system. This is followed by some examples of how the maternal immune system is being activated by an infection, how autism spectrum disorder is affecting the immune system and how patients and research models are affected in different levels by autism spectrum disorders. Lastly, I describe the effect of genetics as intrinsic factors and environmental aspects as extrinsic factors affecting neuronal development and autism spectrum disorders in patients and in research models.

7.1 Neuronal development and Immune system

Neuronal development

7.1.1.1 Gross brain development

The development of the brain, as described in the sixth edition of Neurosciences by Purves et al (Purves et al., 2018) and reviewed by V. S. Chen et al in their histology atlas (V. S. Chen et al., 2017), is summarized in the following paragraphs. During the earliest days of development, the blastula invaginates during gastrulation and forms the three primary cell layers. These primitive cell layers are called endoderm, mesoderm and ectoderm. The mesoderm is incapsulated between the ectoderm and the endoderm, which consists of the invaginated cells. The mesoderm then retracts from the center of the newly formed tissue and thereby creates first the primitive pit, further stretching to two sides as the primitive streak. In this contact region between ectoderm and endoderm, the notochord forms as a transient structure. The cells of the ectoderm directly on top of the notochord develop into the neuroectoderm and will later give rise to all cells of the nervous system. During the following neurulation, the neural tube is formed by the neuroectodermal precursor cells. The cells inside the neural tube are the multipotent neural stem cells. Neural stem cells will proliferate and differentiate into all the other progenitor cells of the nervous system. The prolongation of the neural tube is then guided by cues from structures within the ectoderm and from the other germ layers. This neural tube forms the later spinal cord and develops into the gross brain structures. The development starts at the most anterior part of the neural tube, where a first balloon like structure is constricted and formed. Later, the forebrain is derived from this structure called prosencephalon. Together with the mesencephalon (midbrain) and rhombencephalon (hindbrain) it forms the first three vesicles of the brain. After the cerebral hemispheres are initiated, the five secondary brain vesicles are formed. The former prosencephalon is now developing into telencephalon and diencephalon, forming the cerebral hemispheres and the thalamus and hypothalamus respectively. While the mesencephalon stays undivided, the rhombencephalon develops into metencephalon and myelencephalon. The metencephalon will form the cerebellum and pons, while the myelencephalon will develop into the medulla oblongata. Inside the cerebral hemispheres, the initial cortical layering begins and the ventricular zone with its stem cell layer develops. The developed mammalian brain is covered by its enlarged cerebral cortical hemispheres with their characteristic sulcation. These gyri and sulci allow for a largely increased cortical surface compared to a smooth brain. Encased underneath are the cerebral nuclei with basal ganglia, amygdala, and basal forebrain (Appendix 3 of (Purves et al., 2018)). Ventral to the basal forebrain are the thalamus and hypothalamus, located themselves dorsal of the midbrain. The pons and medulla oblongata connect to the spinal cord. Most ventral to the cortical hemispheres and posterior and connected to the pons, is the cerebellum located. It resembles the sulci and gyri structure of the cerebral cortex. The basic cellular composition of the vertebrate brain can be broadly divided into neuronal cells and glial cells. While neurons are actively involved in the transmission of electrical signals in either an excitatory or inhibitory way, the glia cells cover a broad

spectrum of different supporting cell types with multiple functions. These range from architectural stability and stem cell characteristics (radial glia), immunological functions (microglia and astrocytes) up to acting upon the electric conductivity along neuronal axons (Oligodendrocytes) (Allen & Lyons, 2018).

7.1.1.2 *Murine vs human brain*

In contrast to the characteristic shape of human cortex, the murine brain is lissencephalic and does not feature the strong gyrification (Molnár et al., 2019). The murine olfactory bulb is much more prominent with its 2 % of the total brain volume compared to the human 0.01% (McGann, 2017).

7.1.1.3 *Neuronal cell development*

The neural tube contains neuronal precursor stem cells called neuroepithelial cells. Inside the tissue the neuroepithelial cells start to orientate themselves towards the later ventricle to develop into radial glia cells. These radial glia cells give rise to all neuronal cell types and glial cells. Asymmetrical division of radial glia cells produces one daughter radial glia cell and either one of the different neuronal cell types or a neuronal intermediate progenitor cell (Paridaen & Huttner, 2014). These intermediate progenitor cells most often are of a multipolar shape and divide symmetrically into two postmitotic neurons (Cadwell et al., 2019). Neurons and progenitors do present multiple different morphologies, which can be categorized by their polarity. Calderon de Anda et al. covered different aspects of these in their editorial (Calderon de Anda & Gaertner, 2018). The basic morphology of neurons is tightly linked to their function of receiving and transmitting signals to further neurons. Their branched network of most often multiple dendrites receives signals from axons of other neurons with their dendritic spines. The, in most cases single, in rare cases missing, axon transmits information to either neighboring neurons or over long distances in the central and peripheral nervous system (Chapter 1 (Purves et al., 2018)). The neurons of the cerebral cortex can be mainly classified into inhibitory neurons and excitatory, pyramidal neurons (Marín et al., 2010). In this thesis, I will focus on the pyramidal neurons.

7.1.1.4 *Cortical development*

The six layered neocortex is thought to be responsible for the complex tasks such as perception, language, thoughts and others (Reviewed in (Molnár et al., 2019)). Its development starts with the above-described radial glia cells which provide both structural integrity and stem cell characteristics to proliferate into neuronal progenitors and neurons. Via symmetric division they can proliferate into daughter radial glia cells and thereby increase their number. The apical and basal processes of radial glia cells span the developing cortex and provide an architecture for the neuronal migration (Hansen et al., 2017). The multipolar intermediate progenitor cells, produced by asymmetric division of radial glia cells, develop into bipolar neurons and radially migrate along the radial glial basal processes from the ventricular zone towards the building marginal zone (Molnár et al., 2019). This process is briefly sketched in Figure 1 (C. Chen et al., 2015), with apical radial glia cells included in the apical progenitors (Arai & Taverna, 2017). During this radial migration, the nucleus of the neuron is propelled by nucleokinesis. In this process, the leading edge of neurons stretches towards their target zone. In a second step, the centrosome is moved in between the nucleus and the leading edge. This allows for the last step in which the nucleus is pulled towards the leading edge creating the characteristic saltatory movement pattern (Marín et al., 2010). The protein reelin is thought to play a role in both the attraction of neurons towards the marginal zone, as well as the termination of migration once they reach their target zone (Frotscher et al., 2017).

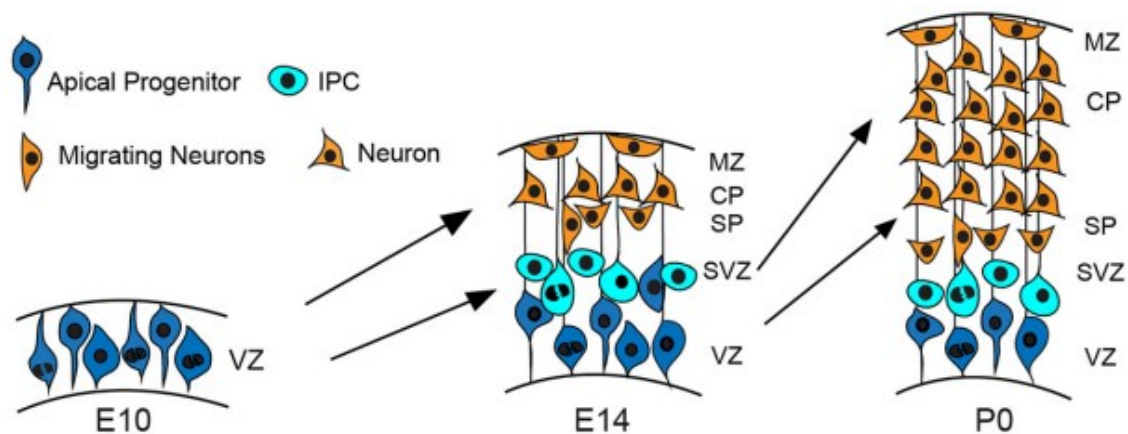


Figure 1: Neuronal differentiation in the developing cortex.

The development of the murine cortex sketched from embryonal day 10 to birth. From the ventricular zone containing the apical Progenitors at E10, the development of the subventricular zone with the Intermediate progenitor cells (IPC), the subplate, cortical plate and marginal zone containing differentiated neurons during and after their migration at E14 until the expanded cortical plate at birth. Figure published in (C. Chen et al., 2015).

During each wave of migration, the newly generated neurons are migrating from the ventricular zone through each earlier formed layer outwards until they reach the marginal zone (Mukhtar & Taylor, 2018). By doing this, the migrating neurons form the six layers of the neocortex consecutively in an inside out fashion, starting with the inner three layers during early neurogenesis, followed by the outer three layers during late neurogenesis (Kwan et al., 2012). The formed layers do not only differ by the timepoint, the neurons migrated into them, but also by the expression of certain markers and the targets for axonal projection of neurons present in the layer. For example in mice, while neurons in the neocortical layers 2-6 do express *Satb2*, the expression of *Ctip2* is fairly limited to layer 5 (Nomura et al., 2018). The expression of the layer-specific genes in neurons can set on as early as during the symmetrical and asymmetrical division from radial glia cells in the ventricular zone, persists during their postmitotic migration through the subplate and already existing layers of earlier born neurons along the glia tracts up to until their own layer formation just below the marginal zone and furthermore until late postnatal timepoints (Kwan et al., 2012). If these layer specific genes are impaired, specific phenotypes and layering deficits can arise. Defects in *Reeler* lead to an inversion of the six cortical layers in between the marginal zone and the subplate as migrating neurons are not capable of breaching through the layers on top (Caviness, 1982). Loss of *Tbr1*, expressed in post-mitotic neurons early during the generation of the deep layers and later in the neurons of the upper layers, results in neurons of the subplate being positioned in between other layers and neurons of deep layers appearing in clusters in upper layers (Kwan et al., 2012). The different projections of neurons can be briefly described in three classes: The *Ctip2* expressing Pyramidal tract neurons, mostly situated in layer 5, project their axons mainly towards the spinal cord. Corticothalamic neurons, placed further up in layer 4, project towards the Thalamus. Finally, there are Intratelencephalic neurons located more distributed among layers 2-6. These neurons express *Satb2* and project to both hemispheres within the forebrain (Cadwell et al., 2019). The Intratelencephalic neurons are also the main local source of input for the other classes (Harris & Shepherd, 2015). Due to the specificity of projections in the cortex and the fine-tuned timing during development, disturbed layering might negatively influence neuronal networks within and between cortical layers and other brain regions.

The cerebral cortex can mainly be classified into the four lobes each hemisphere harbors. The Occipital lobe most caudal, the Temporal lobe extending ventrally from the cortex, the Parietal lobe anterior from the Occipital lobe towards the central sulcus and the Frontal lobe, covering roughly the rostral half of the cortex (Purves et al., 2018, Chapter Appendix 4). The regions targeted in the experiments of this thesis are in the somatosensory cortex located in the Parietal lobe.

Embryonal immune system development

7.1.1.5 *General immune system development*

The immune system is comprised of cells of the innate and adaptive immune response. Hematopoiesis in human fetuses starts in the yolk sac and mesenchymal tissue where pluripotent progenitors of macrophages are produced (P. G. Holt & Jones, 2000). In a second wave the fetal liver and bone marrow starts to become active (Park et al., 2020). After this first development of the innate immune system from the liver, the adaptive immune system starts to develop with B-cell progenies in the bone marrow and T-cell development in the thymus (Hossain et al., 2022). The following paragraph summarizes the description of the immune system by Murphy and Weaver. The innate immune system is regulated by antibody independent receptors. The cells of the innate immune system are, among others, macrophages, dendritic cells, and natural killer cells. Threads are attacked via phagocytosis, complement system and excretion of cytokines. The innate immune system recognizes more general pathogen associated patterns (PAMP, *pathogen-associated molecular pattern*) via *pattern recognition receptors* (PRR). The adaptive immune response is based on specific antibody dependent recognition of threads. These recognized patterns are called antigens. The cells of the adaptive immune response are different subtypes of B-cells and T-cells. The antibody dependent response requires fine tuning of antibodies against the multiple antigens of a thread. B-cells recognize antigens with their B-cell receptor. The B-cell receptor consists of an antibody and a set of transmembrane proteins. The T-cell receptor has a high similarity to the antigen recognizing fragment of antibodies. Upon recognition of a thread, B-cells become activated and undergo multiple proliferation steps before developing into mature antibody producing plasma cells. Depending on their receptor-subtype, T-cells recognize either phagocytosed antigens (presented by major-histo-compability complex MHC-2) or self-antigens (presented from the cytoplasm by major-histo-compability complex MHC-1). T-cells activated by MHC-2 tend to have immune-regulatory or -stimulating function, while activation by MHC-1 leads to a cytotoxic reaction against the targeted cell (Murphy & Weaver, 2018).

7.1.1.6 *Placenta*

During the development in the womb, the placenta acts as a first physical barrier between the maternal and offspring's circulation (Goasdoué et al., 2017). The placentas three major functions are described as processing the maternal-fetal exchange of nutrients, gas and waste, providing the fetus with maternal immunoglobins and excretion of cytokines and hormones for both the maternal and fetal development (Griffiths & Campbell, 2015).

7.1.1.7 *Blood Brain barrier*

The Blood-Brain-Barrier develops early during development to protect the brain from potential hazards in the embryonal blood. It consists of endothelial cells blocking the passage of substances via tight junctions. Furthermore, specific transporters allow for nutrient supply to the brain and disposal of other substances from the brain. This structure is supported by various cell types such as astrocytes, microglia, pericytes and neurons, altogether called Neurovascular unit (NVU) (Goasdoué et al., 2017). In his review, Banks illustrates how different hormones, cytokines, peptides and other molecules may or may not pass the blood brain barrier, which itself, upon stimulation, can produce molecular signals towards the brain or the blood (Banks, 2012, fig. 1).

7.1.1.8 *Early border associated Macrophages and Microglia infiltration*

In the developed brain, around 80 percent of the immune cells are microglia (Morimoto & Nakajima, 2019). These cells develop early from a macrophage like progenitor in the yolk sac and migrate into the brain already before the Blood-Brain-Barrier develops (Ginhoux et al., 2010). The infiltration of microglia into the brain coincides with or just after the onset of neurogenesis and leaves microglia, until the following later astroglia and oligodendrocyte development, the main glial cells present in the neuronal parenchyma (Thion et al., 2018). Their distribution in the cortical layers changes over the course of development. Initially, they migrate to the cortex via the ventricle and pial surface. In mice, infiltration of amoeboid microglia into the different layers takes place around E14, although the cortical plate is still spared until shortly before onset of astrogenesis at E18. At that time, initially ramified microglia distribute around neurons, radial glia and blood vessels along the whole depth of the cortex (Reemst et al., 2016). Also it was shown that in E19 rats microglia do contact multiple neuronal progenitor cells at the same time in the ventricular zone (Noctor et al., 2019). As microglia are a type of tissue resident macrophages, their main function in the brain is their phagocytic activity and excretion of cytokines. This includes important contributions to neuronal development such as engulfment of neuronal progenitors, pruning of axons and spines but also stimulation of spine formation (Cunningham et al., 2013; Miyamoto et al., 2016). These different functions are accompanied by a whole range of morphologies. Thin, long-stretched and ramified processes are thought to be surveying the surrounding tissue, while a reduction and thickening of process length together with an increase in soma size is mentioned to have a stronger focus on phagocytic activity (Antonson et al., 2019; Lier et al., 2021). Though arising from one progenitor, microglia develop a wide heterogeneity throughout different brain regions (as reviewed in (Tan et al., 2019)). Some molecular markers used to identify microglia are P2Y12R (Mildner et al., 2017), TMEM119 (Satoh et al., 2016) and Iba1 (Reviewed in (Jurga et al., 2020)). P2Y12R is detecting ATP and ADP and is guiding the microglia towards a site of injury (Haynes et al., 2006). On the other hand, P2Y12R has also been shown being necessary for microglia-neuron interaction at somatic junctions to support neuronal development (Cserép et al., 2022). The function of TMEM119 in microglia is not clear but TMEM119-positive follicular dendritic cells have been found outside the brain in immunologic active organs (spleen, lymph nodes, tonsils) (Satoh et al., 2016). Iba1 expression is restricted to monocytes, whose tissue resident cells in the brain are the microglia and intruding macrophage (Imai et al., 1996). Iba1 is colocalizing with F-actin in macrophages and microglia and is involved in phagocytosis and membrane ruffling and might also play a role in migration due to its fimbrin-binding activity, an actin-bundling protein (Ohsawa et al., 2000, 2004). In addition to the microglia inside the parenchyma, there are border associated macrophages (BAM). These innate immune cells are located outside the parenchyma close to the vessels inside the brain and lining the meninges and perivascular spaces (Bechmann et al., 2001; Mrdjen et al., 2018).

7.1.1.9 *Later Astroglia and Oligodendrocyte development*

During the late stages of embryonal development at the end of neurogenesis - in mice around E18 - astrogenesis takes place in the developing brain (Reemst et al., 2016). Radial glia cells exit the proliferative phase after a final asymmetric division and develop into astrocytes during migration towards the cortical plate (Noctor et al., 2004). After migration, astrocytes proliferate and divide multiple times and create around half of the astrocytes in the upper layers (Ge et al., 2012). One of the multiple functions of astrocytes is the enclosure of a neuronal synapse. By doing this, the astrocyte prevents neurotransmitter from diffusing into the extracellular matrix (Piet et al., 2004). Equipped with their own receptors, they also contribute to the uptake of transmitters (Zhou et al., 2019, fig. 2). Like microglia, astrocytes also play a role in the immune response in the CNS. Upon stimulation with LPS, they react by upregulation of multiple immune related mRNAs, such as Tumor Necrosis factor alpha (TNF α) and interleukin 6 (IL-6) (Rodgers et al., 2020). The oligodendrocyte precursor cell (OPC) is also

arising from radial glia and migrating away from the ventricular zone before proliferating and developing into mature oligodendrocytes (Bergles & Richardson, 2016). The main function of oligodendrocytes is thought to be the myelination of axons and thereby the support of their electric conductivity (Purves et al., 2018, Chapter 1).

Maternal immune system and maternal immune activation

7.1.1.10 Maternal immune status during pregnancy

The female immune system undergoes multiple changes during pregnancy. Specifically, different parts of the maternal complement system as well as inhibitory molecules are increased but balanced (Abu-Raya et al., 2020). An unbalanced increase in the complement system was shown to be involved in pregnancy related complications such as preeclampsia and pre-term birth (Reviewed in (Denny et al., 2013)). The number of regulatory cells of the maternal immune system, including regulatory B- and T-cells (Breg and Treg), but also neutrophils is increased. On the other hand, compared to non-pregnant women the number of B-cells, T-cells and phagocytotic activity is decreased (Abu-Raya et al., 2020, fig. 1). One important function of the increase in Treg cells was shown to be the prevention of the maternal T-cells being activated against the fetus (Tilburgs et al., 2009).

7.1.1.11 Maternal immune response to viruses

When a virus enters the maternal body during pregnancy, several lines of immune defense become activated (Murphy & Weaver, 2018, Chapter IV). The first reaction of the innate immune system is a rather unspecific inflammation response with cytokine excretion leading to influx of proteins of the complement system via blood plasma, recruiting of phagocytotic cells and further inflammatory cytokine secretion (e.g., TNF- α). Secretion of Interferon α and β is here rather specific for a viral infection of cells. Already in this innate response, certain PAMPS can be recognized by the phagocytes. The Toll like receptor 3 (TLR-3) is expressed on the cell surface and in endosomes and recognizes double stranded RNA, which is specific for Viruses (Reviewed in (Mogensen, 2009, fig. Table 1)). Other recognized patterns are single stranded RNA (TLR-7/8) or glycoproteins from the surface of the virus (TLR-2/4) (Mogensen, 2009). Detection of viral particles by phagocytes leads here to a secretion of IL-12 which in turn induces monocytes and natural killer cells to secrete Interferon γ to further activate phagocytotic activity. In the next step, the dendritic cells migrate from the point of infection to the lymph nodes and activate the adaptive immune response by priming B-cells and T-cells with antigens from the site of infection (Murphy & Weaver, 2018, Chapter IV). Basic T-cell activation upon viral infection can be divided into two groups. CD8⁺ cytotoxic T-cells induce apoptosis and can destroy proteins inside infected cells. CD4⁺ lymphocytes can develop into the various T-helper cells, secrete cytokines, and activate B-cells. B-cells secrete antibodies for viral clearance and antibody dependent cell-mediated cytotoxicity. As a virus infection is primarily intracellular, the cytotoxic T-cells are thought to be the most active T-cells in the adaptive immune response against viruses (X. Chen et al., 2018).

7.1.1.12 Maternal immune response to bacteria

The principle innate immune reaction towards intra- or extracellular bacteria is comparable to the anti-viral reaction. Also, the recognition of intracellular viral or extracellular bacterial infection via TLRs differs only for some PAMPS. While bacterial DNA, RNA and glycoproteins are recognized by the same set of TLRs as their viral counterparts, also the presence of lipoproteins and other membrane compounds is detected by this set. The example of bacterial Flagellin is an exception with no viral counterpart and is recognized by TLR-5 (Mogensen, 2009, fig. 3). Secretion of Interferon γ induces further phagocytotic activity against the bacteria. Extracellular bacteria also induce the production of IL23 in phagocytes, which itself leads to a secretion of IL17 and IL22 (Murphy & Weaver, 2018, Chapter IV). As in viral infections, dendritic cells prime B-cells and T-cells in the lymphoid organs for their activation specific to the bacterial antigens. The T-helper cell Th-17 is responsible for secretion of IL-

17 in both viral and bacterial infections. The two main effects of IL-17 are the stimulation of IL-6, which itself stimulates IL-17, and the activation of neutrophils to tackle the bacterial infection (Murphy & Weaver, 2018, Chapter IV). A maternal infection with bacteria such as *Listeria* reaching cells in the placenta can be very dangerous for the fetus, as this is an environment which is highly regulated against maternal immune activity. Extra villous trophoblasts in the placenta can be infected by *Listeria* but will not be classically targeted by the local decidual NK cells (Tilburgs et al., 2015). Though, the maternal decidual NK cells are capable of selectively transferring granulysin to the infected Trophoblasts which kills the *Listeria* by perforating their membrane without harming the placental cells (Crespo et al., 2020).

7.1.1.13 Maternal vaccination during pregnancy

Maternal vaccination is a rather safe and important medical procedure. It not only protects the mother from infections she is more likely to suffer stronger from during pregnancy, but also against maternal infections that can have harmful consequences for the fetus. In addition, it directly protects the fetus by transferring maternally produced antibodies via the placenta and passively immunizes the unborn child (Etti et al., 2022).

7.1.1.14 Virus / Bacterium / Toxin reaching embryo vs Maternal immune reaction affecting embryo

Different data sets indicate towards different modulators of the maternal immune system to be responsible for a neurodevelopmental impairment in the offspring. When the dam is injected with the viral mimic Poly(I:C) it reacts with increased levels of IL-1 and IL-6 (Smith et al., 2007). Injection with anti-IL-6 antibody reduced the effect in the offspring (Smith et al., 2007). The increase of maternal IL-17 after a bacterial or viral infection also elevates autism-resembling behaviors in the offspring of mice (Yasumatsu et al., 2020). Some viruses themselves can also pass through the placenta and infect the fetus. One of the most prominent might be the ZIKA virus, which was shown to negatively affect the development of both neuronal progenitors (Tang et al., 2016) but also reduces growth in organoid brain models (Garcez et al., 2016).

7.1.1.15 Offspring's immune reaction to maternal immune activation and infection

The expression of immune related genes in the offspring's microglia is reduced after maternal immune activation (Hayes et al., 2022). The maternal immune activation by Poly(I:C) led to an increase in the offspring's macrophage activity. Stimulation with either LPS or LPS and IL-4 or Interferon γ led to an increase in IL-12 or CCL3 in the offspring (Onore et al., 2014). A maternal infection and the transfer of IL-6 to the embryo led to a higher resistance against oral infections but also an increased susceptibility for gut inflammation in the offspring (Lim et al., 2021).

Autism spectrum disorders affecting the immune system

7.1.1.16 Immune dysfunctions in patients with ASD

Impairments in the offspring's immune system have been linked to autism spectrum disorders (ASD). A decrease in the percentage of total lymphocytes and CD4+ T-helper cells in children with autism compared to their unaffected siblings or controls has been already found in 1990 (Yonk et al., 1990). A mutation in the autism risk gene TAOK2 was shown to reduce the proliferation of T-cells in a family struggling with an HPV associated skin disease (Molho-Pessach et al., 2017). Multiple cytokines were observed to be affected in patients from ASD spectrum compared to control groups. E.g. an increase in IL-1 or IL-6 was observed in ASD patients and associated with severity of ASD, "deficits in social sphere" irritability, lethargy and hyperactivity (Gładysz et al., 2018). The density of microglia-distribution was also found to be increased in autistic patients, specifically in the fronto-insular and the visual cortex (Tetreault et al., 2012). Also diseases connected to asthma and allergies were shown to be more prominent in patients with ASD (Hughes et al., 2018, fig. 2).

Autism spectrum disorders in clinic and research

7.1.1.17 Clinical description of ASD

Leo Kanner and Hans Asperger defined in their 1943 and 1944 published works a certain typical behavior in children, that to their knowledge has not been described before (Asperger, 1944; Kanner, 1943). Both describe the status of children as autistic, a term, which Asperger attributed to the German psychiatrist Eugen Bleuler (Asperger, 1944). In their studies, they depicted their patients with a certain self-sufficiency, “happiest, when left alone”, “like in a shell”. Language acquisition was described as parrot-like, questions were answered with the repetition of the question instead of “yes” (Kanner, 1943).

Today’s description of essential features of the Neurodevelopmental Disorder in the current ICD-11 WHO catalogue is the following:

“Persistent deficits in initiating and sustaining social communication and reciprocal social interactions that are outside the expected range of typical functioning given the individual’s age and level of intellectual development. Specific manifestations of these deficits vary according to chronological age, verbal and intellectual ability, and disorder severity.

Persistent restricted, repetitive, and inflexible patterns of behavior, interests, or activities that are clearly atypical or excessive for the individual’s age and sociocultural context.

The onset of the disorder occurs during the developmental period, typically in early childhood, but characteristic symptoms may not become fully manifest until later, when social demands exceed limited capacities.

The symptoms result in significant impairment in personal, family, social, educational, occupational, or other important areas of functioning. Some individuals with Autism Spectrum Disorder are able to function adequately in many contexts through exceptional effort, such that their deficits may not be apparent to others. A diagnosis of Autism Spectrum Disorder is still appropriate in such cases.” (World Health Organization, 2022).

A study covering countries in North America, Europe, Asia, Africa and Australia, estimates the global prevalence of ASD as currently around 1/100, with a rise in number of diagnoses. There are around 4 times more male than female cases and in 33 % of the cases another intellectual disability was present (Zeidan et al., 2022).

7.1.1.18 Neurological implications in ASD

Patients with ASD are, as it is a neurodevelopmental disorder, affected from as early on as prenatal development. Apart from the above-mentioned behavioral implications, there are also neurobiological features, such as impairments in neuronal connectivity, gross brain morphology and neuronal migration present. Larger brain size, called macrocephaly, was shown to be up to 5 times more present in ASD patients than in control groups (Sacco et al., 2015). In children with autism, patches of disorganization have been found in the neocortex (Stoner et al., 2014). Also the connectivity in between brain regions can be impaired, as shown in some 16p11.2 mutation carriers (Bertero et al., 2018). In addition, in children autistic traits have been correlated with smaller brain size and a decrease in gyrification and cortical thickness, even when ASD cases have been excluded from the study (Alemany et al., 2021).

7.1.1.19 ASD symptoms in research models

Different research paradigms have been applied to study ASD. In genetically altered mouse models, behavioral features such as missing social novelty, increased repetitive behaviors (self-grooming), reduced social behaviors and vocalizations, cognitive impairments, marble burying and “reduced

reciprocal social interactions” have been described (Crawley, 2012). To cover the neurodevelopmental aspects of ASD, both animal models and human in vitro models have been used. Human in vitro models utilized either fetal post mortem neuronal progenitor cells, induced neurons or the generation of embryonal or induced pluripotent stem cells (Gordon & Geschwind, 2020). In animal models of autism risk genes, features of neuronal developmental disorders have been observed, such as abnormal brain size, impairments in dendrite and synapse formation and deficits in cortical layering and neuronal migration (de Anda et al., 2012; Richter et al., 2018; Scharrenberg et al., 2022). Others copy the neurochemical imbalances of certain brain regions also found in young human patients (Michetti et al., 2014).

7.2 Intrinsic factors predisposing ASD

Patient based mutations

7.2.1.1 Genetic causes for ASD

ASD, with its wide variety of symptoms, is thought to have both genetic and non-genetic risk factors such as environmental toxins contributing to its development (Cheroni et al., 2020). Also maternal infections during pregnancy play a role for at least some of the affected patients (Tioleco et al., 2021). The SFARI Gene bank from the Simons Foundation lists a large number of genes, assigned to a certain likelihood of their contribution to ASD (The Simons Foundation, 2022). Some of them derive from the review of Satterstrom et al. where over a hundred genes implicated with a risk for autism have been identified, most of which are expressed in neurons and some of which are linked to development (Satterstrom et al., 2020). The genetic variants, potentially involved in the development of ASD are to a high degree de novo mutations. Twin studies also support the heritability, as the fraction of monozygotic twins sharing a diagnosis of ASD has been very high in multiple twin studies, even though it was found that also here additional factors might play a role in the severity (Castelbaum et al., 2020; Frazier et al., 2014). This highlights the broad spectrum of genes impacting the development which can, when altered, lead to a phenomenon like ASD.

7.2.1.2 16p11.2 mutation

The 16p11.2 genomic region is a prominent genetic region carrying a risk potential for the development of ASD. It is located on the small arm of chromosome 16 and carries within the so-called single copy region thirty protein coding genes. Duplications and deletions in this region have been found in about 1% of all diagnosed ASD patients (Weiss et al., 2011). The symptoms of affected patients may include impairments in motor and speech development, affected cognitive functions (memory) or seizures (Fetit et al., 2020). Also micro- and macrocephaly can appear in patients with 16p11.2 duplication and depletion, respectively (Shinawi et al., 2010).

7.2.1.3 TAOK2 mutation

One of the risk-genes located in the 16p11.2 region is the Thousand-And-One-Amino-Acid Protein Kinase 2 (TAOK2). This Serine/Threonine protein kinase exists in two splicing variants, TAOK2 α and TAOK2 β . Both variants contain a N-terminal kinase domain, a central MEK binding domain and a C-terminal regulatory domain which is varying in length depending on the splicing variant (Richter et al., 2018). In human patients, TAOK2 mutations have been found amongst others in the kinase domain (A135P), rendering TAOK2 Kinase dead, in the linker domain (A335V) and in the regulatory domain (P1022*), leading to a premature stop codon, called C-terminal deletion (Richter et al., 2018).

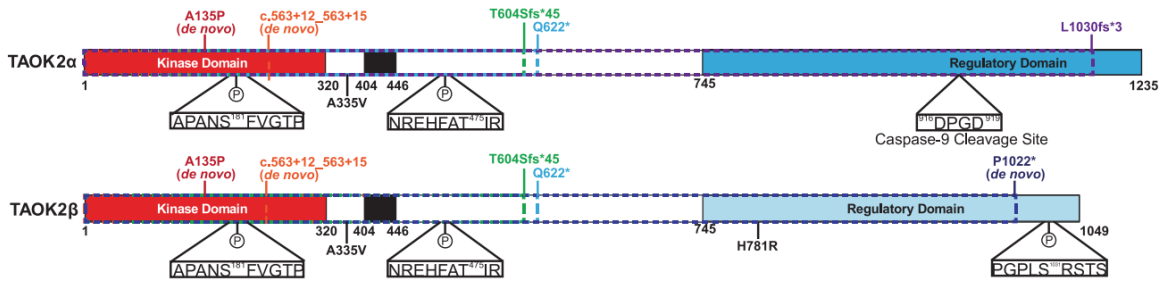


Figure 2: Schematic representation of human TAOK2 isoforms with patient derived mutations. (Richter et al., 2018, fig. 4)

Model based mutations

7.2.1.4 16p11.2 mutation

As mentioned earlier, there are organoid models available for the 16p11.2 deletion and duplication. In these models, processes like neuronal migration, proliferation and synapse formation are impaired and the size of the organoid reflects the micro- and macrocephalus-phenotype of 16p11.2 duplication and deletion patients, respectively (Urresti et al., 2020). In the mouse model, changes in the number of basal progenitor cells are observed together with a decrease in the number of upper layer neurons and memory impairments (Pucilowska et al., 2015). In addition, neurons of the prefrontal cortex, transfected with a marker protein at E15 in 16p11.2 heterozygous deletion mice, were less frequently found in the cortical plate but in a higher number in the intermediate zone at E18-19, compared with their wild type littermates (Scharrenberg et al., 2022).

7.2.1.5 Taok2 mutation

The impairments of 16p11.2 heterozygous deletions are partially reflected in the TAOK2 heterozygous or knockout mice generated by Kapfhamer et al., such as the cortical thinning of 16p11.2 patients, or even exaggerated, possibly due to the homozygous knockout of TAOK2 (Kapfhamer et al., 2013; Richter et al., 2018; Scharrenberg et al., 2022). Patient mutations found in TAOK2, expressed in different models reflected impairments in autophosphorylation and subsequently kinase activity, leading via affected RhoA signaling to impaired spine stability in neurons transfected with human variants of TAOK2β (Richter et al., 2018). Human variants expressed in TAOK2α on the other hand do influence neuronal migration, which I will focus on in the results part (7.1.1 The effect of ASD-related human variants of TAOK2 on neuronal migration) and which just recently have been published (Scharrenberg et al., 2022). Upon acute downregulation of TAOK2 with shRNAs, both the basal dendrite formation and the callosal axon formation is impaired in murine brains (de Anda et al., 2012).

7.2.1.6 Other genetic mutations

The number of genes related to ASD is huge, as described above. For some, genetic models have been developed. Reelin (RELN) has been shown to have a high linkage to ASD in a European cohort (R. Holt et al., 2010). In the heterozygous mouse model, an increased response to a stress stimulus and an neurochemical imbalance has been demonstrated (Michetti et al., 2014). The homozygous patients display lissencephaly and both patients and the homozygous mouse model present an impaired cerebellar development (Lossi et al., 2019). Loss of function in FMRP, the gene for the fragile-x mental retardation protein is causative for the Fragile-X-Syndrome, which is part of the autistic spectrum. Normally functioning FMRP is binding to RNA, e.g. TAOK2, and thereby stalls the translation (Darnell et al., 2011).

7.3 Extrinsic factors predisposing ASD

Human / Patient appearances

Even though the number of genes implicated in ASD is immense, there are not only genetic reasons behind this disorder. Maternal exposure to environmental toxins, heavy metals, organic substances but also infections, malnutrition and other stressors have been implicated in the development of ASD (Cheroni et al., 2020; Vasistha & Khodosevich, 2021). Also sex hormone levels, maternal obesity and in some cases ultrasound have been associated with an increased risk of ASD in the offspring (Bölte et al., 2019).

7.3.1.1 *Viral infection*

Maternal infections by a virus can be potentially harmful for the embryo mainly by two different mechanisms. Firstly, the maternal infection elicits an immune reaction in the mother, e.g., against an infection with Influenza. This immune reaction implicates amongst other factors cytokines such as IL-6, IL-12, IL-17a, antiviral interferons α and β and signaling from the innate immune system to activate the adaptive system. These cytokines do not only circulate in the maternal blood but pass through the placenta and enter the fetal blood stream (Elgueta et al., 2022). Studies in mice support an effect of maternal cytokine levels on the fetal brain, as mRNA for the IL-17a receptor was found to be upregulated in the offspring's brain after increased IL-17a levels in Poly(I:C) injected mothers (Choi et al., 2016). A study on the Boston Birth cohort showed a significant increase in the odds of developing ASD in the offspring when the mother in general had fever or specifically in the third trimester (Brucato et al., 2017).

Secondly, a virus can also directly infect the embryo and either elicit a detrimental immune reaction or harm the neuronal development by infecting the neurons directly. One of the examples for this kind of infection is the ZIKA virus infection, leading to the congenital ZIKV syndrome (CZV) (Teixeira et al., 2020). Common symptoms of children after a maternal ZIKV infection were Hydrocephalus, Microcephalus, calcifications of cortical and subcortical junctions and cerebellar impairments. Also disturbances in neuronal migration in the cortex and other regions have been observed (Marques et al., 2019). In laboratory studies, it was shown that ZIKV is capable of infecting neuronal progenitor cells, derived from induced pluripotent stem cells. The infection leads to a deregulation of cell cycle, transcription and can lead to cell death upon release of the viral particles. Both deregulation of cell cycle and increased cell death decrease the number of progenitors over time upon infection (Tang et al., 2016).

7.3.1.2 *Bacterial infection*

In some cases, bacterial infections during pregnancy can potentially harm the offspring in either a direct or indirect way and pave the path for the development of ASD. In general, bacterial infections of the mother, diagnosed during a hospitalization, has been found to be coupled to increased odds for ASD in the offspring (Zerbo et al., 2015). In the case of chorioamnionitis, a bacterial infection induces a maternal inflammation response against the two fetal tissues, chorion, and amnion. This can elicit a fetal inflammatory response syndrome (FIRS), which induces high level of proinflammatory cytokines, increases the risk for intraventricular hemorrhage and might lead to an increased activation of microglia in critical developmental windows of the fetal brain (Muraskas et al., 2020). In a study with mice, the bacterial cell wall peptidoglycans were able to cross the placenta into the embryo and induce proliferation in neurons via FoxG1, resulting in an increased density of neurons in the cortical plate and memory impairments and behavioral deficits in the offspring (Humann et al., 2016).

7.3.1.3 *Autoimmune disorders in mothers and ASD in offspring*

Apart from an infection, a maternal autoimmune disease can also increase the risk for ASD in offspring. Rheumatoid Arthritis in the mother was found to be significantly associated to an increased risk for

ASD in the offspring (Atladóttir et al., 2009). Another publication showed, that maternal autoimmune disease is significantly related to neurodevelopmental disorders, but not ASD alone (Lyall et al., 2014). The shared link is likely to be the increased immune activation in people affected by autoimmune diseases. A meta-analysis, published in 2022, also saw an increased risk in parental general autoimmune disease and in parts even in paternal involvement for the offspring to develop ASD and ADHD (Ellul et al., 2022).

7.3.1.4 *Toxins*

Another group of effectors, which can prime the unborn child prenatally for ASD are toxins and drugs with toxic effects on the embryo. Lead, a classical environmental toxin contained in fuel and some water pipes, was found to be correlated with intellectual impairments in children. Increase in the blood lead levels were negatively correlated to IQ levels (Canfield et al., 2003). The use of valproic acid, a potent drug in the treatment of epilepsy, was linked to a strong increase in the odds of developing ASD and childhood autism (Christensen et al., 2013). Exposure to environmental burdens such as traffic-related air pollutants nitrogen dioxide and particles with less than 2.5 μm or 10 μm both during gestation and the first year of life were associated with an increase in the odd for children having ASD (Volk et al., 2013).

Models for extrinsic factors

7.3.1.5 *Influenza infection*

Maternal infection is an often-used model for NDDs. In a mouse model, an infection with influenza during pregnancy leads to strong behavioral impairments in the offspring, associated with ASD and Schizophrenia. Exploratory behavior in the open field was strongly reduced compared to mice born to non-infected mothers, and also the social interaction between mice from infected mothers was almost three times less than from non-infected mothers (Shi et al., 2003). Due to the common view that the maternal immune reaction and not the virus itself is acting on the fetus, the maternal infection is more frequently replaced by maternal Poly(I:C)-treatments. Still, an influenza infection can also harm the fetus by eliciting an inflammation response at the placenta. This activation of the immune system can damage the placenta and thereby reduce its capability to transfer oxygen, leading to hypoxia of the fetus and potentially damaging the fetal brain (Liong et al., 2020).

7.3.1.6 *ZIKA infection*

In contrast to Influenza, ZIKV is capable of directly infecting the fetus inside the womb. Upon mild maternal infection of pregnant mice, the female offspring was found to have reduced basal dendrites in the hippocampus, while the males even displayed a reduction in both apical and basal dendrites in the hippocampus (Stanelle-Bertram et al., 2018). A study of maternal infection, where the infection was not found in the fetus two days post infection, still an increase in proinflammatory cytokines and a morphological change of Iba1+ immune cells in the brain was observed. The infection also lead to a change of connectivity between medial prefrontal cortex and ventral hippocampus and increased the repetitive self-grooming behavior (Ma et al., 2021). As mentioned earlier, in an in vitro model of human brain organoids and neurospheres, ZIKV was capable of infecting the neurons and lead to cell death and strongly reduced growth of the spheres (Garcez et al., 2016).

7.3.1.7 *Maternal immune activation (Poly(I:C) and LPS)*

As mentioned earlier, one of the main effects of maternal infection on the offspring is mediated by maternal immune activation. This immune activation is transferred to the offspring via cytokines and other mediators of the innate and adaptive immune response. As the innate immune response reacts to rather broad PAMPs instead of specific pathogens, this has been utilized to stimulate the maternal immune systems with the PAMPs, rather than with live pathogens. A viral infection can be recognized by double stranded RNA, a feature well mimicked by the synthetic substance Poly(I:C). The

corresponding bacterial patterns of the bacterial surface are the lipopolysaccharides (LPS) (Meyer, 2014). Prenatal treatment of mice with Poly(I:C) induces an autistic like behavior with a reduction in social, but an increase in repetitive behavior (Andoh et al., 2019). Also, prenatal treatment with LPS reduces the sociability, but increases the repetitive marble burying behavior in a mouse experiment and thereby reflects the human symptoms (Fernández de Cossío et al., 2017). After MIA with Poly(I:C) in mice, a change in gene expression in the fetus was detected. Genes for anti-viral molecules, response to interferon and chemokines were upregulated, while some genes for neuronal function, neurulation and neural development were among the most down-regulated gene (Baines et al., 2020). On the cellular level, MIA induces microglial activity. In rats, a prenatal LPS injection activates microglia and increases their phagocytotic activity against neuronal precursor cells. This subsequently leads to a reduced number of neuronal precursor cells in the neocortex (Cunningham et al., 2013). A well written overview about MIA and its consequences on development can be found in (Estes & McAllister, 2016).

7.3.1.8 *Interleukins*

Instead of eliciting a maternal immune activation and its cytokine secretion in a mouse model, a direct injection of cytokines into the dams was considered in some studies. Injection of the proinflammatory cytokine IL-6 in pregnant mice leads to behavioral changes in the offspring, also observed in other ASD models. In addition, they presented that co-administration of an anti-IL-6 antibody prevents the effect of MIA via Poly(I:C) on social deficits and gene expression of adult offspring (Smith et al., 2007). Another result of maternal IL-6 injection in mice is an increased neuronal precursor pool and impaired olfactory neurogenesis (Gallagher et al., 2013). In a mouse model of MIA, Poly(I:C) injected dams were pretreated with anti-IL17 antibodies. This rescued neuronal migration and behavioral phenotypes such as cortical patches after MIA, reduced sociability and increased repetitive behavior (Choi et al., 2016).

7.3.1.9 *Other factors*

Apart from primary immunological factors, there are also other contributors to an impaired neuronal development, which might act via mechanisms shared with the models of MIA.

When 2-4 week old mice were stressed by separation from their mother, their hippocampal microglia did not develop properly but lacked changes in cell density and gene expression patterns involved in inflammatory responses, normally developing hippocampal microglia present (Delpech et al., 2016). When pregnant rats were stressed by enforced swimming, it activated the offspring's microglia. In culture, these microglia expressed increased levels of CD40, a surface receptor required for their activation. In addition, IL-6 and other proinflammatory cytokines or their RNA was stronger expressed than in the control cultures of microglia (Ślusarczyk et al., 2015).

Prenatal valproic acid uptake was already mentioned above as a factor involved in human development of ASD. In mice, it elicits alternations in timing precision in behavior testing, a feature that is also known in some ASD patients in their estimation of interval timing (Acosta et al., 2018).

Maternal diabetes in mice, resulting in high oxidative stress due to hyperglycemia, leads to autism-like reduction of ultrasonic vocalizations and impaired behavior in sociability test-settings (Wang et al., 2019).

7.3.1.10 *In situ treatment*

Whenever animal experiments are performed one should always consider the 3R-principle. Replace animal experiments wherever possible with experiments not requiring animals or using animal which are considered to not being able to suffer, reduce the number of animals used for the experiments and refine the experiments in a way to cause less harm, stress and suffering for the animals involved (National center for the Replacement Refinement and Reduction of Animals in Research, n.d.; W.M.S. Russell & Burch, 1960). Slice cultures and acute slices of murine brains are a valuable model to close

the gap between a cell culture and the organism. Figure 3 depicts the process of preparing acute cortical slices as it was done for this thesis.

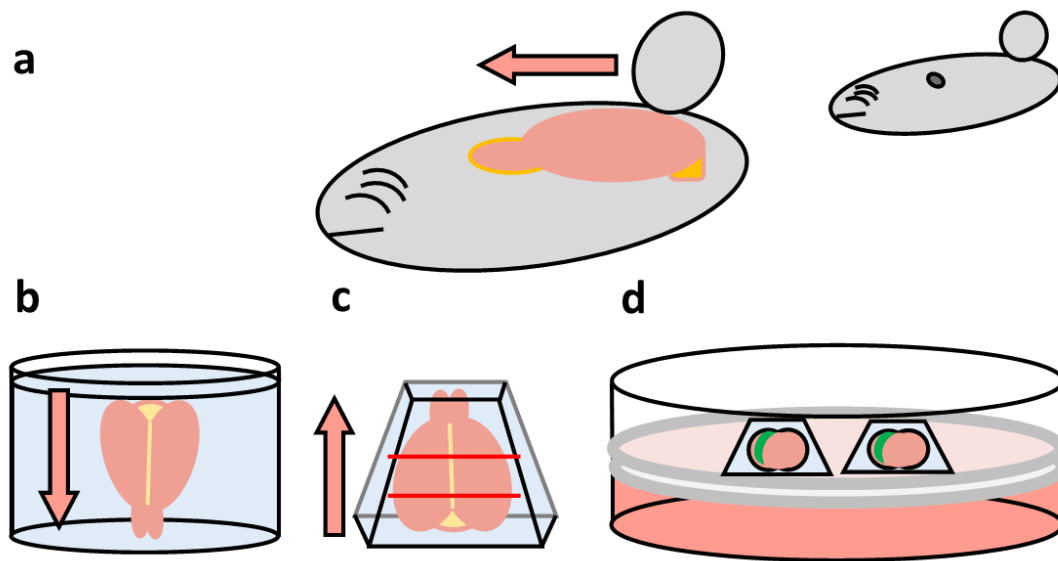


Figure 3: Acute cortical slice cultures

The murine brain is located in the murine skull with the olfactory bulb facing rostral (a and arrow). After taking it out of the skull, it is placed in the low melting agarose with the olfactory bulb facing downwards (b and arrow). When the agarose is solidified, an agarose block with the brain is carefully cut. Leftover agarose is trimmed in a slightly pyramidal shape following the brains anatomy, the olfactory bulb now facing upwards (c and arrow). At the vibratom, coronal brain slices of the somatosensory cortex are prepared (area roughly in between the red lines of c) and incubated on an insert in a culture dish with medium in the incubator (d, coronal brain slices with green transfected neurons on grey insert over red culture medium)

Experiments on the effect of LPS on synaptic stability have been performed in organotypic hippocampal cultures of mice. Here, IL1 β was identified as required for LPS induced activation of microglia and their destruction of synaptophysin. Microglia depletion or anti IL1 β antibody application prevented the LPS-induced presynaptic loss of synaptophysin (Sheppard et al., 2019).

8 Hypotheses

The emergence of Autism spectrum disorder is linked to known familiar or de novo genetic variations but also sporadic cases with presumably non-genetic contributions, such as maternal infection during pregnancy (Atladóttir et al., 2010; Brucato et al., 2017; Satterstrom et al., 2020). In ASD patients, the brain morphology has been found to be alternated in different ways, ranging from macrocephaly to impaired connectivity and “disorganized patches” in the neocortex (Bertero et al., 2018; Sacco et al., 2015; Stoner et al., 2014). Some neuronal impairments, such as changes in the gross brain morphology or cortical layering are also present in the experimental genetic model of the ASD-risk genes TAOK2 and 16p11.2 (Richter et al., 2018; Scharrenberg et al., 2022; Urresti et al., 2020). Also experimental models of maternal immune activation show impairments of neuronal and cortical development (Choi et al., 2016). Neuronal migration in the neocortex is one crucial part of neuronal development. Therefore, I want to find out how intrinsic and extrinsic insults, associated with ASD, influence neuronal migration. This further leads to the question of the molecular mechanisms affected by those insults, during neuronal migration, and if they can be addressed as a therapeutic target.

Within this thesis I want to test the following:

- To test whether neuronal migration is affected in mice which carry mutations in ASD-risk genes.
- Test if acute immune activation by Poly(I:C)- or LPS-treatment *in situ* in the developing cortex of mice during late embryonal development affects the migrating of neurons.
- Finally, test if maternal immune activation (MIA) by a viral infection or Poly(I:C)-injection in mice during early embryonal development affects the cortical layering.

Therefore, I examined the effects of intrinsic genetic and extrinsic immunological interventions on neuronal migration in the murine somatosensory cortex. As intrinsic factors, loss of 16p11.2 and human variants of TAOK2 represent the genetic contribution involved in the development of ASD in humans. For the extrinsic contribution, I applied two different approaches of immune activation, modeling an early maternal immune activation and a late embryonal cerebral immune activation, to cover a broader spectrum of extrinsic factors involved in the development of ASD in humans.

9 Methods

9.1 Contribution

The procedures described in the paragraphs 9.2.1.7, 9.2.1.8, 9.2.1.10 to 9.2.1.14 were mainly conducted by me.

The analyses described in 9.3 were conducted by me. The analyses for results 10.1 were partially conducted in collaboration with the authors mentioned.

The procedures described in 9.2.1.4, 9.2.1.5, 9.2.1.6, 9.2.1.9 were thankfully carried out entirely by others.

For the experiments described in results 10.1 and 10.3 I was provided with images named with a random number. I analyzed the experiments blinded to the conditions.

9.2 Preparation

Solutions

9.2.1.1 *Slicing and fixation*

9.2.1.1.1 Buffer

PBS: NaCl 137mM, KCl 2.7mM, Na₂HPO₄ 10mM KH₂PO₄ 1.8 mM.

Antibody buffer: PBS, 0.3% Triton X 100, 1% Donkey Serum.

Blocking buffer: PBS, 1% Donkey Serum.

Fixation solution

Brains and tissue were fixed in 4% PFA in PBS.

9.2.1.1.2 Slicing solution

Brains were sliced with the vibratome in PBS, ice cold.

9.2.1.1.3 Slice culture medium

Adapted from (Calderon de Anda, 2013): Neurobasal medium, 1x B27, 200mM Glutamine, 1x Peniciline/Streptomycine, 5% , 1x N2Horse serum

9.2.1.2 *Staining*

9.2.1.2.1 Lectin Dye

The dye solution was carefully pipetted into the slice culture medium carrying the cortical slice cultures on cell culture inserts to a final concentration of 5µg/mL. It was taken care that the time of the stock solution vial outside the refrigerator and not in the dark was limited to the possible minimum.

9.2.1.2.2 Antibodies

WAKO polyclonal rabbit anti Iba1 #019-19741 (1:1000), Abcam rat anti Ctip2 #18465 (1:100), Abcam rabbit anti SATB2 #ab34735 (1:100), Invitrogen Alexa 568 donkey anti rabbit #A10042 (1:300), Invitrogen Alexa 488 donkey anti rat # A21208 (1:300), Invitrogen Alexa 647 donkey anti rabbit # A31573.

9.2.1.2.3 Hoechst nuclear staining

Nuclei were visualized with Hoechst (Invitrogen, 33258; 1:10.000)

9.2.1.2.4 Mowiol mounting medium

Mowiol 4-88 powder was dissolved following the instructions. The solution was stored at -20°C in single use aliquots. Before use, aliquots were quickly thawed in ice, carefully mixed without creating bubbles and used with a cut-off tip due to the high viscosity of the solution.

9.2.1.3 Immune treatment

9.2.1.3.1 LPS

LPS powder was carefully mixed and dissolved following the instructions to a stock solution of 10ng/μL. The stock solution was split into single-use aliquots and stored at -20°C.

9.2.1.3.2 Poly(I:C)

Poly(I:C) powder was dissolved following the instructions to a stock solution of 5μg/μL. The stock solution was split into single use aliquots and stored at -20°C.

Animal work

9.2.1.4 Mouse Models

Mouse Models for the genetic approaches are described in (Scharrenberg et al., 2022).

9.2.1.5 In Utero Electroporation

In utero electroporation was conducted by qualified and licensed personnel. All procedures were done following the protocol described elsewhere (Richter et al., 2018). The procedure is approved by Tierversuchsantrag Bewilligungsnummer N109/2020 Behörde für Justiz und Verbraucherschutz, Freie und Hansestadt Hamburg.

9.2.1.6 Maternal immune activation

9.2.1.6.1 Poly(I:C) injection

Procedures were conducted as described elsewhere (Jacobsen et al., 2021). Embryonic brains were explanted at E17.5.

9.2.1.6.2 Influenza infection

Procedures were conducted as described elsewhere (Jacobsen et al., 2021). Embryonic brains were explanted at E17.5.

9.2.1.7 Preparation of murine organs

9.2.1.7.1 Preparation of embryos

The pregnant mouse was deeply anesthetized with Isoflurane and, after checking deep narcosis by pinching the paw, quickly decapitated. The abdomen was cut open and the uterus was exposed. The fetuses were taken out one after each other and quickly decapitated. The heads were placed in ice-cold PBS. After all heads have been transferred to the ice-cold PBS the brain preparation was performed.

9.2.1.7.2 Preparation of murine brain tissue

The head was held with forceps in the ocular cavities, ventral facing upwards. A miniature scissor was placed with the tip at the neck where the central nerve cord is exposed. Small cuts were made towards the ears at the bottom of the calotte. It was especially taken care to not penetrate the underlying brain with the scissors. The cuts were continued to the top of the ocular cavity crossing from one side to the other. Once the top of the calotte was loosened enough it was carefully flipped open with another pair of forceps. The brain stem was cut in between the skull and the brain to avoid any strain onto the tissue. The exposed brain was carefully taken out without touching the cortex and placed in a multi-well plate filled with ice-cold PBS.

9.2.1.8 Identification of transfected hemisphere

Where applicable, brains were swiftly moved with the multi-well dishes to a binocular fluorescent microscope. Using the fitting laser and filter set, the localization and efficiency of transfection of neurons was checked and rated.

9.2.1.9 Cryosectioning

Brains were fixed in a 4% PFA solution at 4°C overnight, followed by a 30 % sucrose PBS solution at 4°C overnight. After embedment in OCT, brain slices were cut using a cryostat and transferred to the microscope slides. The tissue was stained by immunohistochemistry (IHC) against cortical layer markers and imaged.

9.2.1.10 Preparation of acute slice cultures

Brains were sliced after mounting in an agarose block using a vibratome. All solutions, if not stated otherwise, were kept ice-cold. The method was adapted from a published protocol (Calderon de Anda, 2013). Freshly prepared brains were placed olfactory bulb first in 1% low melting agarose solution at 40°C. The brains were carefully swirled to remove any air bubbles attached to the tissue and dilute leftover buffer in the surrounding agarose solution. When all the remaining air bubbles had been taken away, the brains were placed in the initial position and the dish was placed on an ice-cold metal plate to support the solidification process of the agarose solution. Once the agarose was solidified, the brain was cut out of the agarose with some millimeters surrounding agarose left to stabilize the brain. The agarose block was placed and glued onto the sample dish of the vibratome. Brain slices were cut with a thickness of 240µm and placed on cell culture inserts submerged into cell culture medium. Four to six brain slices are to be placed on one insert. For pairwise comparison experiments, consecutive brain slices are to be placed on paired inserts marked accordingly. When all brain slices were collected, the inserts were placed in an incubator at 36°C 5% CO₂. Acute slice cultures are allowed to rest for 1-2 hours after cutting before treatment. See Figure 3 for illustration of the described preparation.

9.2.1.11 Treatment of slices

The quality of slice cultures was checked under the binocular microscope before any treatment. To be included in the experiments, the paired inserts per brain must carry comparably transfected and healthy-looking brain slices from comparable regions of the somatosensory cortex.

From the brains chosen to be included in an experiment, one of the inserts was randomly assigned to the treatment and the other one to the untreated control. The slices were treated by adding Poly(I:C) in PBS (final concentration 50µg/mL) or LPS in PBS (final concentration 100ng/mL) to the slice culture medium and mixing shortly by swirling around the medium and lifting the insert. The added volume for the treatment was below 2% of the total cell culture medium surrounding the insert and was not replaced in the control. The slices were left in the solution for up to 18h before imaging.

Imaging

9.2.1.12 Mounting

Cryostat tissue samples were collected with the slide directly from the cryostat and stained on slide. The vibratome sections were stained in a multi well chamber and afterwards transferred to the slide. Leftover buffer was carefully taken away without letting the slice run dry. Mounting solution was applied and the slices were covered by a cover glass. The mounting solution was left to harden at room temperature for 12-24 hours, long term storage was done at 4°C. Imaging was performed at least 24 hours past mounting.

9.2.1.13 Live imaging

The microscopes 1 and 2 (for details, see 14.1) were used for live imaging of cortical slices. The preparation procedures were comparable. The climate chamber surrounding the microscope stages was heated to 35°C and a constant CO₂ inflow was applied. Once the target parameters were reached, the chosen inserts were transferred from the incubator to the stage. Regions of interest were the transfected neurons in the developing cortex. Overview images covering the complete transfection area and the complete brain slice were taken. Afterwards coordinates for automated image acquisition

were chosen to cover the complete area of migration in the following live imaging. Live imaging was performed for 6-10 hours with one acquisition either every 20 or 30 minutes. Imaging was conducted either in parallel for the two conditions (microscope 1) or consecutively (microscope 2). Each acquisition consisted of the region of interest, covered by stitching, if necessary, in all z-layers that contained neurons. The step size between each z-layer was 5 μm . During live imaging disturbances were avoided by limiting access to the room.

9.2.1.14 *Imaging fixed tissue*

Fixed tissue mounted on slides were imaged on either one of the two microscopes. Overview images of the complete slice were taken in 4x or 10x magnification and stitched, if necessary. Overview images were acquired in the GFP, RFP, DAPI and brightfield channels. The regions of interest were the areas with transfected or stained cortical neurons. These regions were imaged in a higher magnification (10x-20x) and z-stacks of 5 μm . Stitching was done where necessary to cover the complete region of interest. The regions of interest were acquired in GFP, RFP and DAPI channels.

9.3 Analysis

Microglia

9.3.1.1 *Microglia fixed tissue*

9.3.1.1.1 Microglia morphology

To analyze the morphology of microglia, microscopic images of fixed cortical slices cultures were used. The ImageJ plugin Cell counter was chosen to track the position and classification of the microglia into three morphologies (“round”: no protrusions; “amoeboid”: roundish condensed soma with 1-4 short thick protrusions; “ramified”: more irregularly shaped than amoeboid with multiple thin and long protrusions) (Cunningham et al., 2013; Delpech et al., 2016; Rezaie & Male, 1999). The results data table from the plugin was saved as a csv file containing the running number of the tracked cells, the morphological classification, and the x- and y-coordinates of the tracked cell. I used a self-written RStudio script to analyze the obtained information from all the csv tables produced in this study. Each table was opened and the information about the classification and x- and y-coordinates were read out. The number and percental fraction of each morphological category was calculated. The data output was further analyzed in GraphPad Prism (GraphPad Software LLC, 2022).

9.3.1.1.2 Microglia localization

Microglia localization given by x- and y-coordinates were obtained from the morphological classification. For each analyzed image a corresponding csv file containing the x- and y-coordinates of the marginal zone was created using FIJI (Rasband, 2022) and the segmented line tool. The shortest distance of each microglia to the marginal zone was calculated using a personal RStudio script. The coordinates of the marginal zone and the microglia were read in, the distances among them were calculated and the shortest distance between each microglia and a point within the marginal zone was selected and saved. The factor of micron to pixel was applied to numerical values where required. The positions of microglia were plotted with the RStudio plugin “ggplot” differentiated by their classification.

9.3.1.2 *Microglia time lapses*

9.3.1.2.1 Microglia velocity

I used the red channel (568 nm) from the live time lapse images for the microglia velocity analysis in ImageJ. Where needed, filters were applied (Mask unsharp, enhance contrast to a fixed fraction of saturated pixels applied on all slices). The movement of microglia was tracked in z-stack images over the time course of imaging with the Trackmate tool in ImageJ (Rasband, 2022). Primary microglia spot

detection was performed with Laplacian of Gaussian (LoG) filter or via manual detection. No further filter was used. Further spots were added manually where microglia were missed out. Spots in the marginal zone were excluded and deleted due to a high density and overlap of cells. Spots on signals not from microglia but from blood vessels or a not identified source were also deleted. Linear Assignment Problem (LaP) Tracking was performed with 50 μm linking distance, 150 μm gap distance and 2 frames. Csv files were exported with tracking parameters. Total distance moved (sum of single steps in tracks) and number of frames in track were exported and quotient for distance moved per frame was calculated. These values were further statistically analyzed in GraphPad Prism (GraphPad Software LLC, 2022) and data was plotted.

9.3.1.2.2 Microglia movement activity

Actively moving microglia were defined by a velocity of more than 0.1 $\mu\text{m}/\text{min}$. The ratio of actively moving microglia to not moving microglia was calculated for all microglia combined.

Neurons

9.3.1.3 *Neurons fixed tissue*

9.3.1.3.1 Neuronal position

The position of neurons was analyzed in images of fixed cortical slice cultures post live imaging. Images were opened in ImageJ. Filters were applied where necessary (Unsharp mask radius between 1 and 10, mask weight 0.6). GFP signals of neurons were tracked with the point selection tool. All tracked points of one image were saved as ROIs in a zip file. In addition, the marginal zone was tracked with the segmented line tool and the coordinates of segmentations including start and end points were saved in a csv table. Using a personal RStudio script, the coordinates of neurons were extracted from the ROIs. The coordinates from the marginal zone were read out of the segmented line coordinates. The coordinates from the lines connecting the segments were calculated in steps of 1 pixel in y dimension. The distances between each neuron and all the coordinates of the marginal zone were calculated and the shortest distance for each neuron stored. The shortest distances from all neurons to the marginal zone were transferred to GraphPad Prism for further analysis.

9.3.1.3.2 Cortical layering

In the images from cryosectioned murine brains (see 9.2.1.9), the position of neurons relative to the marginal zone was tracked and analyzed like described above.

9.3.1.4 *Neurons live imaging*

9.3.1.4.1 Neuronal population migration

The position of neurons was tracked in the first and last frame of each time lapse as described above. The distances towards the marginal zone were calculated as described above. As the distribution of neurons differed strongly between the experiments, normalization was applied. The mean distance of neurons in the first frame was subtracted from the distances in the first and last frame. The resulting distribution is spread around $Y = 0$. Values below 0 represent neurons closer to the marginal zone than the average distance in frame 1, values above 0 represent neurons further away.

9.3.1.4.2 Polarity of neurons

In the above-described tracking of neuronal position in ImageJ with the point selection tool, two different groups of neurons were tracked. The bipolar neurons can be described as stretched with a protrusion on each side reaching away. The other group contains either a multipolar morphology with more than two protrusions or a round morphology with less than two protrusions. As a result, two zip files with ROIs per slice culture and frame were created and further analyzed in RStudio. The zip files with the coordinates of the neurons were read in the RStudio environment and the fraction of bipolar neurons in the complete population was calculated.

9.3.1.4.3 Bipolar ratio

For each experiment the ratio of bipolar to all neurons was calculated for the first and last frame of imaging. In addition, the change of the bipolar fraction was calculated. The results were plotted in GraphPad Prism (GraphPad Software LLC, 2022).

9.3.1.4.4 Bipolar Migration

The migration of bipolar neurons was tracked like the neuronal population migration.

9.3.1.4.5 Single neuron velocity

The time lapse series from the cortical slice cultures were opened in ImageJ. Maximum intensity projections were performed on the z-stacks. 5-10 radially migrating neurons were chosen from each series. The neurons had to be visible the entire time series and should show a dominantly radially migrating motion. The position of the neurons was tracked with the point selection tool and the ROIs of each neurons track was saved in a separate zip file. Using a personal script in RStudio the tracks were analyzed and the distances moved between each frame were calculated. The mean distance moved per 10 minutes imaging was calculated. In the next step the continuity of movement was analyzed. The distance moved between each frame was divided by the average distance moved between two frames in this time series. The number of movements larger than 2 times the average distance moved was stored and further analyzed in GraphPad Prism (GraphPad Software LLC, 2022).

10 Results

10.1 Neuronal migration and autism spectrum disorder related genetic variations

The effect of ASD-related human variants of TAOK2 on neuronal migration

TAOK2 is a gene highlighted as an ASD risk gene (<https://gene.sfari.org/database/human-gene/TAOK2>). Studies point towards an effect of mutations in TAOK2 on neuronal development (Richter et al., 2018). I analyzed how the introduction of ASD related human variants of TAOK2 into murine cortical neurons alter their radial migration. The two isoforms of TAOK2, alpha and beta, contain a kinase domain N-terminally and the regulatory domain C-terminally (Richter et al., 2018). The *de novo* patient mutation A135P is in the kinase domain and reduces the kinase activity. The mutation A335V is in the linker in between the kinase and regulatory domain. The mutation P1022* translates into a stop codon and leads to a disruption inside the regulatory domain. Figure 4 displays the effects of the above-mentioned human variants on neuronal migration. Overexpression of TAOK2 α wild type led to a significant reduction of the median distance of neurons to the marginal zone, compared to the control neurons. The variants TAOK2 α A135P and TAOK2 α A335V on the other hand led to a significant increase in the median distance of neurons to the marginal zone because of impaired migration. Interestingly, the impaired migration was not observed after transfection with the TAOK2 β variants A135P, A335V or P1022*. On the contrary, the overexpression of the TAOK2 β -WT isoform led to a small but significant increase in migration and therefore reduction in the median distance of neurons to the marginal zone. The position of neurons in the single brains is displayed in Supplementary Figure 1.

The effect of mutations in the ASD susceptible region 16p11.2 on neuronal migration

TAOK2 is located in the ASD risk region 16p11.2. This region is known for copy number variations and mutations in 16p11.2 can lead to NDD and ASD. Therefore, this region provides a well-suited platform to analyze the intrinsic factors perturbing neuronal migration. As I demonstrated in Figure 4 (published in (Scharrenberg et al., 2022)), expression of human variants of TAOK2 α influences neuronal migration. Furthermore, it was shown that neuronal migration is impaired in mice carrying the 16p11.2 del Het genotype compared to wildtype controls (Scharrenberg et al., 2022). I then analyzed if TAOK2 α can recover the effects of a heterozygous deletion of 16p11.2. Figure 5 shows the distribution of neurons following transfection of a control plasmid, TAOK2 α WT or TAOK2 α A135P in cortical neurons of 16p11.2 del Het mice (as published in (Scharrenberg et al., 2022)). A reduction of the median distance of neurons to the marginal zone after transfection of TAOK2 α WT compared to the control transfected neurons is observed. This indicates that expression of TAOK2 α WT rescues the migration-phenotype of 16p11.2 del Het mice. The TAOK2 α A135P mutation on the other hand did not rescue the impaired neuronal migration in the 16p11.2 del Het model. The neuronal migration in single slices can be found in Supplementary Figure 2.

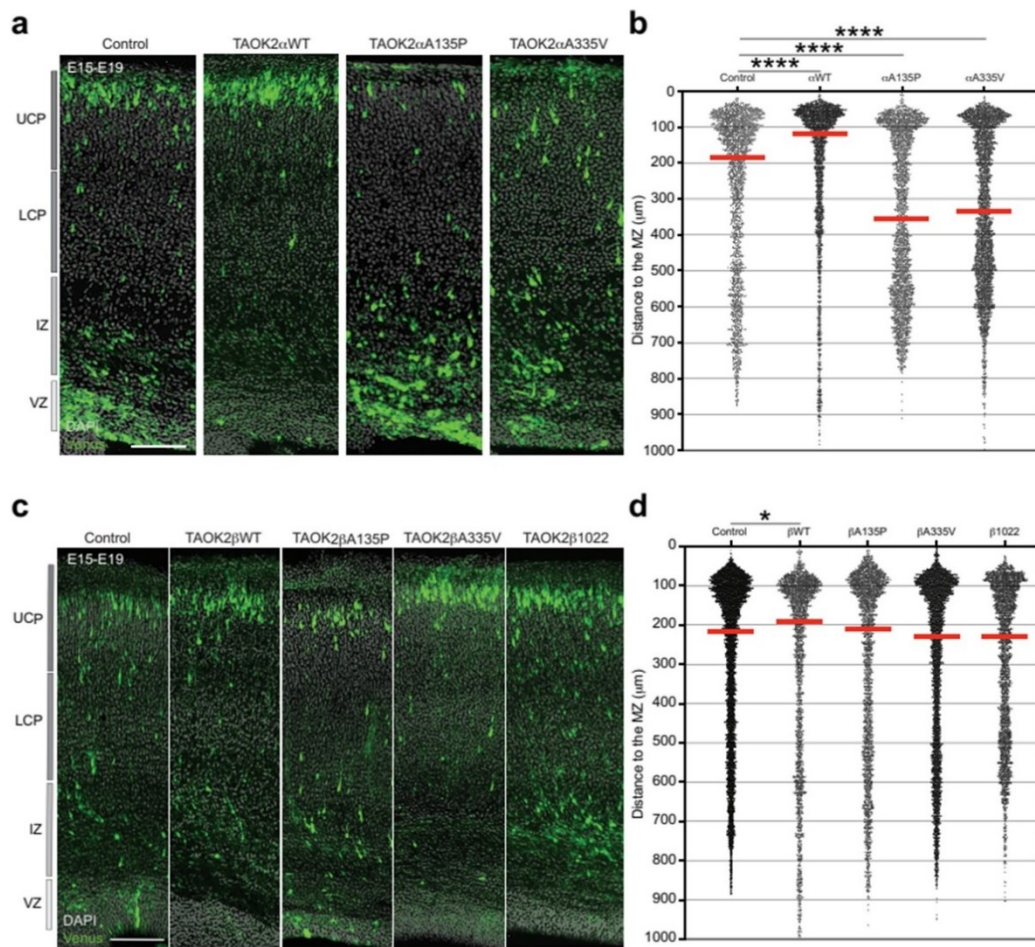


Figure 4: Human variants of TAOK2 affect neuronal migration in mice. (Scharrenberg et al., 2022)

10.1.1.1 Figure 4: Human variants of TAOK2 affect neuronal migration in mice.

Neuronal migration in the developing cortex is impaired in ASD-associated human variants of TAOK2 α but not of TAOK2 β . b. Overexpression of TAOK2 α WT led to a decrease in the median distance of transfected neurons to the marginal zone, while overexpression of human variants TAOK2 α A135P and TAOK2 α A335V led to an increase in the distance of neurons (One-way ANOVA $p < 0.0001$, post hoc Dunnett's multiple test $p < 0.0001$; Number of brains used: control, TAOK2 α WT = 3 brains; human variants = 4 brains; red line depicts median distance). d) TAOK2 β WT also leads to minor reduction in the distance of neurons towards the marginal zone, but TAOK2 β A135P, TAOK2 β A335V and TAOK2 β 1022 do not have a significant effect on the migration of neurons (One-way ANOVA $p = 0.0002$, post hoc Dunnett's multiple test: Control vs TAOK2 β WT $p = 0.0138$; Number of brains used: control = 5 brains; TAOK2 β WT and variants = 4 brains; red line depicts median distance). Bar is scaled to 200 μ m. In collaboration with M Richter, R Scharrenberg and FC de Anda (Scharrenberg et al., 2022).

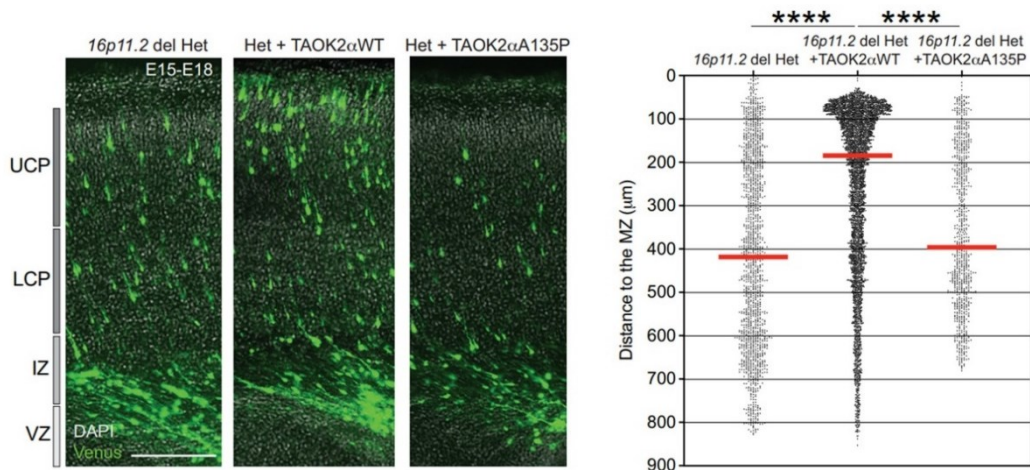


Figure 5: Neuronal migration is impaired in Het 16p11.2 deletion and recovered by TAOK2.

10.1.1.2 Figure 5: Neuronal migration is impaired in Het 16p11.2 deletion and recovered by TAOK2.

Neuronal migration in the developing cortex of mice is impaired in the 16p11.2 del Het mouse model and can be rescued by TAOK2 α WT but not by the human variant TAOK2 α A135P. The distances of neurons in the 16p11.2 del Het mouse model transfected with the control plasmid or the TAOK2 α A135P human variant are increased compared to neurons in this model transfected with TAOK2 α WT (One-way ANOVA $p < 0.0001$, post hoc Dunnett's multiple test between the control or TAOK2 α A135P and TAOK2 α WT $p < 0.0001$; Number of brains transfected with: control = 4, TAOK2 α A135P = 3, TAOK2 α WT = 6; red line depicts median distance. In collaboration with M Richter, R Scharrenberg and FC de Anda (Scharrenberg et al., 2022).

10.2 Neuronal migration and immune perturbations in situ

Neuronal development starts during the prenatal period. During this time the embryo is not isolated but connected to the mother by the umbilical cord. This allows not only for transmission of nutrients but also transmission of cytokines, infections and other potentially harmful substances. I analyzed the effect of LPS and Poly(I:C) treatment on neuronal migration in cortical slice cultures. This in situ model is a possibility to examine the effect of external factors on neuronal migration. In the following paragraphs I present results from three different characteristics in neuronal migration: The position, the neurons reach at the end of this experiment; the change of position relative to the marginal zone, the whole population of transfected neurons covers within this experiment; and finally, the speed selected neurons migrate with. Additionally, I analyzed how microglia are affected in their migration and morphology by the different treatments.

The effect of LPS and Poly(I:C) treatment in situ on neuronal positioning

Neuronal migration takes place over the time course of several days. I therefore treated the slice cultures with an agent mimicking the presence of either bacteria or viruses for several hours and analyzed the position of neurons after 24 to 36 hours. I compared the radial migration of neurons towards the marginal zone in the treated brain slices with the neurons in the control slices from the same brain. Figure 6 shows the distances of neurons to the marginal zone relative to the neurons in the control slices. There is no clear effect of the LPS treatment on the migration of neurons detectable.

The distance of all neurons treated with LPS taken together does not differ from the control neurons. The differentiation into mean distances per experiment displays the different effects LPS had in the different experiments. Eventually these effects cancel each other out. On the other hand, there is an effect in the Poly(I:C) treated slices detectable. Both, the summation of all Poly(I:C) treated neurons and the mean distances of neurons treated compared with the controls exhibit an increase in distance towards the marginal zone. This can be translated to a reduction in migration.

This in situ model of cortical brain slices consists in principle of all cell types present in the corresponding regions in the murine brain. The treatment with Poly(I:C) and LPS therefore not only acts on the migrating neurons, but also on the present immune cells. I focused on the analysis of microglia, as described in Supplementary Figure 3 and Supplementary Figure 4. In the fixed tissue, I was able to identify three distinguishable phenotypes and the localization of microglia relative to the marginal zone. Examples of these morphologies can be found in Supplementary Figure 3e. As described in Supplementary Figure 3, in the LPS treated experiments was a significant higher proportion of round microglia than in the control slices. While the fraction of amoeboid microglia was indifferently changed, the LPS treated experiments also presented a clear and significant reduction of the ramified shaped microglia fraction. The Poly(I:C) treated experiments also presented a clear but not significant trend towards a higher fraction of round microglia compared with the control experiments. But, different than in the LPS experiments, only three out of four experiments showed a reduction of ramified microglia fraction compared with the control experiments. I analyzed the position of microglia as the distance to the marginal zone. Because of the high dispersion of distances (Supplementary Figure 4), I decided to standardize all values within each experiment (see Supplementary Figure 5 a and b). I subtracted the mean distance of the control microglia and divided it by the standard deviation of the control values. The resulting graph presents the distances of microglia to the marginal zone relative to the mean distance of the control microglia. The distances of all microglia treated with LPS combined did not show a significant change compared with the control microglia. The distances to the marginal zone of microglia treated with Poly(I:C) are significantly reduced compared with the distances of control microglia. The distribution of microglia in their specific phenotype can be seen in Supplementary Figure 4. An interesting observation can be made from Supplementary Figure 5 where the distances of microglia and the distances of neurons, normalized by subtracting the mean distance of the control slices, are shown. The position of treated microglia and neurons more proximal or distal to the marginal zone compared to their untreated controls occurs to be contrary to each other in most experiments.

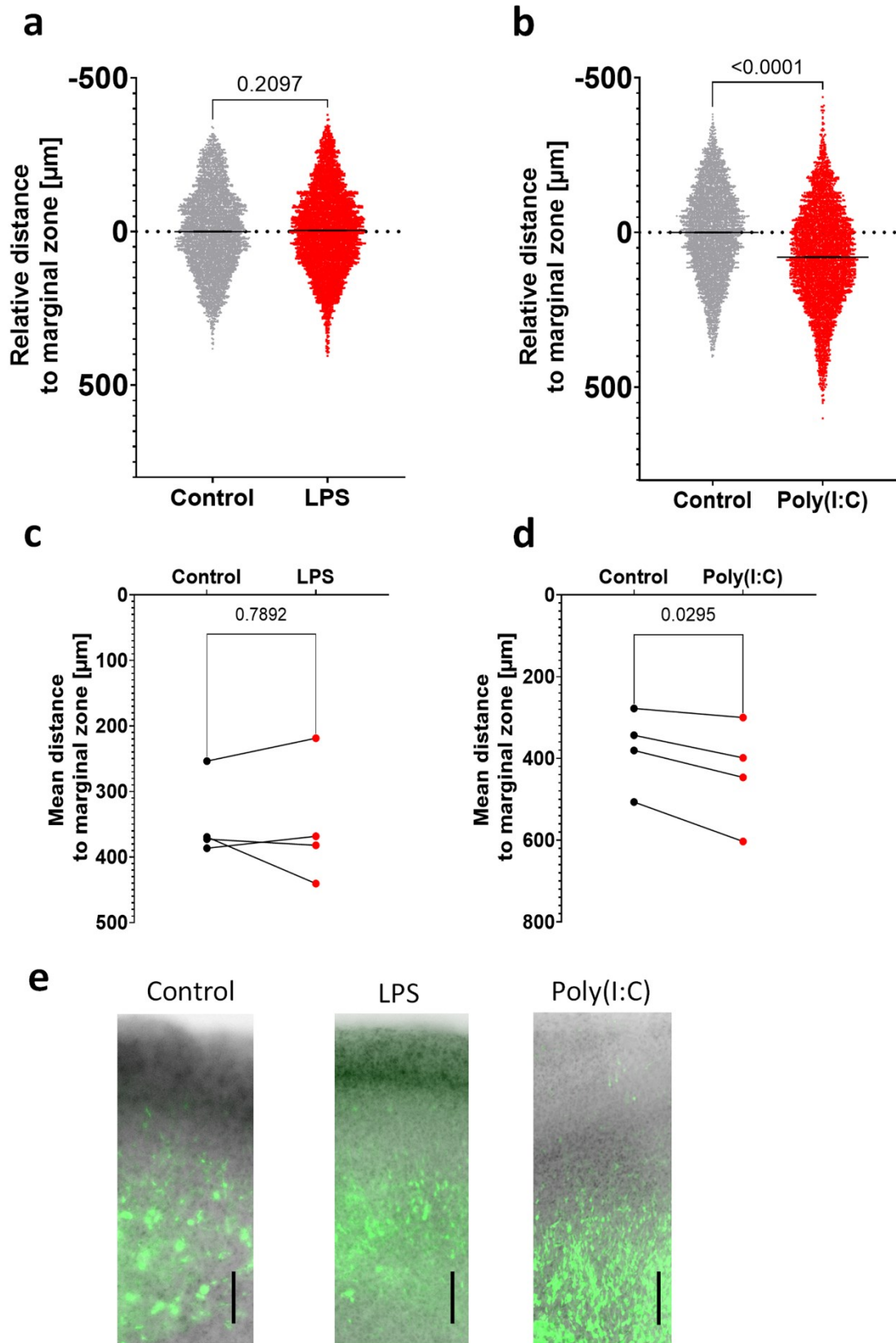


Figure 6: Immune treatment affecting the position of neurons after migration.

10.2.1.1 Figure 6: Immune treatment affecting the position of neurons after migration.

Murine embryonic cortical neuronal progenitors were transfected at E15 with the fluorophore venus. At E17 cortical brain slices were prepared and half of the slices of each brain were treated with either LPS or poly(I:C) or left untreated as control. Panels a (LPS) and b (Poly(I:C)) show the position of neurons in μm distance to the marginal zone, relative to the mean distance of neurons in the control slices of that experiment. A smaller distance compared to the control reference returns a negative value, a larger distance returns a positive value. The distance of Poly(I:C) treated neurons is significantly increased (b: unpaired t test, P value <0.0001 , ctrl N: 4003, ctrl mean \pm Std Error of mean: 0 ± 2.26 , Poly(I:C) N: 4233, Poly(I:C) mean \pm Std Error of mean: 79.69 ± 2.436) but not the LPS treated neurons (a: unpaired t test, P value 0.2097, ctrl N:3966, ctrl mean \pm Std Error of mean: 0 ± 2.129 , LPS N: 4617, LPS mean \pm Std Error of mean: -3.644 ± 1.975). The panels c (LPS) and d (Poly(I:C)) show the mean distance of all neurons per experiment and condition, paired by experiment. The distances between ctrl and LPS do not differ significantly (c: paired t test, P value 0.7892, two tailed, 4 pairs). The distances of neurons treated with Poly(I:C) are significantly increased compared to the control neurons (d: paired t test, P value 0.0295, two tailed, 4 pairs). Panel e shows three example images of fixed slices after treatment with LPS, Poly(I:C) or untreated neurons (green: Neurons, grey: DAPI., scale bar $100\mu\text{m}$).

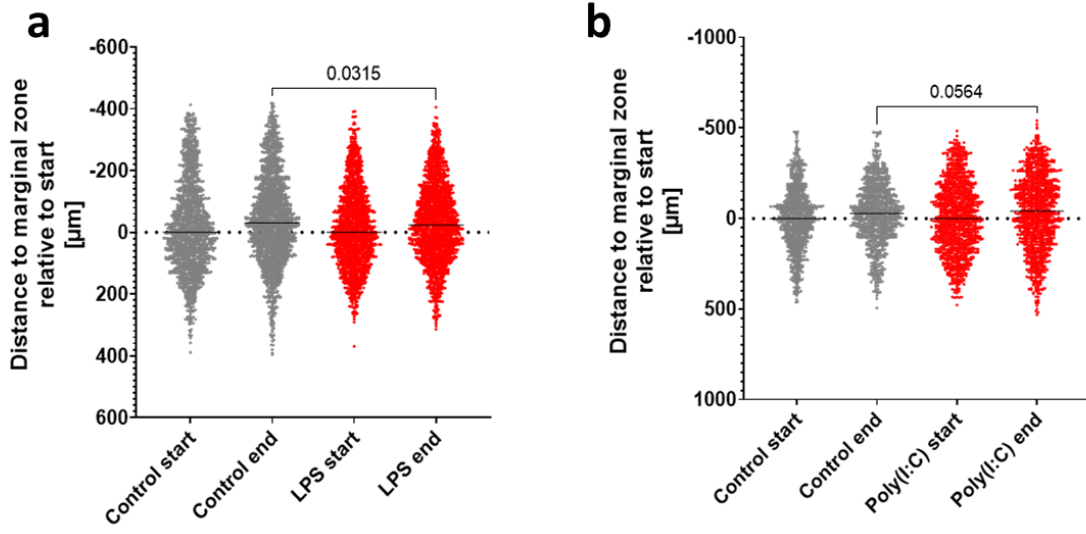
The effect of LPS and Poly(I:C) treatment *in situ* on neuronal migration and bipolarity
To directly analyze neuronal migration upon MIA, I tracked the position of neurons *in situ* with live imaging. The morphology of neurons changes between distinctive phenotypes during their radial migration. Between the round progenitors and the multipolar connected neurons in their respective cortical layer, the neurons have a bipolar morphology during their migration. I therefore differentiated in my migration analysis between specifically the bipolar neurons and all neurons. Figure 7 shows the migration of neurons to the marginal zone, comparing the distance at the start and end of imaging. The distance covered during migration was significantly reduced for the complete population of neurons after treatment with LPS but was not when only the bipolar neurons were analyzed (Figure 7a and c). After treatment with Poly(I:C), only the migrated distance of bipolar population was affected but not when the complete population was analyzed (Figure 7b and d). The bipolar fraction of all neurons was significantly lower in LPS treated neurons compared to their control slices while the fraction was not significantly changed in the Poly(I:C) condition. Figure 7g shows example images of neurons at the start (red) and at the end (green) after 8-10h of imaging. The dashed line indicates the outer border of the marginal zone as the end of the slice and direction of migration.

The detailed distribution of neurons per experiment can be found in Supplementary Figure 6 for Poly(I:C) and Supplementary Figure 7 and Supplementary Figure 8 for LPS experiments. The raw positions of neurons treated with LPS, Poly(I:C) and control neurons combined per condition can be found in Supplementary Figure 9.

10.2.1.2 Figure 7: Migration of neuronal populations in live imaging.

The panels a (LPS) and b (Poly(I:C)) show the distance of treated and untreated neurons to the marginal zone at the beginning and at the end of the live imaging (duration between 8 and 10 hours, identical within each experiment). The distances of untreated control and treated neurons are normalized by subtracting for each condition the median distance of the neurons at the beginning of imaging from all neurons of this condition for both time points. Negative distances are more proximal to the marginal zone than the median distance at the beginning, positive values are more distal than the median distance at the beginning of imaging. The distance of LPS treated neurons to the marginal zone is significantly increased at the end of imaging compared to the untreated neurons, while the distance for Poly(I:C) treated neurons is not significantly altered (a LPS: Mann Whitney test, median distance control neurons at the end of imaging: $-30.96\mu\text{m}$, N:1709; Median distance of LPS treated neurons at the end of imaging: $-22.84\mu\text{m}$, N:1685, approximate P value 0.315; b Poly(I:C): Mann Whitney test, median distance of control neurons at the end of imaging: $-28.83\mu\text{m}$, N: 906; median distance of Poly(I:C) treated neurons at the end of imaging: $-41.35\mu\text{m}$, N:1104, approximate P value 0.0564). The panels c and d only take the bipolar fraction of neurons from a and b into account. LPS treated bipolar neurons did not change their distance to the marginal zone between start and end of imaging significantly different than their untreated bipolar controls. Treatment with Poly(I:C) lead to a significant reduction of distance migrated towards the marginal zone compared to their untreated bipolar control neurons. (c LPS: Mann Whitney test, median distance of bipolar control neurons at the end of imaging: $-29.46\mu\text{m}$ N:1519; median distance of LPS treated bipolar neurons at the end of imaging: $-24.37\mu\text{m}$, N: 1334, approximate P value 0.1541; d Poly(I:C): Mann Whitney test: median distance of bipolar control neurons at the end of imaging: $-71.40\mu\text{m}$, N: 659; median distance of Poly(I:C) treated bipolar neurons: $-43.13\mu\text{m}$, N: 730, approximate P value 0.0047). The neurons treated with LPS do display a significantly lower fraction of bipolar neurons at the end of live imaging, compared with the control neurons (e: two-tailed paired t test, 4 pairs, mean fraction within each experiment and condition analyzed, P value 0.0488). The fraction of bipolar neurons in the Poly(I:C) treated slices does not significantly differ from the controls (f: two-tailed paired t test, 4 pairs, P value 0.1768). The panel g shows the position of neurons in LPS treated (left) and Poly(I:C) treated slices (right) in red at timepoint $t_1=0\text{h}$ and in green at timepoint $t_2=10\text{h}$, the scale bar is $100\mu\text{m}$. The signal in both channels is adjusted for illustrative reasons to reduce background signal.

Complete neuronal population



Bipolar neuronal population

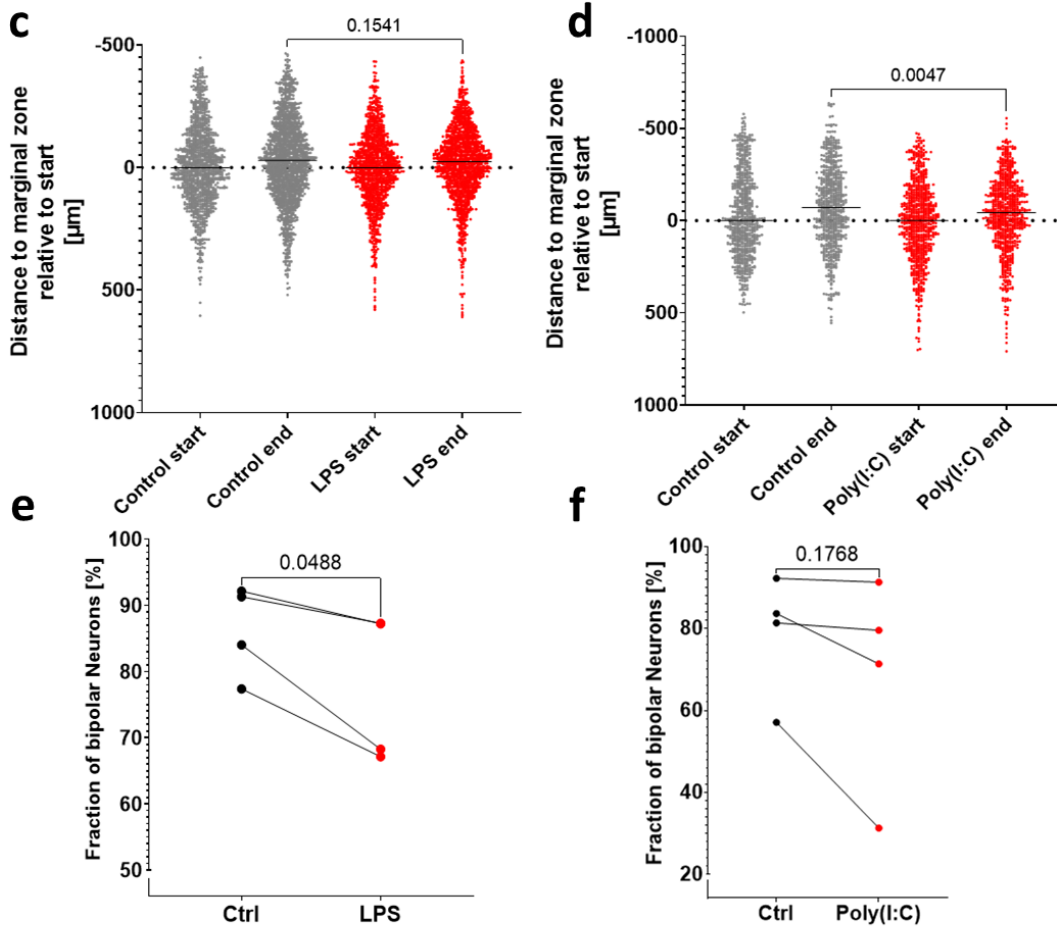
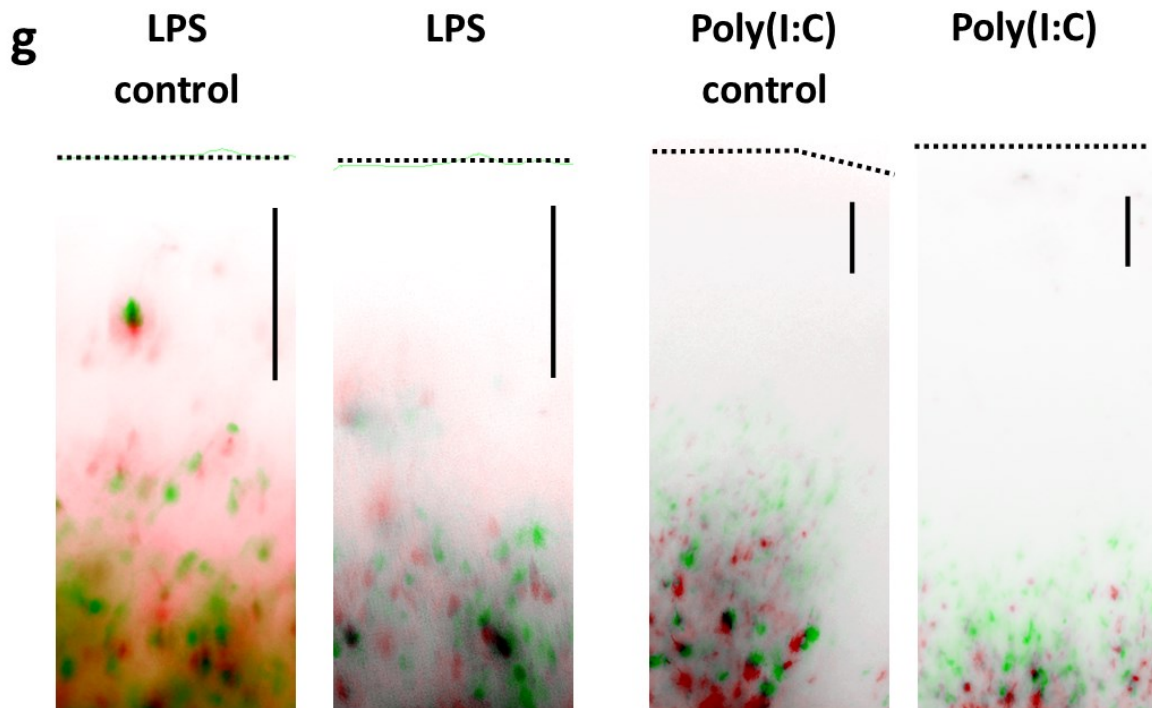


Figure 7: Migration of neuronal populations in live imaging.

(continuation)



Red neurons = Start of live imaging at 0h

Green neurons = End of live imaging at 10h

Dashed line indicates meningeal border of cortical slice

The effect of LPS and Poly(I:C) treatment in situ on single neuron velocity

I then analyzed the velocity of single neurons during their radial migration. This is characterized by a dominantly straight radial movement towards the marginal zone. Figure 8 a depicts the mean velocity in treated or untreated neurons during the time lapse. There was no significant difference between the velocity of treated and untreated neurons. Examples of migrating neurons either treated with Poly(I:C) or as a control can be seen in b, with an interval of 30 minutes in between red and green and green and blue, respectively.

The saltatory radial migration of neurons is characterized by a stationary phase of the nucleus while the soma reaches out towards the marginal zone and leaping movements of nucleokinesis where the nucleus is pulled towards the target zone. Within the limited points of observations (one image every 20 to 30 minutes for up to 10 hours) I tracked the different velocities neurons migrate with. I approached the analysis of the regularity of migration by calculating the number of frames in which the neuron migrated with more than twice the average migration velocity of that neuron. The number of these events are display in the part c and d of Figure 8. The Poly(I:C) treated neurons have a modulus of three events of higher velocity movements during their migration, while the corresponding control distribution has a modulus of two events. The experiments with LPS treated neurons are more evenly distributed and do not differ strongly from control neurons. Also, the regularity of migration with regards to the mean velocity was not significantly different between the treated and untreated neurons for either treatment. The detailed distributions of neuronal velocity and saltatory movements per experiment can be found in Supplementary Figure 10.

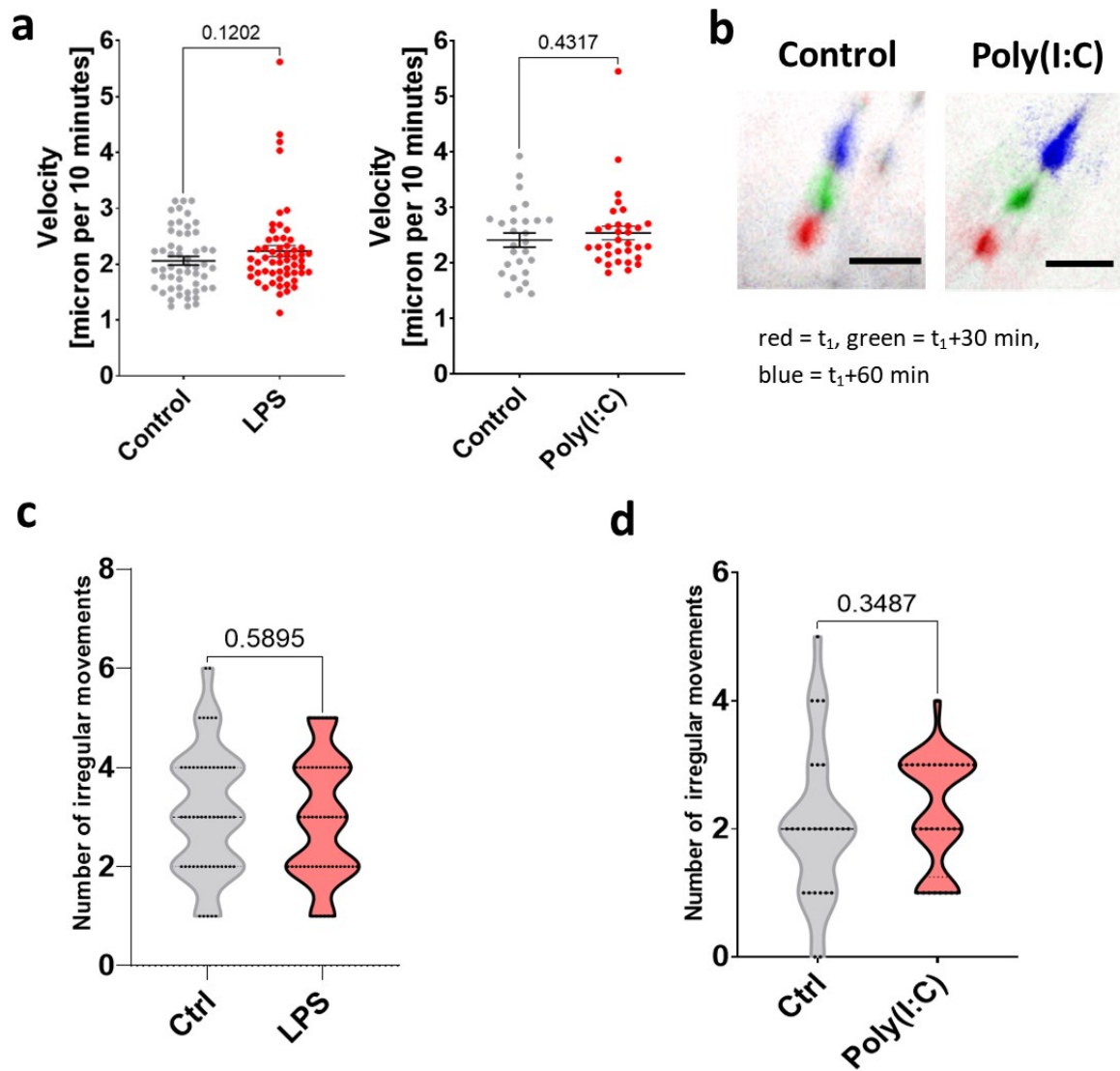


Figure 8: Single neuron velocity and mode of migration.

10.2.1.3 Figure 8: Single neuron velocity and mode of migration.

The position of radially migrating GFP-expressing cortical neurons were tracked during the complete course of live imaging. The panels in a display the velocity of these neurons, left for LPS treatments, right for Poly(I:C). Examples for the migration of neurons in three consecutive frames with 30 minutes in between can be found at b (red = t_1 , green = t_1+30 min, blue = t_1+60 min, scale bar of $25\mu\text{m}$, intensity adjusted for illustrative reasons to reduce background signal). The velocity does not differ in LPS- (Kolmogorov-Smirnov test, P value: 0.1202) or Poly(I:C)- (Kolmogorov-Smirnov test, P value: 0.4317) treated neurons significantly from their control neurons. The saltatory movement of migrating neurons results in a change of velocity over time. Panels c (LPS) and d (Poly(I:C)) display the number of steps each neuron moved with a velocity more than two times the mean velocity of that neuron. No significant changes in the number of irregular movements were recorded for either of the two treatments (c: LPS vs. ctrl: $p=0.5895$, Number of cells tracked: LPS=57, control=54; d: Mann Whitney test: Poly(I:C) vs ctrl: $p=0.3487$, Number of cells tracked: Poly(I:C)=32, control=27).

Microglia constantly scan their surroundings for potential threats with their elongated processes and by actively migrating through the cortex. In the live imaging time lapses, I analyzed this microglia migration by tracking the position of microglia each frame and linking the most likely connections

between consecutive frames. Supplementary Figure 4c and d present the velocity of microglia after different treatments. The velocity of microglia ranged from nearly stationary with around $1\mu\text{m}/10$ minutes observation time to highly motile tracks of $15\mu\text{m}/10$ minutes observation time. There was no significant difference between Poly(I:C) treated and control microglia. The velocities of LPS treated microglia also do have a distribution comparable to the controls' but are slightly shifted to higher velocities with a median velocity of LPS treated microglia of $0.8946\ \mu\text{m}/10$ min and control microglia with a median velocity of $0.726\ \mu\text{m}/10$ min. This leads to a significant difference in the overall velocity distribution. The detailed distribution of microglia velocity can be found in Supplementary Figure 11.

10.3 Neuronal migration and maternal immune activation

The way internal and external factors impair neuronal migration is not answered in full yet. The above-described cortical slice culture exemplifies a partly controlled model of immunogen substances affecting neuronal migration in situ. In vivo, the pathogen is sometimes acting directly on the fetal neurons, but foremost it is the mother being affected. While some pathological substances and pathogens are transferred to the fetus via the placenta, for others it is the transferred maternal immune reaction that is thought to have an impact on the fetus. In the following paragraph I examined the effect of maternal immune activation on the cortical layering in vivo.

The effect of maternal immune activation on neuronal migration

The cortical architecture consists of several distinct layers of neurons. They can be discriminated by either the timepoint they migrate into the specific layer or by molecular markers distinct for their layer. Distortions in these layers can lead to impairments of neuronal connectivity and function. I analyzed the position of Ctip2- and Satb2-positive neurons in mice, who experience maternal immune activation by maternal influenza infection (H1N1) or Poly(I:C) injection during pregnancy. Representative slices showing the staining specific for the respective layers can be seen in Figure 9a. Figure 9b displays the distances of neurons to the marginal zone marked by either Ctip2 or Satb2 staining. There is a significant difference in distribution between the Ctip2-positive neurons of offspring from both H1N1 and Poly(I:C) affected mothers compared with offspring from control mothers, as seen in part b for all Ctip2 neurons combined. The distance of neurons from offspring of H1N1 infected mothers do have the strongest increase compared to the controls, while the Poly(I:C) infected mothers' offspring displays an intermediate effect. As shown in Figure 9d, the mean distances per brain do not differ significantly. The Satb2-positive neurons also differ significantly between the three groups in the comparison of all neurons (Figure 9c). This difference is not on a significant level, when only the mean distances of the brains are compared, as done in e. The distance distributions per brain are displayed in Supplementary Figure 12. It can be observed that in the distance distributions for both markers in the control animals, the males from a litter (see naming) have an increased distance to the marginal zone compared with the females. For the influenza group two out of three males have an increased distance compared to their female littermates. For the Poly(I:C) treated group two out of three holds true for Satb2 while in Ctip2 it is only one male brain with neurons displaying a higher mean distance to the marginal zone compared with the female littermates. Supplementary Figure 13 displays the frequency distribution of distances to the marginal zone of Ctip2-positive neurons with the respective treatment of their mothers. Part b displays the differential histograms. Bars to the left mean a higher percentage of neurons in the control samples, bars to the right are caused by a higher fraction of neurons in the treated samples. The control outnumbers the H1N1 samples in the distances closest to the marginal zone (top bars) and have a tipping point at the $250\ \mu\text{m}$ bin ($225\text{-}275\mu\text{m}$ distance to the marginal zone). The Poly(I:C) treated experiments display a more complex differential distribution.

The fraction of neurons in the top $150\mu\text{m}$ bins is slightly higher in the Poly(I:C)-treated samples than in the controls. In the bins $200\text{-}250\mu\text{m}$ away from the marginal zone, the fraction of neurons is higher in

the control samples than in the Poly(I:C)-treated samples. This difference is larger than the one in the top 150 μ m and highlights a slightly larger fraction of neurons in the top 250 μ m in the control samples than in the Poly(I:C)-treated samples. In the lowest bins (400-500 μ m distance to the marginal zone), the fraction of neurons present is higher in the samples treated with Poly(I:C) than in the control samples. Taken together, this leads to the small but significantly larger distance to the marginal zone of neurons in the Poly(I:C)-treated samples compared to neurons in the control samples presented in Figure 9.

The Satb2 frequency distribution can be seen in Supplementary Figure 14. Both treatments lead to a reduced fraction of neurons in most of the bins covering the first 250 μ m, when compared to the control sample. In the following bins (300-450 μ m), the percentage of neurons is higher in the treated samples than in the control samples. The distribution of the most distant neurons does only differ slightly between treated and control animals.

9

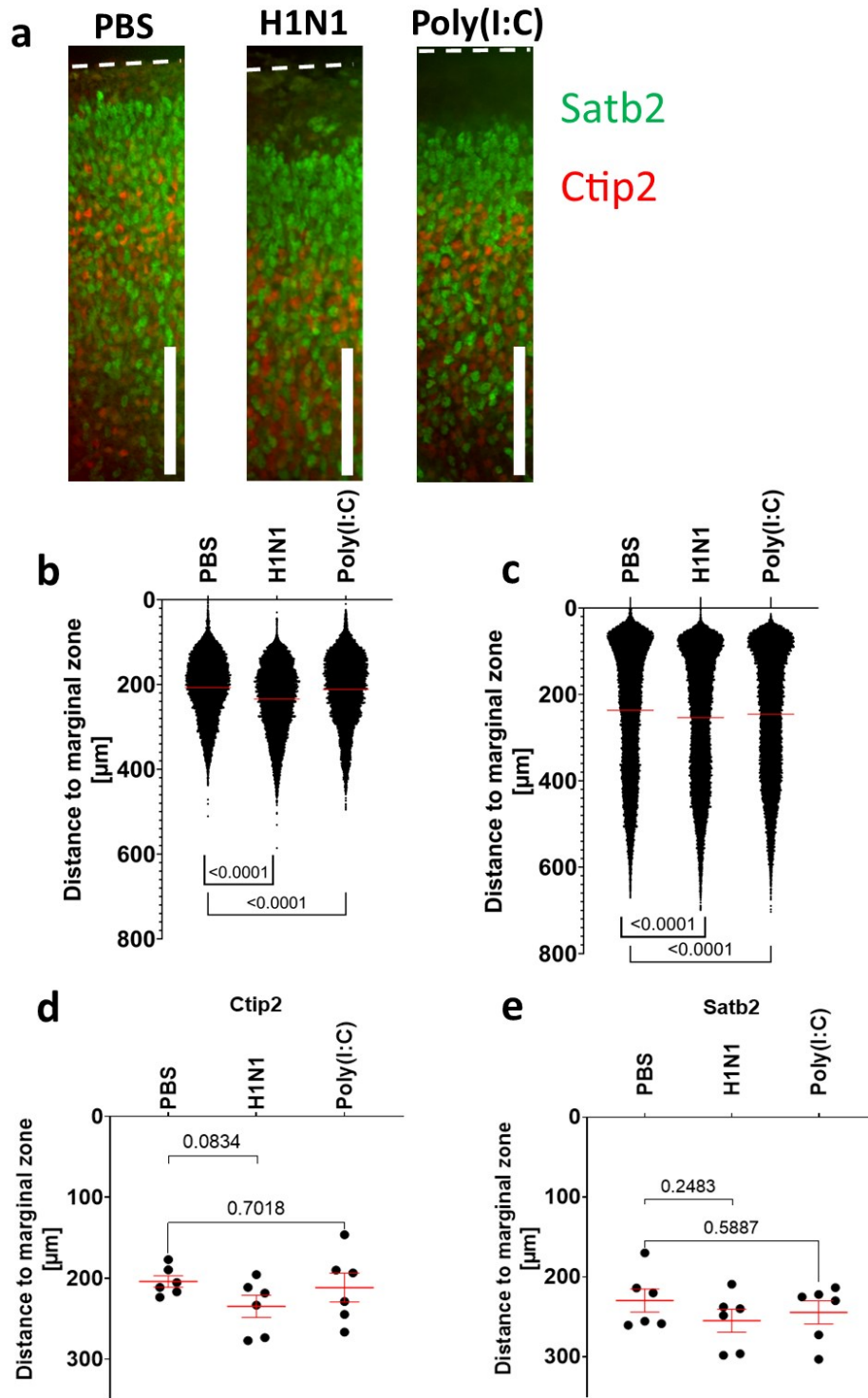


Figure 9: Cortical layering after maternal immune activation.

10.3.1.1 *Figure 9: Cortical layering after maternal immune activation.*

Pregnant mice were treated with either a H1N1 infection or a Poly(I:C) injection at e5.5. Their offsprings neuron were stained for the lamination markers *ctip2* and *satb2* in cortical slices of E17 brains. a) Examples of cortical layering in offspring of (from left to right) H1N1-, PBS and Poly(I:C) treated mothers. *Ctip2* positive neurons in red and *Satb2* positive neurons in green, scale bar at 100 μ m. b) The distribution of *Ctip2* positive neurons differed significantly among all three conditions (Welch's t test of mean distances to marginal zone: PBS: 207.1 μ m, N: 15592, H1N1: 234.2 μ m, N: 18020, Poly(I:C): 211.5 μ m, N: 13578; treatments compared to PBS both two-tailed P value < 0.0001;). c) Also the distribution of *Satb2* positive neurons was significantly different among the three maternal treatments (Welch's t test of mean distances to marginal zone: PBS: 236.7 μ m, N: 28437, H1N1: 253.6 μ m, N: 29090, Poly(I:C): 245.8 μ m, N: 24234; treatments compare to PBS with both two-tailed P value > 0.0001). d) The mean distance of neurons per brain in *ctip2* positive neurons did not differ significantly among the three conditions (Welch's t test of the mean distance to the marginal zone: PBS: 203.9 μ m, N: 6, H1N1: 234.8 μ m, N: 6, two tailed P value 0.0834; PBS to Poly(I:C): 211.6 μ m, N: 6, two-tailed P value 0.7018). e) The same holds true for the mean distance per brain of *satb2* positive neurons (Welch's t test of the mean distance to the marginal zone: PBS: 229.7 μ m, N: 6, H1N1: 254.9 μ m, N: 6, two-teailed P value 0.2483; Mann Whitney test between the median distances of the conditions PBS: 237.7 μ m, N: 6 and Poly(I:C): 227.4 μ m, N: 6, two tailed exact P value 0.5887).

11 Discussion

11.1 Genetic intrinsic factor

In this thesis I describe the effects of intrinsic and extrinsic ASD-risk factors on neuronal migration. The overexpression of ASD-risk gene *TAOK2α*'s patient derived variants in cortical neurons of mice resulted in their position being more distal to the marginal zone than neurons transfected with either *TAOK2α* wildtype or the fluorophore Venus as a control. Differently, the transfection of *TAOK2β* wildtype did result in neurons being slightly more proximal to the marginal zone than the control neurons while the neurons transfected with human variants of *TAOK2β* did not differ in their position. Neurons in the 16p11.2 het del mouse do have a reduced migration compared to their wildtype littermates (Scharrenberg et al., 2022, fig. 8). In Figure 5, the expression of *TAOK2α* alone was sufficient to recover the migration deficits in the 16p11.2 het del model. The autism linked human variant of *TAOK2β* did not recover the described deficits.

In between the *in utero* electroporation at e15 and the analysis of the neuronal position at E19, radial neuronal migration to the upper cortical layers takes place in the neo cortex. The observed differences in the localization of neurons are therefore most likely to be attributed to neuronal migration. *TAOK2* is the only gene in the 16p11.2 locus known that, when affected by mutations, phenocopies the symptoms of 16p11.2 deletion or duplication. In addition to the above described effect, a human variant of *TAOK2* lacking its regulatory domain affects the outgrowth of dendrites in a way comparable the phenotype in a 16p11.2 duplication model (see (Blizinsky et al., 2016; Richter et al., 2018)).

The *TAOK2α*A135P and *TAOK2α*A335V mutations are both situated in or in close proximity to the kinase domain (Richter et al., 2018). The functional relevance of *TAOK2α* kinase domain for the migration is further supported by the fact that *TAOK2* phosphorylation level in the cortex is increasing during the migration time window of upper layer neurons, while lower layer neurons during earlier migration without increased phosphor-*TAOK2* levels were unaffected by lack of *TAOK2* (Scharrenberg et al., 2022). It was shown that migration deficits in neurons where *TAOK2* is knocked out by shRNA can be rescued by inducing MKK7/JNK, an effector of *TAOK* (de Anda et al., 2012; Scharrenberg et al., 2022). As inactivation of JNK by genetic means or via an inhibitor lead to reduced migration, *TAOK2s* role in migration is further supported (Kawauchi et al., 2003). A decreased migration after deletion of 16p11.2 was also found in human patient organoids. In here, lower fractions of neurons migrated in dissociated organoids of both 16p11.2 duplication and deletion carriers compared to organoids from control cells (Urresti et al., 2020).

The fact that neuronal migration deficits in both models, the *TAOK2* model and the 16p11.2 model, can be found during late mid gestation, further supports their shared contribution in neuronal migration deficits observed in the 16p11.2 ASD patients (Scharrenberg et al., 2022).

11.2 Infection related external factors in neuronal migration

While the effect of genetic manipulations in neurons on neuronal migration are intrinsic and can be perceived as rather direct, the external influence of the immune system is considered more indirect. I focused on two approaches, reflecting two different external insults to the murine immune system. The treatment of acute cortical slices with LPS and Poly(I:C) is supposed to induce an acute inflammatory response in the embryonal brain tissue. The maternal immune activation by Poly(I:C) injection and infection with influenza is an insult, by which supposedly only the maternal immune reaction to the viral infection or viral infection like treatment is affecting the embryo.

During cortical development, the timing of developmental steps in the healthy state is predefined and essential for a proper localization of neurons (Mukhtar & Taylor, 2018). MIA potentially harms the offspring both during mid but also late stages in the development and leads to impairments in behavior

and down to the level of neuronal receptor function (Meyer et al., 2008). A very early maternal immune activation at E5 by either viral infection or Poly(I:C) injection lead to a reduced weight in the fetuses at E17.5, pointing towards a developmental impairment (Jacobsen et al., 2021). A Danish cohort study found a correlation between maternal viral infection in the first trimester and ASD (Atladóttir et al., 2010). Another study showed that maternal infection specifically in the third trimester lead to an increase in the risk for of ASD cases in a birth cohort (Brucato et al., 2017). These hints lead to the decision to assess the effect of maternal immune activation on neuronal migration at an early and a very late time point of development. Due to the delay between infection and immune activation, the maternal immune activation by either Poly(I:C) activation or influenza infection was chosen for the early time point in this approach. For the very late timepoint, the *in situ* treatment with LPS and Poly(I:C) was chosen. This procedure elicits a rather immediate and direct effect during the short time window of upper cortical neuronal migration between the IUE, the slicing of the brains, treating them and imaging the neurons during their migration.

Immune activation in acute slices

11.2.1.1 Neuronal migration in the somatosensory cortex as observed *in situ*

Radial neuronal migration in the developing cortex can be understood as a multi-step process, that can be affected at different points. The onset of migration could be delayed, neurons can be actively migrating towards upper layers or persist in lower layers, the velocity of single neurons (Scharrenberg et al., 2022, fig. 4) or certain populations migrating towards the marginal zone can be affected. Finally, the targeted zone the neurons settle after migration to form a specific layer could be changed. In my *in situ* experiments, I analyzed the position of neurons as the outcome of neuronal migration, the movements of the bipolar subpopulation and the whole neuronal population, changes in the number of bipolar cells from the whole neuronal population and finally the velocity of single neurons.

My results regarding the outcome of neuronal migration in the somatosensory cortex after LPS treatment are inconsistent with some experiments pointing towards an increased migration and other towards a decreased, resulting in no net change of neuronal position when analyzing all neurons together (see Figure 6a and c). On the other hand, the analysis of all Poly(I:C) experiments combined and the mean distance per experiment showed that the Poly(I:C) treated neurons were positioned significantly more distal to the marginal zone than their controls (see Figure 6b and d). Interestingly, the position of treated neurons and microglia relative to their untreated controls in the axis between ventricular and marginal zone is opposed between these two cell types in some experiments (see Supplementary Figure 5), eventually resulting in Poly(I:C) treated neurons being more distal to the marginal zone than their controls (Figure 6) and the microglia from the same condition being more proximal to the marginal zone than their untreated control cells (Supplementary Figure 3). I can only speculate about the reasons and effects of this behavior. During brain development, microglia transiently leave the cortical plate (Hattori et al., 2020; Squarzoni et al., 2014). But there has been no difference in the position of microglia reported following maternal immune activation (Squarzoni et al., 2014). Future experiments will tell if under certain immunological circumstances microglia create a microenvironment that repels neuronal migration and therefore lead to a decreased migration of neurons.

For Figure 7, I analyzed whether the displacement of the neuronal population or the bipolar fraction was affected by the treatments possibly leading to an impaired migration behavior that was not detectable in the analysis of the resulting position of neuronal migration. In the LPS experiments, the neurons migrated a significantly shorter distance towards the marginal zone, while the bipolar selection did not migrate significantly differently. On the other hand, at the end of the experiment, the bipolar fraction of LPS treated neurons was significantly smaller than the bipolar fraction of control neurons. This could be an additional explanation for the lower shift of the general LPS treated

population.

In the Poly(I:C) treated slices, the movement of the complete neuronal population was not significantly changed. Figure 7 presents the significant decrease in the migration of bipolar neurons in the treated samples compared to their controls. At the end of imaging, the bipolar fraction of neurons was still more distal to the marginal zone in the treated samples than in their controls. There was not a significant decrease in the fraction of bipolar neurons in the Poly(I:C) treated samples.

The fraction of bipolar neurons in the control slices was overall in the expected magnitude of about 80% (see (Scharrenberg et al., 2022, fig. 4)). During neuronal migration, neurons change between a multipolar and bipolar phenotype before finally migrating from the ventricular zone towards the marginal zone while presenting the bipolar phenotype (Noctor et al., 2004). A reduced bipolar fraction or the lack of switching from multipolar to bipolar neurons over time can mean a lower fraction of migrating neurons resulting in a placement of neurons closer to the ventricular zone (Huang et al., 2017). This can ultimately lead to a displacement of neurons in the cortical layers and might affect neuronal networks (Pan et al., 2019).

Next, I analyzed the migration velocity of single neurons. In here, no significant differences between the immune activation *in situ* and the control slices could be detected. The overall velocity was in an expected range (see (Scharrenberg et al., 2022, fig. 4)). It is possible that I might have missed some finer movements due to the imaging frequency of one image each 20-30 minutes, but the fact that my control values are very close to the published velocity of neurons in radial migration supports the validity of my results. The radial migration of neurons consists of continues and discontinues movements, based in their mechanism of migration (named somal translocation and locomotion in (Nadarajah et al., 2001)). To check if the neurons mode of migration is affected by my treatments, I analyzed the variability of neuronal velocity with periods of increased velocity defined as irregular leaps. But here as well I did not find a significant variation in the treated neurons. This could either be the behavior not being differentially affected or, due to the low sampling rate described above (compared to one image every minute up to one image every 10 minutes in (Nadarajah et al., 2001)), specific variations in the velocity have not been captured by this approach.

A reduction in the velocity of radial neuronal migration together with an unchanged proliferation rate of newborn neurons could have resulted in a higher density of freshly differentiated neurons close to the ventricular zone and thereby negatively affecting the migration through this improperly formed layer. Neurons migrate radially alongside radial glia fiber. As these glia cells differentiate to other cell types at a specific time point, slow migration might especially affect late developing neurons of the upper layers that could lose these glia cells as guidance for their migration (Itoh, 2016).

11.2.1.2 Behavior of microglia post treatment with Poly(I:C) and LPS in situ

The treatment and activation of microglia in slices is a procedure already performed by others in different experimental setups (Johansson et al., 2005; Papageorgiou et al., 2016; Sheppard et al., 2019). Microglial morphology is described in many publications ranging from a ramified morphology with extensively stretched processes to a short and condensed amoeboid morphology (Antonson et al., 2019; Cunningham et al., 2013). In here, the morphologies are associated with a certain degree of activation by a threat. The ramified morphology is considered resting or scanning the surrounding environment. Once encountering activating signals, ramified microglia can develop into the more condensed amoeboid morphology.

In Supplementary Figure 3 I presented a significant activation of microglia by LPS treatment, judged by their change in morphology. The Poly(I:C) treatment induced a reduction of ramified morphology towards the other morphologies in three out of four experiments, with the fourth one having a clear

increase in microglia having a ramified morphology. This points towards a successful activation of microglia in this experiment by both LPS and Poly(I:C), evaluated at the late time point of fixation past the live imaging.

Most studies focus on the distribution or morphology of microglia during postnatal timepoints or in adult mice (Silvin & Ginhoux, 2018; Tan et al., 2019). Unfortunately, little is known about the distribution of different specific morphologies of microglia in the cortex during prenatal development, so numbers to set my results into perspective are lacking. Still, studies show an increase in the amoeboid morphology and an decrease in the ramified morphology past a maternal immune activation, supporting the general trend I presented (O'Loughlin et al., 2017). Finally, the applied model of analyzing microglia directly and in parallel to the neuronal migration in situ is supported by the recent finding, that microglia in situ are transcriptionally closer to adult acutely prepared microglia than microglia cultured in vitro (Delbridge et al., 2020). This points towards a more in vivo like situation in the slices compared to other forms of culture.

Maternal immune activation

The second model for an external factor affecting the neuronal development is a maternal infection or immune activation with a virus or virus like particle that does not directly proceed to the developing embryo. Here, the early timepoint of treatment was chosen to allow for the maternal immune activation to build for as long as possible. Maternal immune activation was already shown to impair the cortical lamination (Wu et al., 2018). Also markers for early born neurons (Ctip2) and to a lesser extent also later born neurons (Satb2) did show impaired organization after maternal LPS treatment (Chao et al., 2016). To inspect both the actual infection and the effect purely by the maternal immune activation, I analyzed the effect of a maternal Influenza infection and a maternal immune activation by injection of Poly(I:C). The expression of Ctip2 in the murine cortex is strongest in layer 5 and less strong in layer 6, the expression of Satb2 for later born neurons is mainly spread over layer 2 to 4 (Chao et al., 2016).

I could show that in the offspring of influenza infected mothers Ctip2 and Satb2 positive cells are localized more distal to the marginal zone than their controls. This effect was, to a lower extent, also visible in the offspring of Poly(I:C) injected mothers. The shift in cellular distribution was not preserved in the comparison of mean distances of each fetus. I analyzed the shape of the distributions by a differential frequency distribution between the neurons of PBS control animals and treated animals. The distributions showed a lower fraction of cells in the treated groups for both markers in the 200-250µm most proximal to the marginal zone. Vice versa did the distribution of cells in the treatment groups show a higher number of neurons in the area following these first 250µm, pointing towards a general shift in the neuronal localization towards the ventricular zone after maternal infection or immune activation.

The distribution of Satb2 positive neurons overlapped strongly with the Ctip2 positive cells and reached even closer towards the ventricular zone. Still, the highest density of Satb2 neurons was more proximal to the marginal zone than the highest density of Ctip2 (see Figure 9: Cortical layering after maternal immune activation.) and the distribution of neurons positive for either marker was conserved in the treatment groups. These distributions recapitulate the published distributions of Ctip2 and Satb2 positive neurons in the neocortex (Britanova et al., 2008; Harb et al., 2016).

Though I chose a different analytical model, I can confirm previous findings (as described in (Wu et al., 2018)) that maternal immune activation affects the distribution of Ctip2 and Satb2 positive neurons also in an experimental model of a very early influenza infection and of maternal immune activation by Poly(I:C). While the shift in Satb2 positive neurons from the cortical plate towards layers more distal to the marginal zone is more drastic in the mentioned study, my results highlight the more long-term

effect of a maternal immune activation during early pregnancy even on later born upper layer neurons.

Maternal immune activation via Poly(I:C) or viral infection are known to be inducing the production of IL-17a (Choi et al., 2016). Recently it has been shown, that IL-17a leads to a phosphorylation of Erk1 / 2 and a decreased phosphorylation of one of the downstream targets of mTORC1, phospho-RPS6, in neuronal progenitors derived from embryonal stem cells (Gomes et al., 2022). The activation and inhibition of Erk1/2 was already shown to impact migration of neurons *in vitro* (Xu et al., 2016; Yang et al., 2013). Even though their described effect on the migration of neurons is different to my observations, it still points towards Erk1/2 as possible mediators of maternal immune activation on neuronal migration. The activation of RPS6 by phosphorylation is regulated by pathways involving both mTORC1 and ERK. Many mouse models harboring mutations that lead to alternations in the phosphorylation of RPS6 are linked to neuronal developmental disorders and neurological perturbations (Biever et al., 2015, p. 8f). These findings might explain my observed changes in neuronal migration after maternal immune activation.

Overall, I was able to show that both genetic and immunological insults influence the neuronal migration in the developing murine cortex. My results also reflect the differential penetrance of genetic perturbations that directly and immediately affect cortical neurons of interest and more indirect systemic insults. In the case of MIA, the immunological insult is dependent on maternal cytokines such as IL-17a (Choi et al., 2016) being transferred to the embryo. In the immune activation *in situ*, LPS and Poly(I:C) treatment might act directly on the neurons (Leow-Dyke et al., 2012; Ritchie et al., 2018) or via microglia (Baghel et al., 2018; Lehnardt et al., 2003) to elicit a reaction relevant for neuronal migration in rather stressed environments such as the acute preparation of cortical slices (Delbridge et al., 2020). In the experiments considering genetic perturbations, the overexpression of an autism risk gene and its variants can act immediately and directly on the neurons. This is also recapitulated in the visible effects of my treatments, that are more evident to the eye in the genetic approaches compared to the immunologic insults.

11.3 Limitations of this study

Not all performed experiments were included in this final analysis. I performed the first experiments to train the slice culture protocol and to test the used culture and slicing media. In the following experiments, those were excluded that did not have the slicing plane in an angle that allowed for a comparable analysis or undisturbed path of the radial migration. Finally, experiments, brains and slices were excluded where either the site of transfection was not in the desired region, the brains or slices were notably disturbed during preparation or when the slices or neurons did show strong signs of cell death and tissue damage just before or during live imaging.

Neuronal migration from the ventricular zone in the murine cortex follows a strictly regulated series of inside-out development into the different layers (V. S. Chen et al., 2017). Neuronal progenitors can therefore be specifically targeted via *in utero* electroporation and their fate in the cortical layers in control conditions can be well augmented. The expected position of neurons, *in utero* electroporated at E15, would be expected to form a major population in layer 2/3 which is formed from E16 onwards, with a minority of cells distributed into deeper layers down the ventricular zone (See (V. S. Chen et al., 2017; Scharrenberg et al., 2022, fig. 1) for the developmental timeline and positions of neurons in comparable IUE experiments). In the experiments in 10.2 “Neuronal migration and immune perturbations *in situ*”, the development of the neurons in the cortical slices was delayed in some experiments, independently of their treatment. The neurons did not form a defined layer but stayed rather dispersed over a longer distance between ventricle and marginal zone. Still, the experiments 13 Poly(I:C), 16 LPS and 22 LPS do show a trend towards the desired shape of neuronal distribution (see Supplementary Figure 5).

This delay in development was not visible in the control slices of the experiments examining the impact of ASD-related mutations on neuronal migration. In the genetic experiments, the embryos did develop undisturbed in between the IUE at E15 and the sacrificing of the embryos at E19 and immediate fixation and analysis of the brains. Contrary to this, the embryonal brains in the *in situ* experiments were electroporated at E15 but already explanted at E17, sliced and kept in slice culture for the remaining time and analysis until fixation at E19. The handling of the brains, the slicing procedure and the slice culture itself might have had a negative impact on the development of the neurons which might have delayed their migration during the remaining time until their fixation at E19.

In the experiments investigating the velocity of single migrating neurons, the number of single neurons tracked is, compared to the total number of neurons migrating, low. But I decided to only track radially migrating bipolar neurons with an undisturbed visibility over the whole tracking which reduced the number of available neurons drastically. But again, the claim of an unbiased sampling of neurons can be supported by the resulting magnitude of velocity in the expected range.

I assessed the level of microglia activation under live imaging conditions. In Supplementary Figure 4, I showed an increase in the velocity of microglia This is conflicting with a comparable experiment, that was performed in an inflammation model of cerebral palsy in rabbits, where LPS was directly injected in the uterus at E28, three days before the subsequent generation of slice cultures. This created an inflammatory environment and lead to a morphologically activated microglia phenotype with reduced surface to volume ratio in slice cultures. The microglia of these prenatally inflamed rabbits displayed a decrease in migration speed compared to the untreated controls (F. Zhang et al., 2016). Overall, the velocities of microglia recorded in my experiments have been slower by a factor of 2-3 compared with the above-mentioned experiment. Also, the control and treated microglia in the LPS experiments do have decreased velocity compared to the microglia in the control conditions of Poly(I:C) treated brain slices. As the brain slices were handled in the same way, regardless of the experiment and treatment to be applied later, I cannot determine what has been the cause for this difference in overall velocity between the different experiments. One could speculate about the slicing process, the handling-induced stress, and the treatment with LPS and Poly(I:C) initiating a remodeling of the extracellular matrix. This could be the outcome of an astrogliosis-like state of microglia. Astrocytes transform upon sensing of neuronal damage into an active state in a process called astrogliosis. Activated astrocytes fulfill beneficial functions after injury or trauma such as restoring the blood brain barrier and inducing vascularization to replace damaged vessels, but astrogliosis is known to inhibit the regeneration of axons by specific scar tissue. Also the production of proinflammatory and cytotoxic cytokines has been reported for activated astrocytes, which can be harmful for the surrounding tissue (D. Zhang et al., 2010). At the developmental timepoint of my experiments with cortical slices at E17, astrogliogenesis is just at the brink of starting (Farhy-Tselnicker & Allen, 2018). GFAP, an astrocyte marker, was absent in murine amygdala before P0 in an experiment about glial activation after maternal immune activation (O'Loughlin et al., 2017). But it was shown, that microglia and astrocytes both act on phagocytosis of neurons and can compensate each other (Damisah et al., 2020). Therefore, one could assume comparable behaviors of microglia and astrocytes in a state of stress induced by slicing, tissue damage of other causes and other threats, which might have negatively influenced the cultures.

11.4 Alternative models

Genetic markers for microglia and neurons

In this thesis, neurons were visualized by either GFP expression or by antibodies directed against their layer specific markers while microglia were either stained by a conjugated lectin or an antibody directed against Iba1. All methods do have their up- and downsides, but also their specific reason for applying them in these models. The expression of GFP after IUE allows to target a defined population

of neurons both in number (by the amount of plasmid electroporated), position and timing. In addition, this method permits observations and experiments regarding the development of these specific neurons even with live imaging. The downside, specifically in the experiments where immune activation and microglial activation is in focus, is the reaction of microglia against the IUE itself. It has been shown that microglia leave their distribution in the cortical plates and localize towards the ventricle after an IUE or the already the presence DNA in the ventricle (Hattori & Miyata, 2018). One also must consider the stress the animals are facing in the surgical procedure even with a high standard of care and anesthetics used. This stress is not only critical in the view of animal ethics but can also affect the development of the embryos (Reviewed in (Lautarescu et al., 2020)). Microglia staining was done by an antibody directed against Iba1 in fixed samples and by staining with a lectin coupled dye in live imaging. Both methods share microglia and macrophages as their targets and lack specificity between these two cell types. But in the range of these experiments, the differentiation between these two is not necessary, as microglia are expected to be in the large majority in the brain parenchyma at this point of development and immune activation. Macrophages are thought to be infiltrating upon injury or infection but in our experimental model the treatment is applied in situ which does not allow for a further influx (See (Puntambekar et al., 2011) for information about the influx of macrophages into the CNS). Nevertheless, the lectin staining also did stain blood vessels in the brain which led to a certain general background of the staining but was also problematic to distinguish from microglia at certain colocalizations. An alternative to microglia staining could be an engineered mouse model expressing fluorescent proteins specifically by microglia (Kaiser & Feng, 2019). If one can rule out disturbances of microglia function in this model, this might be a useful alternative.

Acute slices

The experiments of immune activation by LPS or Poly(I:C) directly acting on brain tissue have been performed in acute slices. As described above, these slices have the benefit of near in vivo characteristics regarding their composition and structural integrity. But unfortunately, astrogliosis or a microglial counterpart with their immunological activation are potentially harmful in an experimental setting where microglial activation is in the focus. Slice-cultures, cultivated over longer periods of time are perceived as stable and with reduced inflammation processes compared to acute slices (Delbridge et al., 2020). Neuronal migration on the other hand depends on the structural integrity and polarization of the cortex and longer slice cultures might lose their integrity after longer cultivation. An alternative to study the effects of direct embryonal infection could be the injection of LPS or Poly(I:C) directly into the embryo in a procedure similar to the IUE. Thereby one would lose the quality of “sister slices” of one brain treated differently in control and treatment in situ but would keep the genetic similarities and the comparable prenatal environment in sibling embryos injected with LPS, Poly(I:C) or PBS. Analysis of the cortical layering would be possible in fixed brains, thereby avoiding the microglia activation during cultivation.

A last alternative to acute slices could be the application of a cranial window in combination with ex-utero development of mouse embryo. (Aguilera-Castrejon et al., 2021) Studying a mouse embryo with a cranial window would avoid the process of cutting into the brain. An ex-utero approach might be necessary to keep the embryonic brain alive over the extended time of imaging.

11.5 Alternative analysis methods

Parameters Microglia Tracking

Microglia were tracked using the semi-automatic Trackmate tool in ImageJ. The applied parameters in the LaP tracking were chosen to be maximal 50µm linking distance, 150µm gap distance and 2 frames for the maximum gap length. These parameters were carefully chosen to minimize unspecific tracks to be connected by too high values filled in, but also to include fast moving microglia. In this method, all

assigned microglia were manually checked and if necessary deleted or unassigned microglia included.

An alternative could be to apply more advanced automated image and motion detection. It might be necessary for this to further improve the signal to noise ratio of the analyzed live imaging and to avoid unspecific staining of further structures in the regions of interest.

Microglia morphology

Microglia morphology was visually rated and assigned to one of three morphologies. This limits the categories to rather rough morphological qualities (condensation of soma, thin or thick processes, number of processes) and is, to a certain degree, dependent on the subjective assignment of the researcher. An alternative could be the automated detection and segmentation of microglia by morphOMICs, which makes the analysis more independent of the subjective impression of the researcher and includes finer parameters in the description of microglia. (Colombo et al., 2022)

11.6 Follow up experiments

The relevance of an experiment, where only the few transfected neurons are affected by a genetic modification and act within an otherwise unrelated system was highlighted by Vomund et al. They discovered that in a rat, the functional knockdown of a gene by *in utero* electroporation in a set of neurons is sufficient to induce changes in the rats amphetamine sensitivity and behavioral habituation. (Vomund et al., 2017).

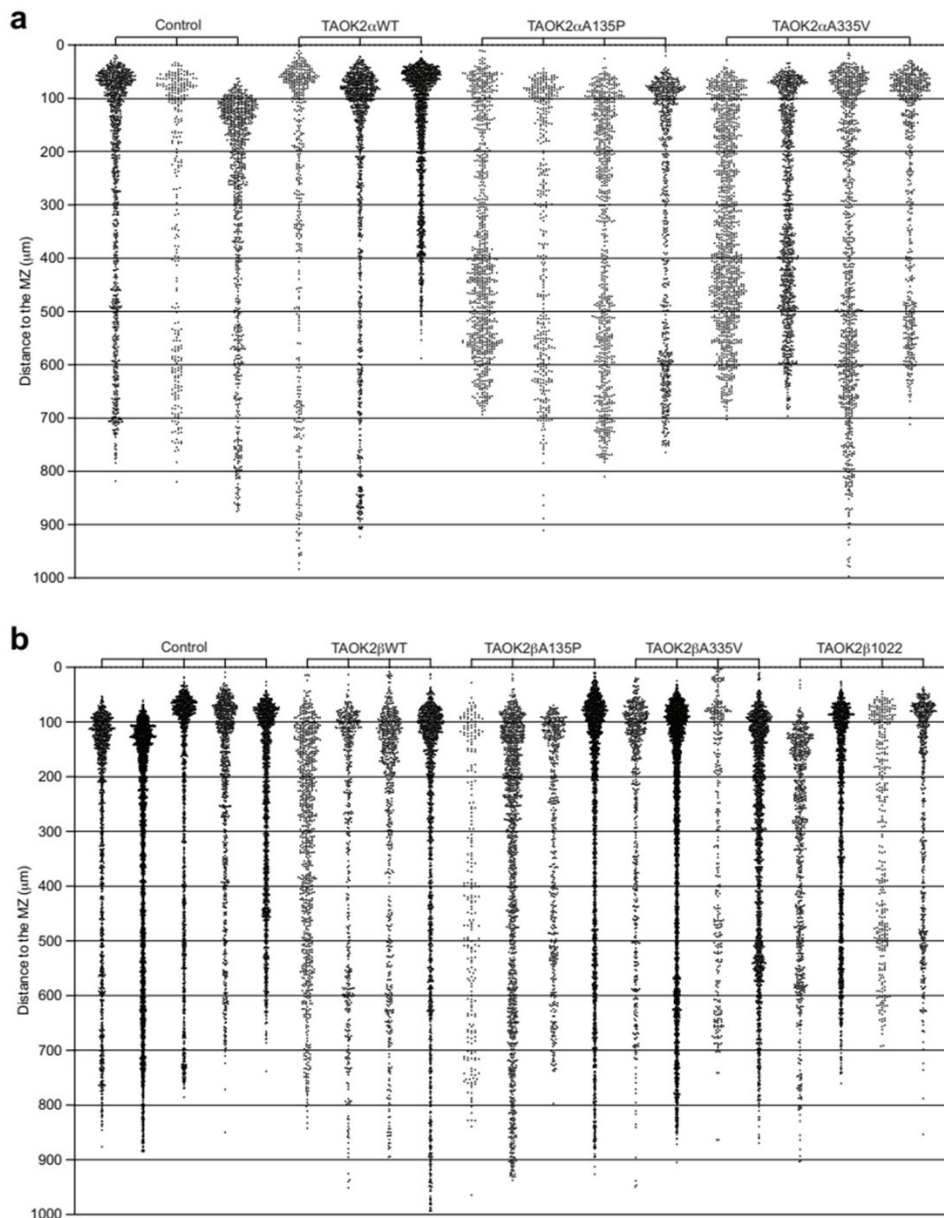
16p11.2 heterozygous deletion and ASD associated human variants of TAOK2 lead to impaired neuronal migration at mid to late gestation in the developing cortex. TAOK2 reintroduction into neurons of the 16p11.2 del Het mouse model rescues this impairment and further suggests being responsible for the migration defects in the 16p11.2 mouse model. In these experiments, two genetically modified mouse models have been used and human mutations of ASD risk gene TAOK2 have been introduced to a selected population of cells via IUE. This experimental setup made it possible to directly compare the neuronal migration behavior of different transfections in littermates, thereby keeping other maternal or prenatal genetic and environmental factors tightly comparable. Still, apart from control transfections with a visual marker only, this model allows only observations of genetically modified neurons in a genetically different environment. Follow up experiments to further study the responsibility of TAOK2 for the described neuronal deficits of the 16p11.2 het del mouse model could be the permanent and stable reintroduction of TAOK2 into the mouse genome. This would provide insights into the effects of TAOK2 on migration in a genetically homogenous brain. In addition, this would provide the possibility to study the connectivity issues, already described in both TAOK2 and 16p11.2 concerning mutations (Bertero et al., 2018; Richter et al., 2018).

TAOK2 mutations are not only associated with neuronal development but also with functions of the immune system (Molho-Pessach et al., 2017). As the development of NDDs is considered to be partially multifactorial, applying the experimental system of immune activation either maternally or in situ could further highlight the involvement of a “second hit” also in the development of ASD.

Even though this would burden additional stress on the mice, one could consider combining the maternal immune activation with the IUE to also track a specific population of neurons during their migration after maternal immune activation at early gestational time points.

Microglia are acting upon their surroundings mainly by phagocytosis and signaling via direct cell-cell contacts and cytokines. It would be very interesting to analyze the RNA expression profile of neurons in general and specifically regarding their expression of cytokine receptors and stress induced molecular pathways during their migration dependent on the immune activation.

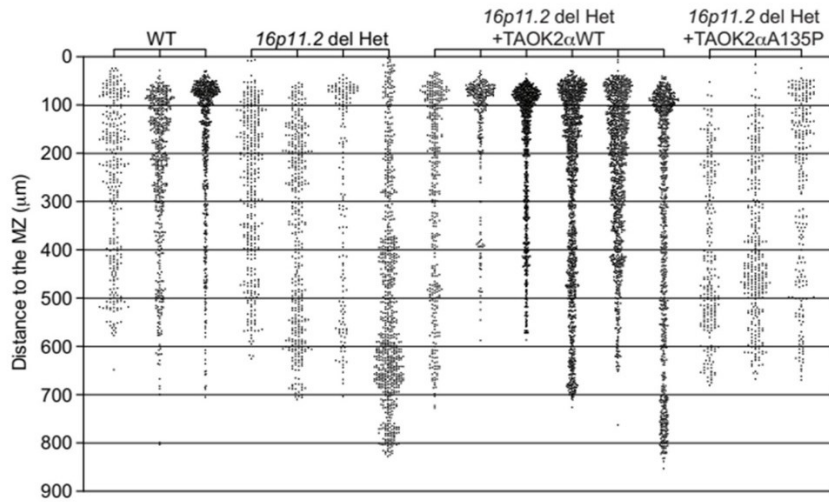
12 Supplementary figures



Supplementary Figure 1: Neuronal migration by slice after transfection with human variants of TAOK.

12.1.1.1 Supplementary Figure 1: Neuronal migration by slice after transfection with human variants of TAOK

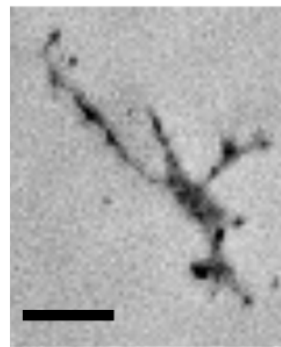
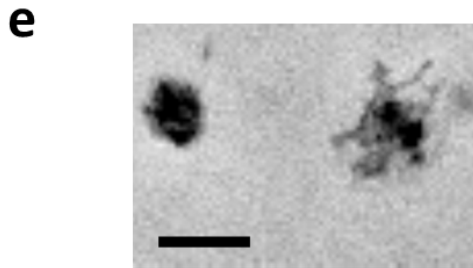
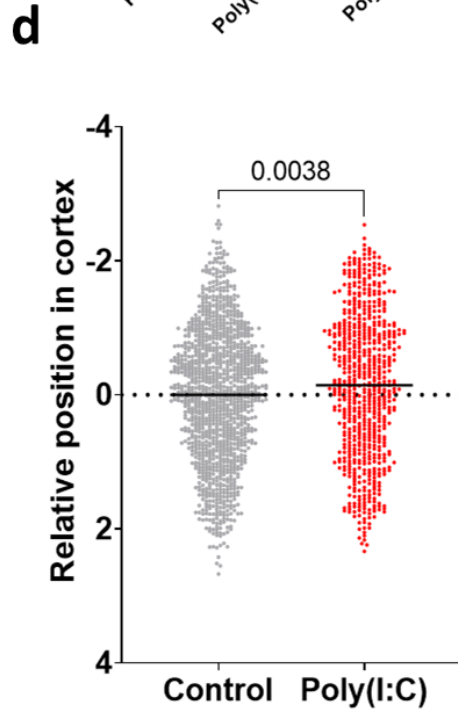
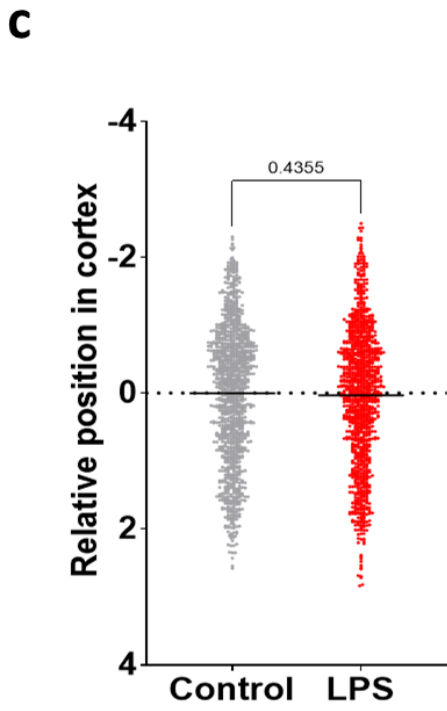
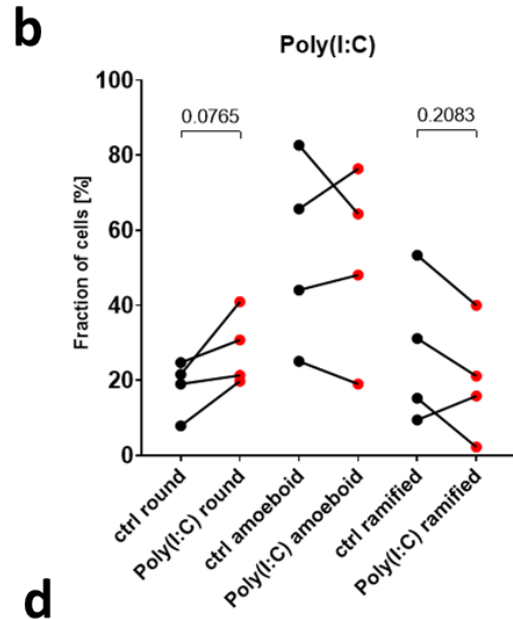
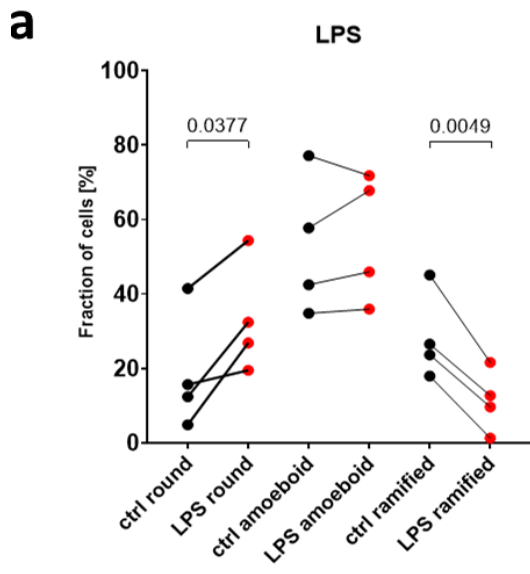
Position of neurons in individual brain slices analyzed in Figure 1, a TAOK2 α , b TAOK2 β . In collaboration with M Richter, R Scharrenberg and FC de Anda (Scharrenberg et al., 2022).



Supplementary Figure 2: Neuronal migration in 16p11.2 het mice by slice after transfection with human variants of TAOK.

12.1.1.2 Supplementary Figure 2: Neuronal migration in 16p11.2 het mice by slice after transfection with human variants of TAOK.

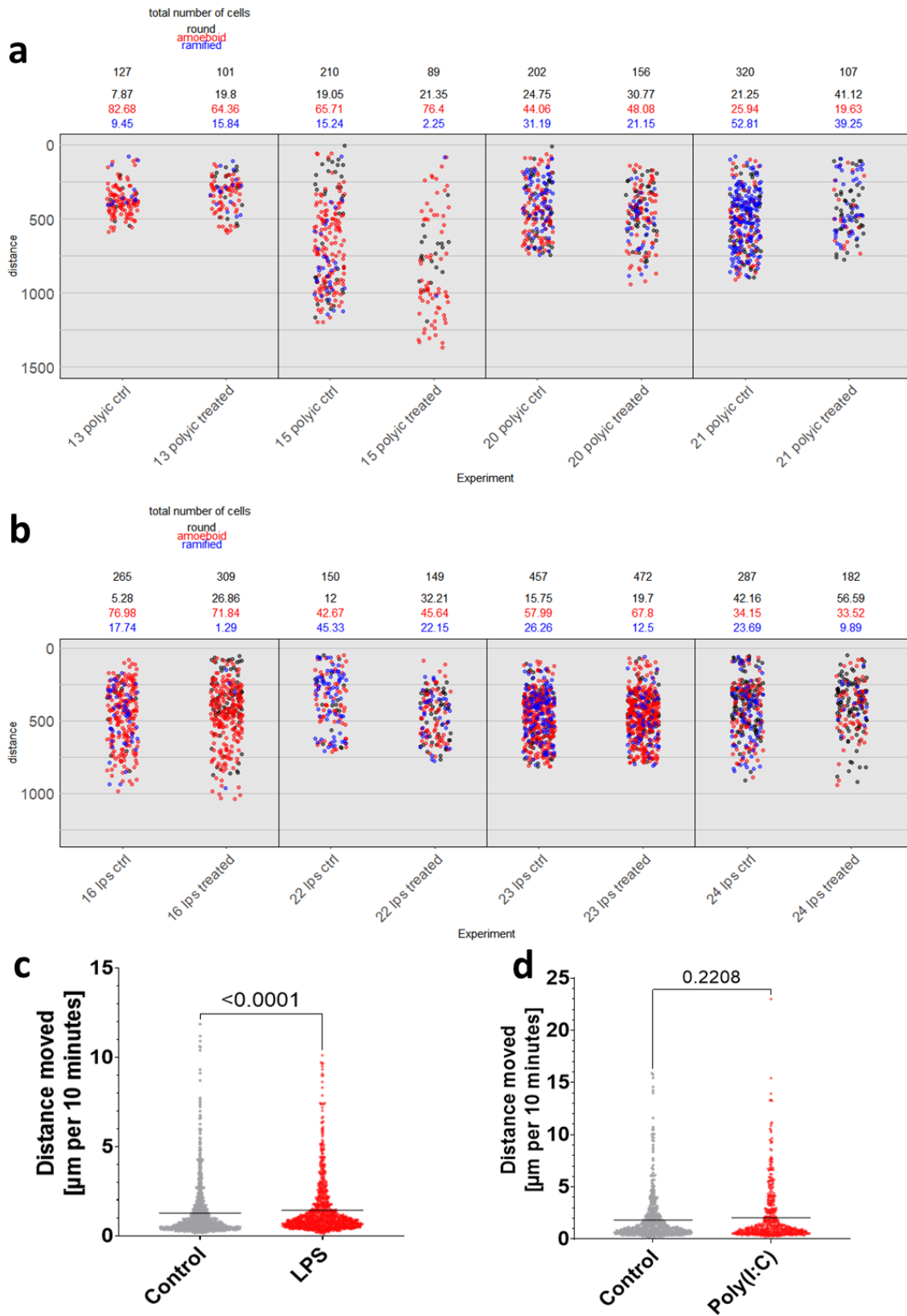
Position of neurons in individual brain slices analyzed in Figure 2. In collaboration with M Richter, R Scharrenberg and FC de Anda (Scharrenberg et al., 2022).



Supplementary Figure 3: Morphology and localization of Microglia.

12.1.1.3 *Supplementary Figure 3: Morphology and localization of Microglia*

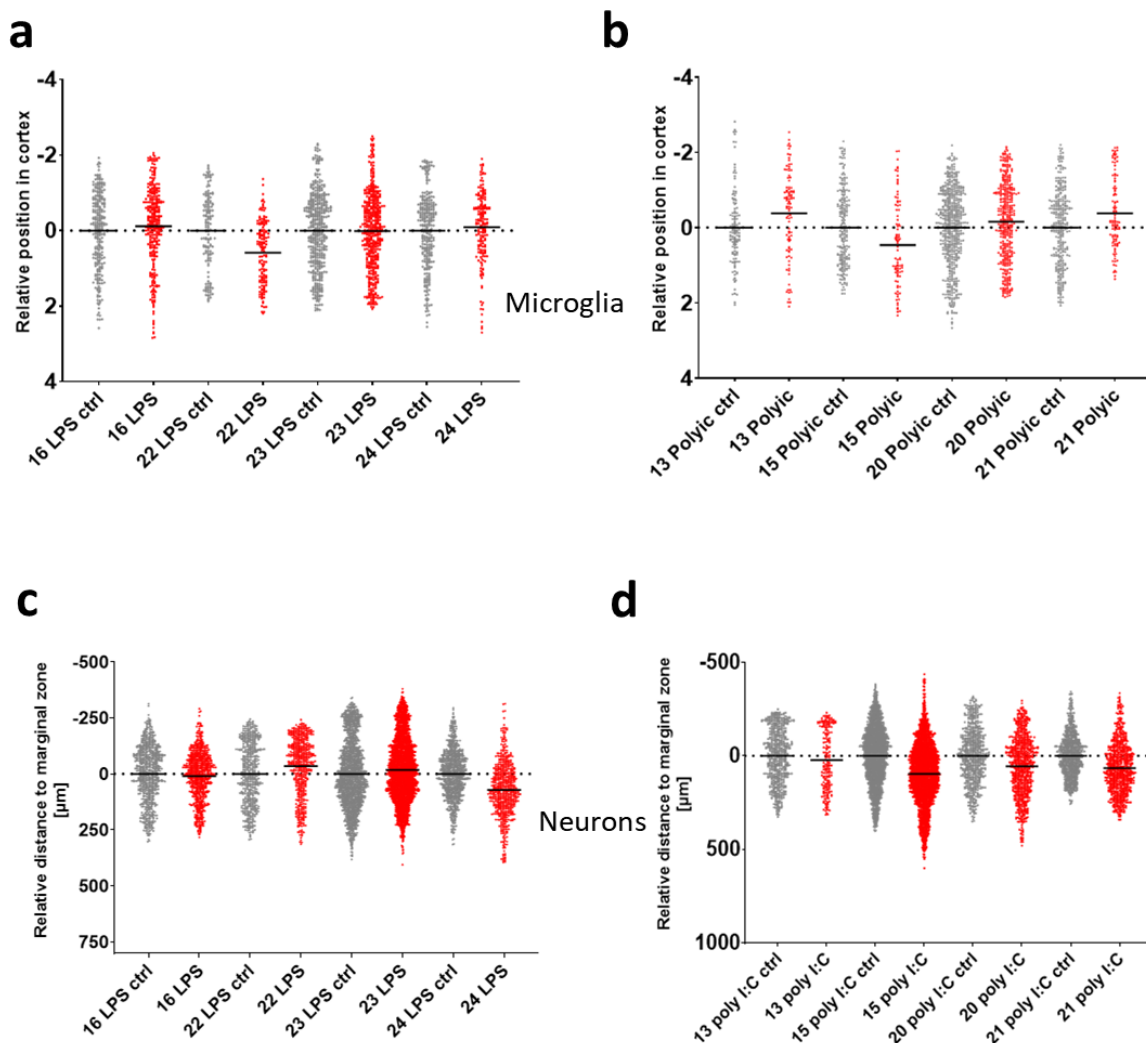
Murine embryonic cortical neuronal progenitors were transfected at E15 with venus. At E17 cortical brain slices were prepared and half of the slices of each brain were treated with either LPS or poly(I:C) or left as untreated as control. Microglia were visualized by Iba1 staining of fixed tissue. The panels a (LPS) and b (Poly(I:C)) show the morphological analysis into round, amoeboid and ramified. The values are mean percentages within each experiment and are paired to their control. The LPS treatment does affect the morphology of microglia significantly (a Paired t test of LPS round vs ctrl round: two-tailed P value 0.0377, 4 pairs; paired t test of LPS ramified vs control ramified: two-tailed P value 0.0049, 4 pairs). The Poly(I:C) treatment does not affect the distribution of morphologies (b paired t test of Poly(I:C) round vs control round: two tailed P value 0.0765, 4 pairs; paired t test of Poly(I:C) ramified vs. control ramified: two tailed P value 0.2083, 4 pairs). The panels c (LPS) and d (Poly(I:C)) show the distance distribution of microglia towards the marginal zone, the mean is displayed. All values of one experiment were standardized by subtracting the control slices' mean distance and dividing by the standard deviation of the control slices. The distribution of microglia does not differ significantly between LPS treatment and control slices (c: two-tailed unpaired t test, P value 0.435, N control: 1162, mean control: 0, N LPS: 1111, difference mean control – mean LPS +/- SEM: 0.03283 +/- 0.0421). It does differ significantly between control and Poly(I:C) treated slices (d: two-tailed unpaired t test, P value 0.0038, N control: 1209, mean control: 0, N Poly(I:C): 677, difference mean control - mean Poly(I:C) +/- SEM: 0.1434 +/- 0.0494). Examples of the three different morphologies are shown in e (from left to right: round, amoeboid, ramified; the scalebar is 20µm).



Supplementary Figure 4: Position and migration velocity of Microglia.

12.1.1.4 *Supplementary Figure 4: Position and migration velocity of Microglia.*

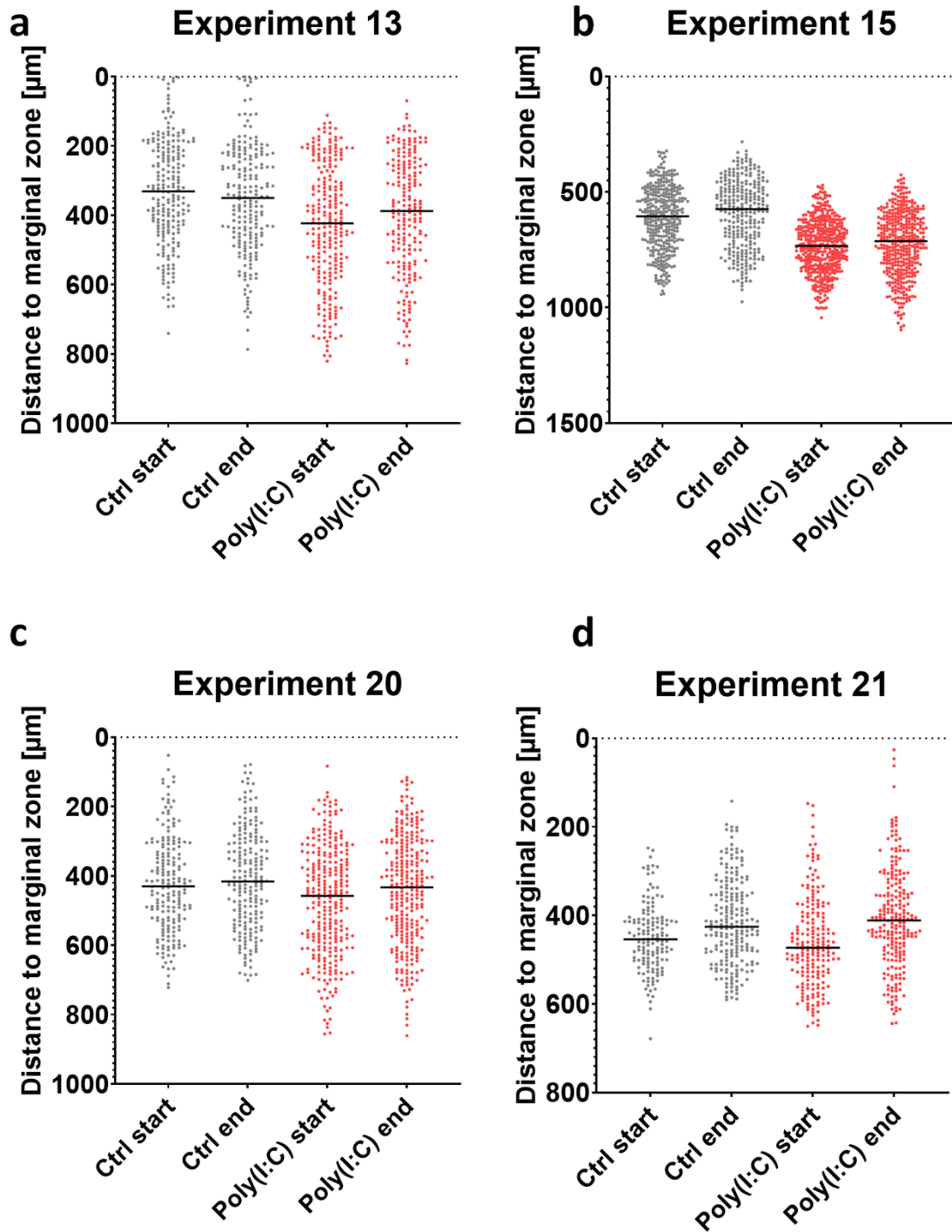
The panels depict the position and morphology of individual microglia in the different experiments (a) Poly(I:C), b) LPS). The numbers above the panels depict the total number of microglia detected in this experiment and the fraction of round, amoeboid and ramified microglia (black, red, blue). Panel c and d display the velocity of microglia in the slice cultures. LPS treated microglia display a significantly increased velocity (c median velocity of LPS treated vs control microglia, Mann-Whitney test, control: $0.7260\mu\text{m}/10$ minutes, N: 1105, LPS: $0.8946\mu\text{m}$, N: 964, two-tailed approximate P value <0.0001). Poly(I:C) treated microglia are not significantly affected in their velocity (d median velocity of Poly(I:C) treated vs control microglia, Mann-Whitney test, control: $0.9904\mu\text{m}/10$ minutes, N: 546, Poly(I:C): 1.001 , N: 539, two-tailed approximate P value 0.2208).



Supplementary Figure 5: Relative position of microglia and neurons.

12.1.1.5 *Supplementary Figure 5: Relative position of microglia and neurons*

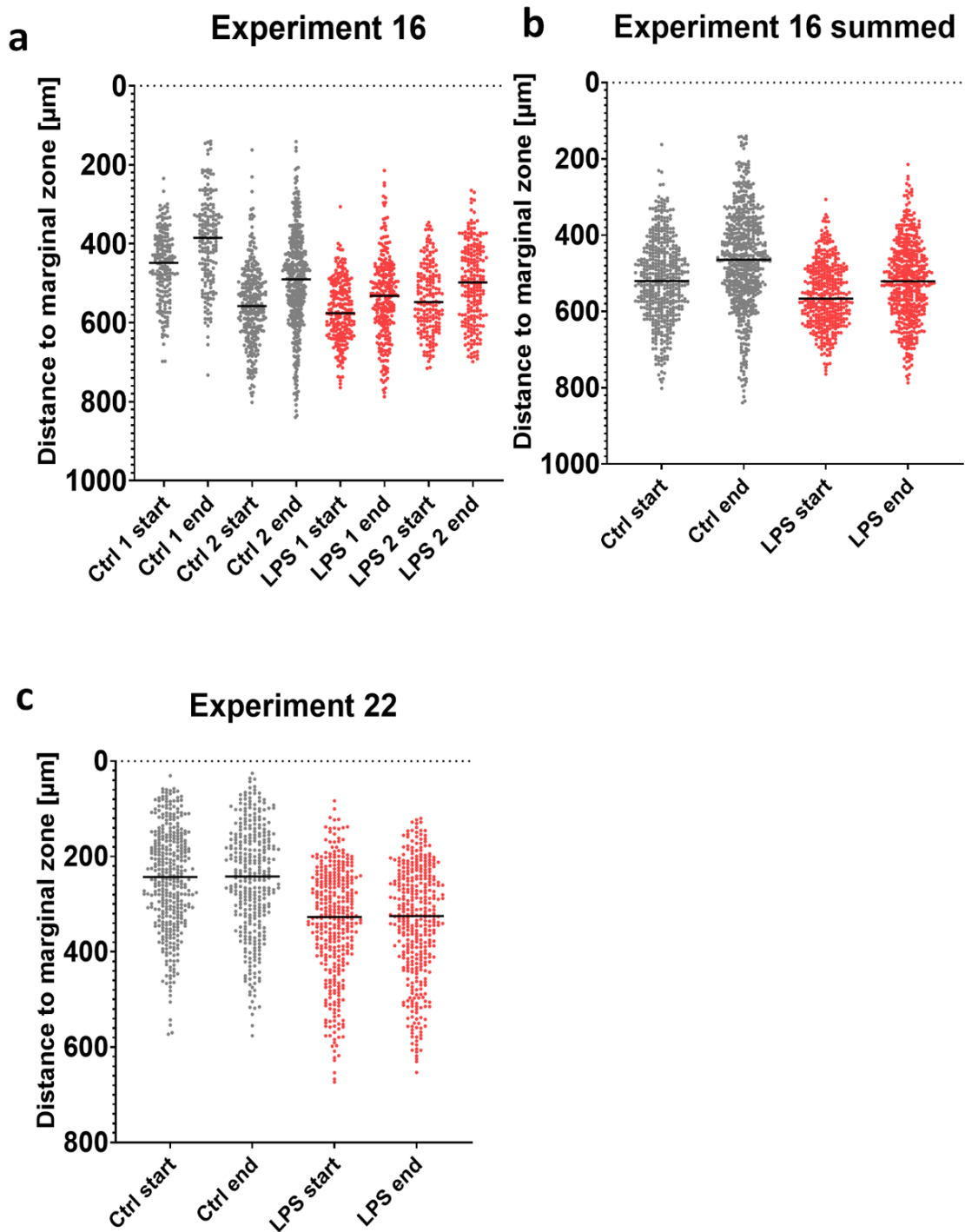
The panels a (LPS) and b (Poly(I:C)) display the deviation of microglia position from the mean of their respective control relative to the marginal zone. In the panels c (LPS) and d (Poly(I:C)), the position of neurons is depicted relative to the mean distance of their respective control neurons.



Supplementary Figure 6: Migration of Poly(I:C) treated neurons.

12.1.1.6 Supplementary Figure 6: Migration of Poly(I:C) treated neurons.

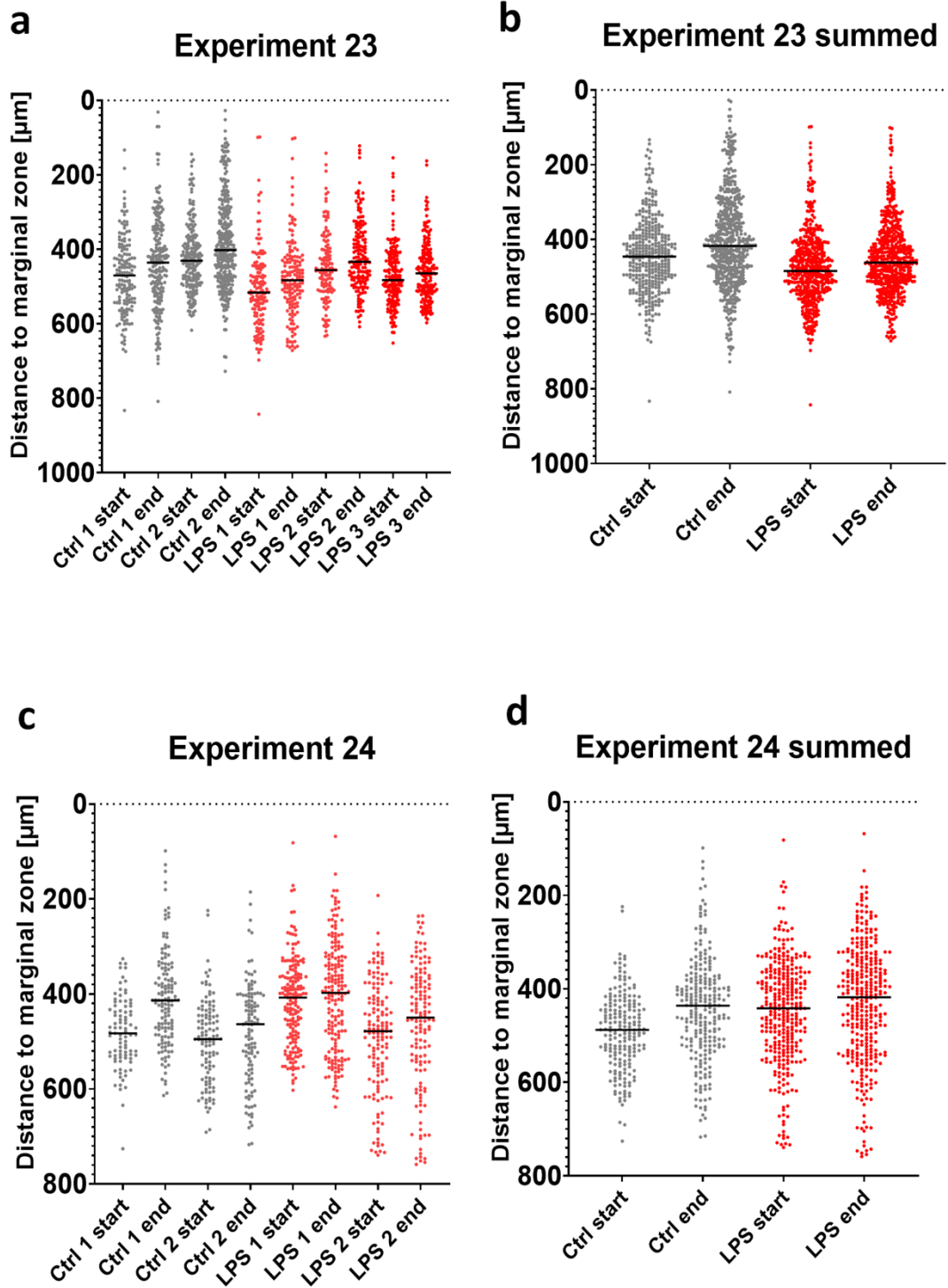
The position of neurons as distance to the marginal zone in control and Poly(I:C) treatment. Displayed are the distances in each experiment at the start and end of imaging, the line is drawn at the median.



Supplementary Figure 7: Migration of LPS treated neurons in Experiment 16 and 22.

12.1.1.7 Supplementary Figure 7: Migration of LPS treated neurons in Experiment 16 and 22.

The position of neurons as distance to the marginal zone in control and LPS treatment. (a) Multiple slices in an experiment (b) are summed per condition and timepoint. Displayed are the distances in each experiment at the start and end of imaging, the line is drawn at the median.

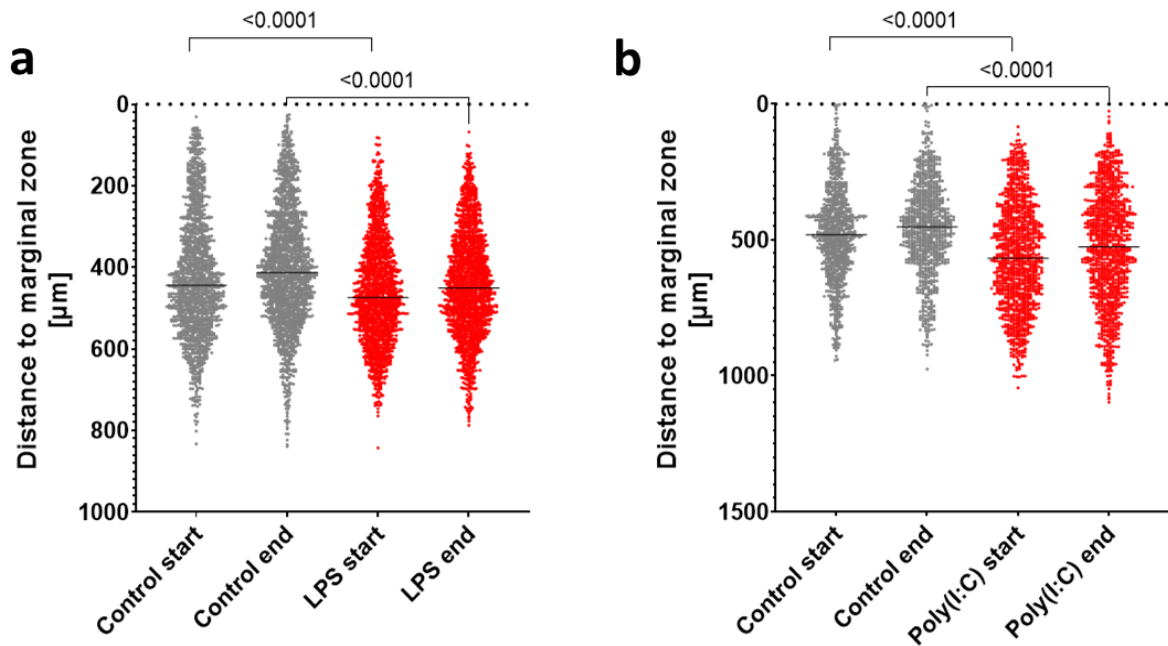


Supplementary Figure 8: Migration of LPS treated neurons in Experiment 23 and 24.

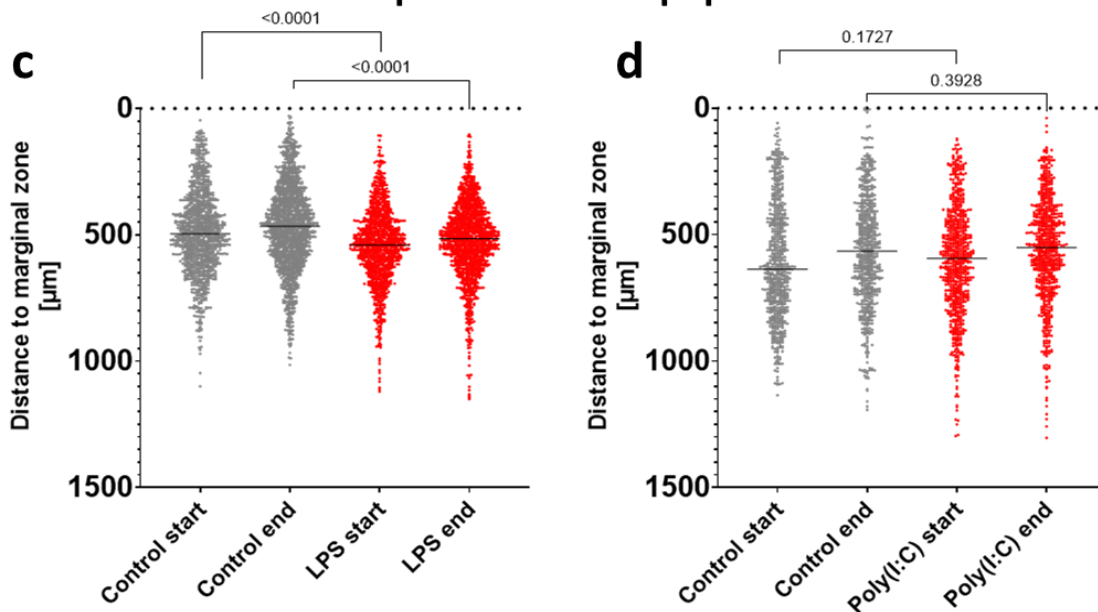
12.1.1.8 Supplementary Figure 8: Migration of LPS treated neurons in Experiment 23 and 24.

The position of neurons as distance to the marginal zone in control and LPS treatment. (a+c) Multiple slices in an experiment (b+d) are summed per condition and timepoint. Displayed are the distances in each experiment at the start and end of imaging, the line is drawn at the median.

Complete neuronal population



Bipolar neuronal population

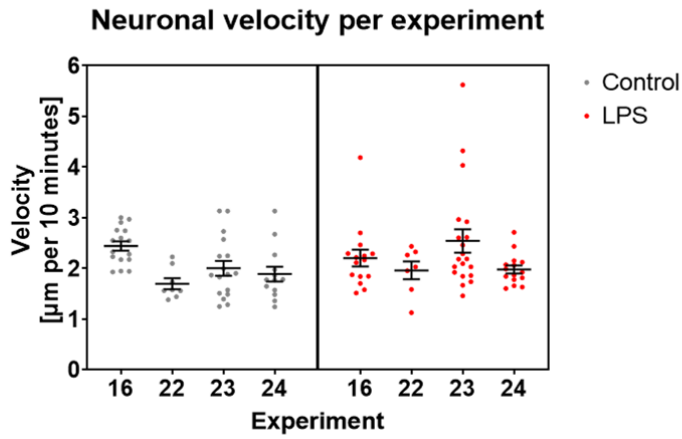
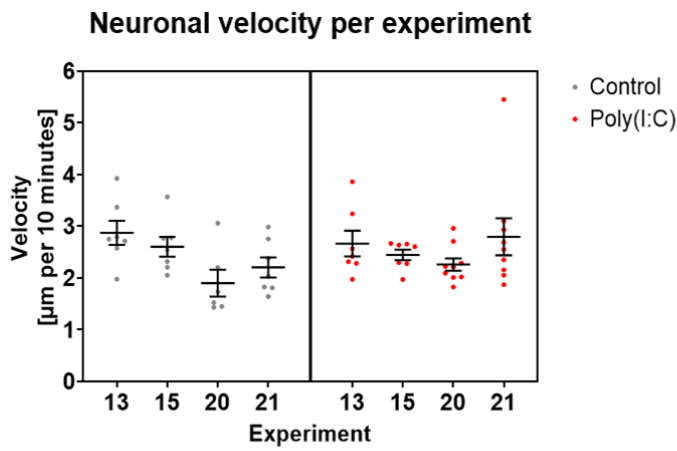
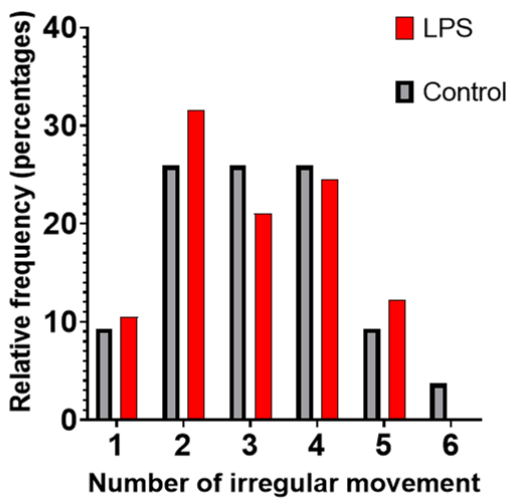
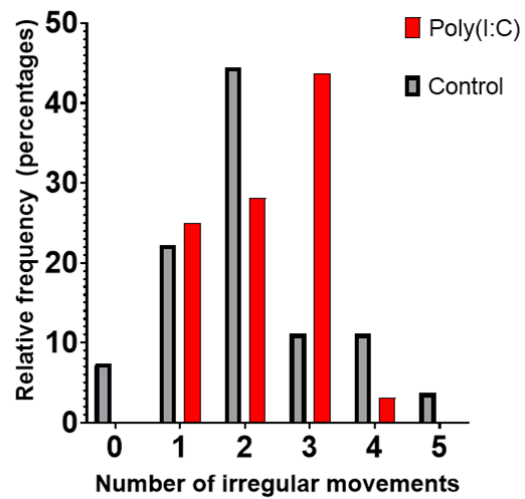


Supplementary Figure 9: Migration of neuronal populations in live imaging.

12.1.1.9 Supplementary Figure 9: Migration of neuronal populations in live imaging.

The position of neurons relative to the marginal zone at the beginning and at the end of time lapse imaging is plotted in a and b for LPS and Poly(I:C) treated neurons and their respective control neurons. The position of the neurons for the treatment and control differs significantly in both the start and end of live imaging (8-10h later, identical duration within each experiment) (a LPS Mann Whitney test, median distance to marginal zone at the start of imaging: control: 443.8 μm , N: 1409; LPS: 473.6, N: 1550, two-tailed approximate P value <0.0001; end of imaging: control: 412.9 μm , N: 1709, LPS: 450.7 μm , N: 1685, approximate P value: <0.0001; b Poly(I:C) Mann Whitney test, median distance to

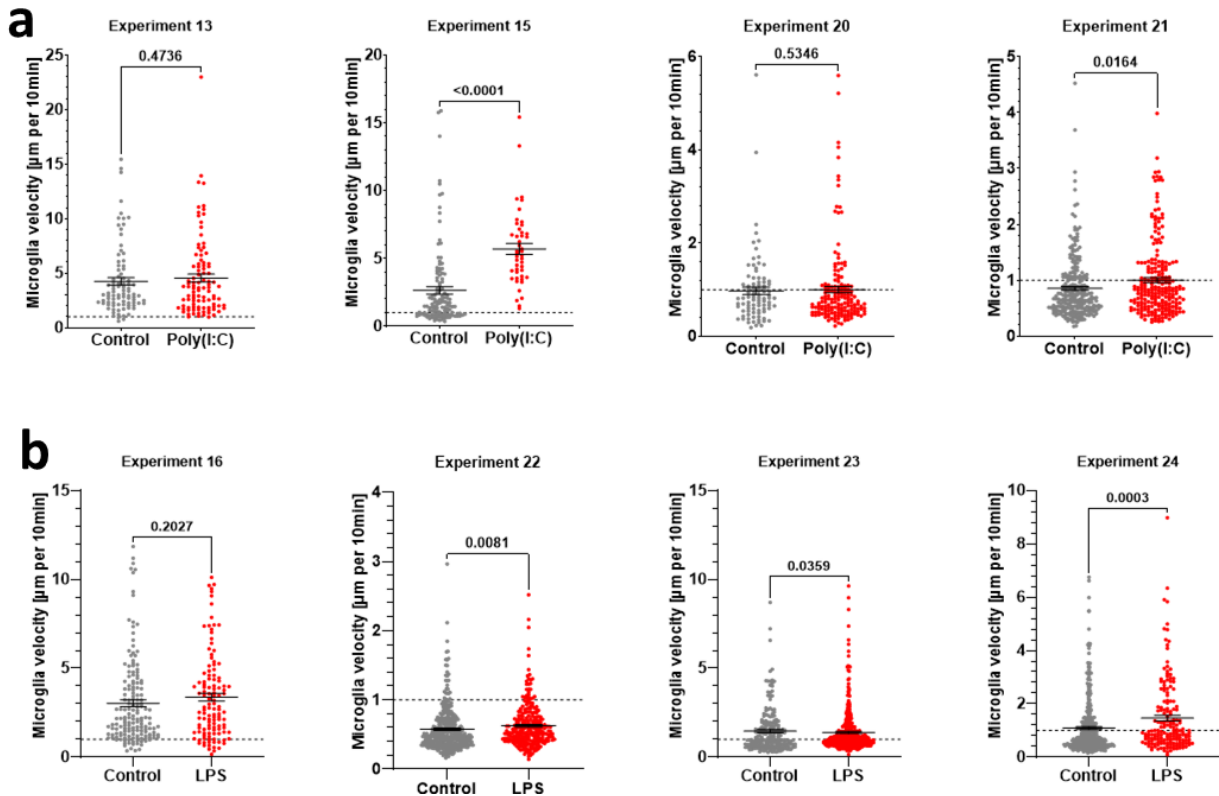
marginal zone at the start of imaging: control: 480.7 μ m, N: 903; Poly(I:C): 567.0 μ m, N:1148; two-tailed approximate P value: <0.0001; end of imaging: control: 451.9, N: 906, Poly(I:C): 5525.7 μ m, N: 1104, two tailed approximate P value: <0.0001). Also the position of bipolar neurons at the start and end differed significantly between control LPS treated neurons, but did not do so between Poly(I:C) and control (c LPS Mann Whitney test, median distance between bipolar neuron and marginal zone at the start of imaging: control: 495.4 μ m, N:1150, LPS: 540.0 μ m, N: 1132, two-tailed approximate P value <0.0001; end of imaging: control: 465.9 μ m, N:1519; LPS: 515.6 μ m, N:1334, two-tailed approximate P value: <0.0001; d Poly(I:C) Mann Whitney test, median distance to the marginal zone at the start of imaging: control: 637 μ m, N:674, Poly(I:C): 594.8 μ m, N:744, two tailed approximate P value 0.1727; end of imaging: control: 565.6 μ m, N:659, Poly(I:C): 551.7 μ m, N:730, two-tailed approximate P value 0.3928)

a**b****c****d**

Supplementary Figure 10: Single neuron velocity and mode of migration.

12.1.1.10 Supplementary Figure 10: Single neuron velocity and mode of migration.

In a (LPS) and b (Poly(I:C)) the velocity of single neurons for each experiment is displayed as mean with the standard error of mean. Irregular movements, defined as movements with a velocity more than two times the mean velocity of the specific neurons, are displayed as bar graphs in c and d.



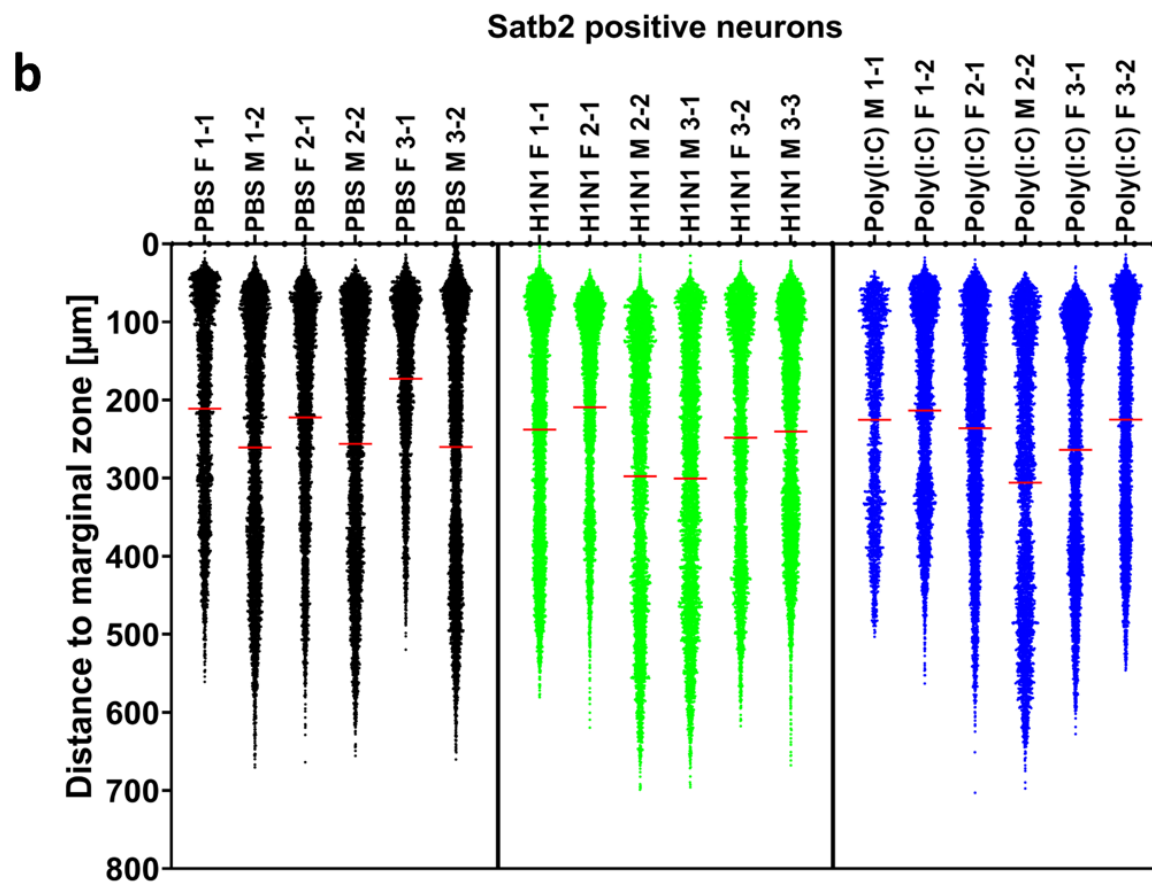
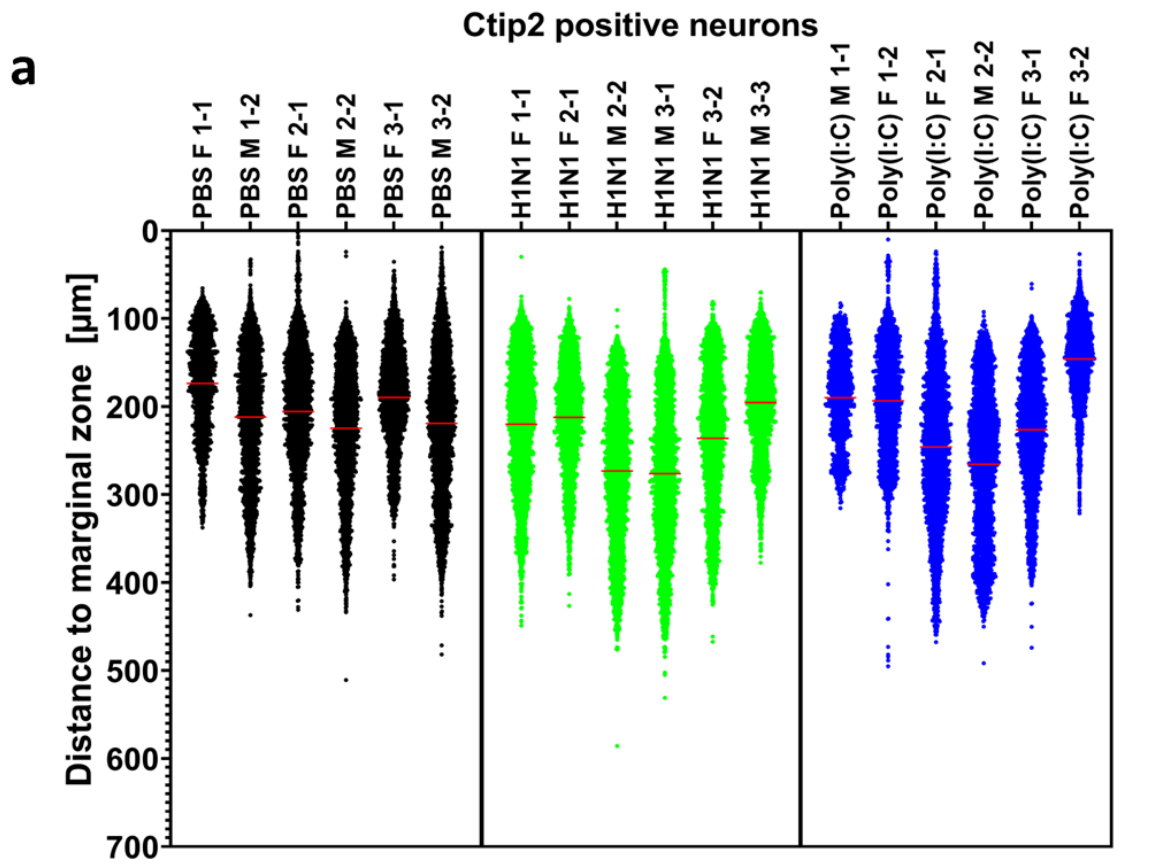
Supplementary Figure 11: Microglia velocity after LPS and Poly(I:C) treatment in situ.

12.1.1.11 Supplementary Figure 11: Microglia velocity after LPS and Poly(I:C) treatment in situ.

The velocity of microglia in the live imaging, displayed for the single experiments. Individual experiments showed a significant increase in velocity compared to their control (Kolmogorov-Smirnov test, a: Poly(I:C) P values: Exp 13 $p = 0.4736$, Exp 15 $p < 0.0001$, Exp 20 $p = 0.5346$, Exp 21 $p = 0.0164$; b: LPS P values: Exp 16 $p = 0.2027$, Exp 22 $p = 0.0081$, Exp 23 $p = 0.0359$, Exp 24 $p = 0.0003$).

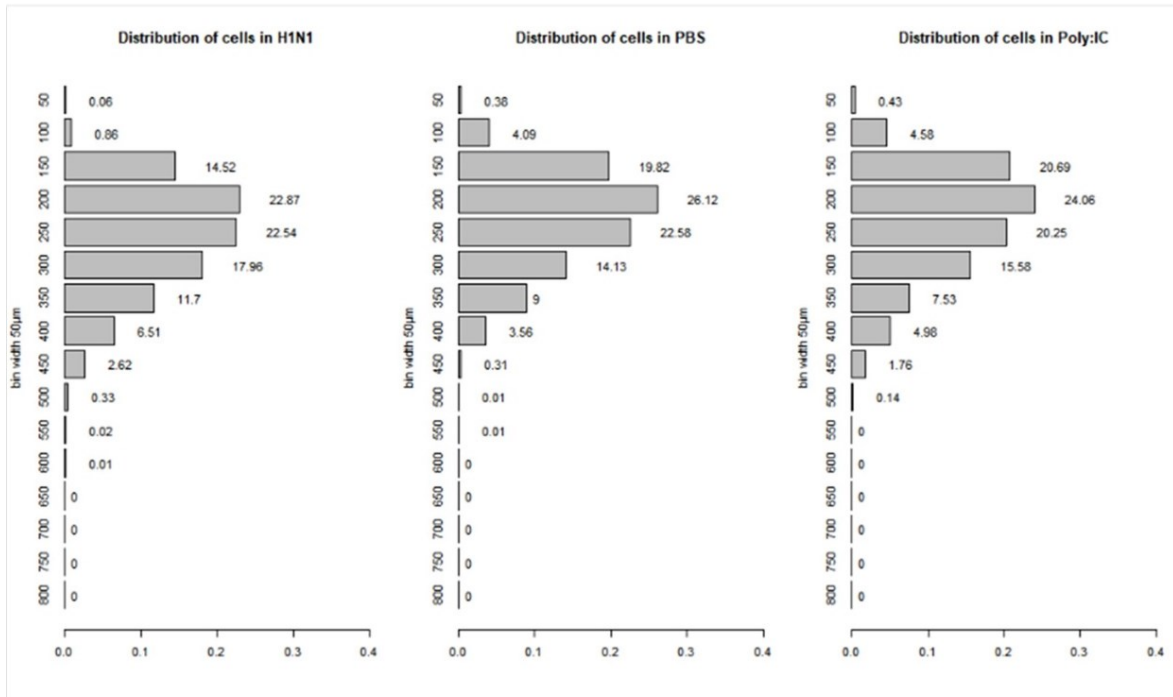
12.1.1.12 Supplementary Figure 12: Cortical layering after maternal immune activation.

The position of a) *ctip2* or b) *satb2* positive neurons in cortical slices after MIA is displayed as distance to the marginal zone. Displayed are the individual values for each embryo, consisting of 1-2 slices per brain. Embryos from H1N1 infected mothers are plotted in green (middle), embryos from mothers treated with PBS are plotted in black (left) and embryos from mothers treated with Poly(I:C) are plotted in blue (right).

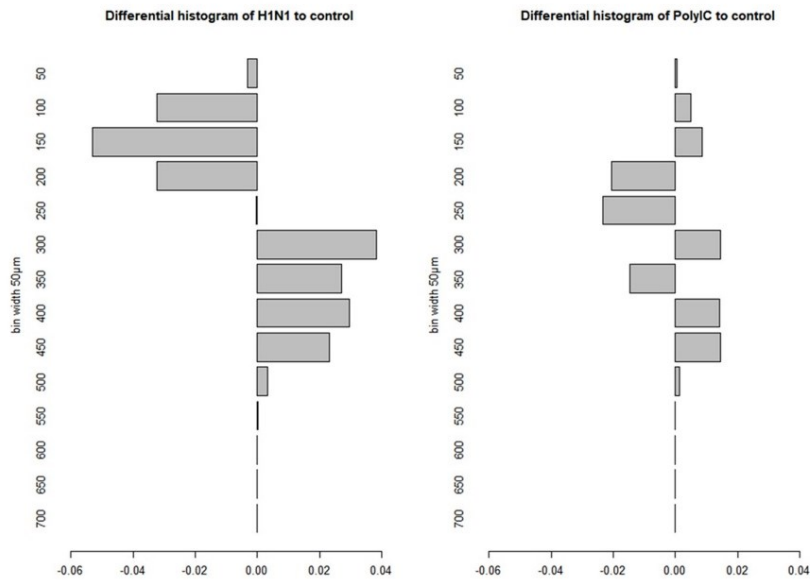


Supplementary Figure 12: Cortical layering after maternal immune activation.

a



b

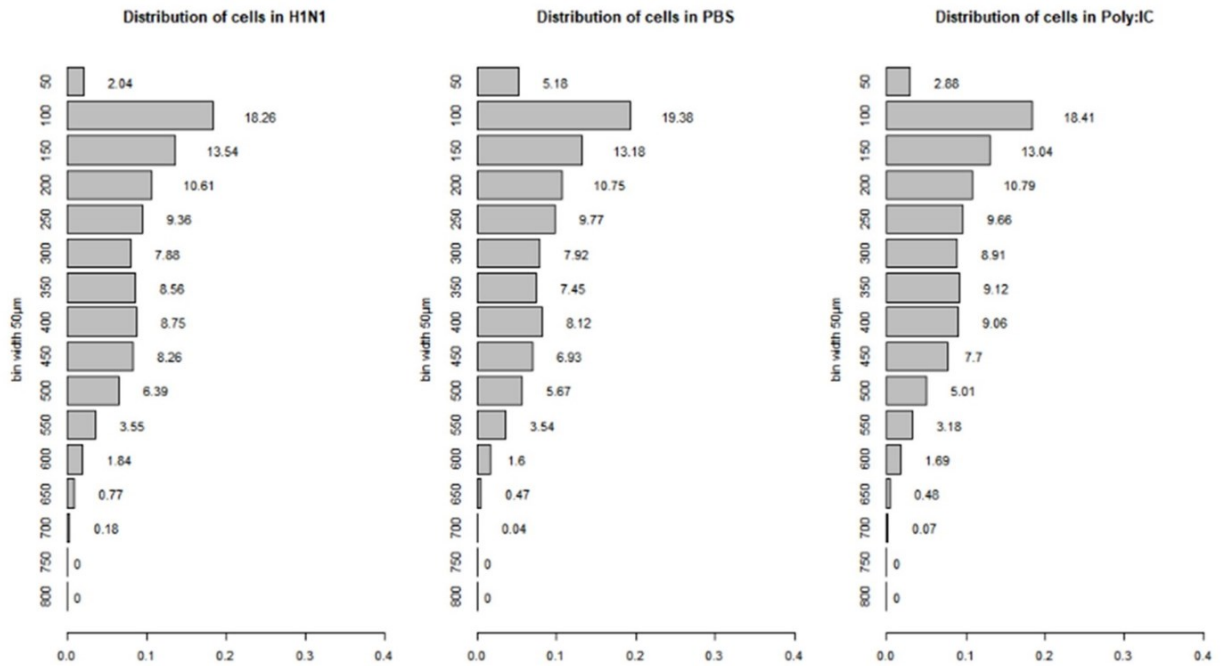


Supplementary Figure 13: Frequency distribution of *Ctip2* positive neurons.

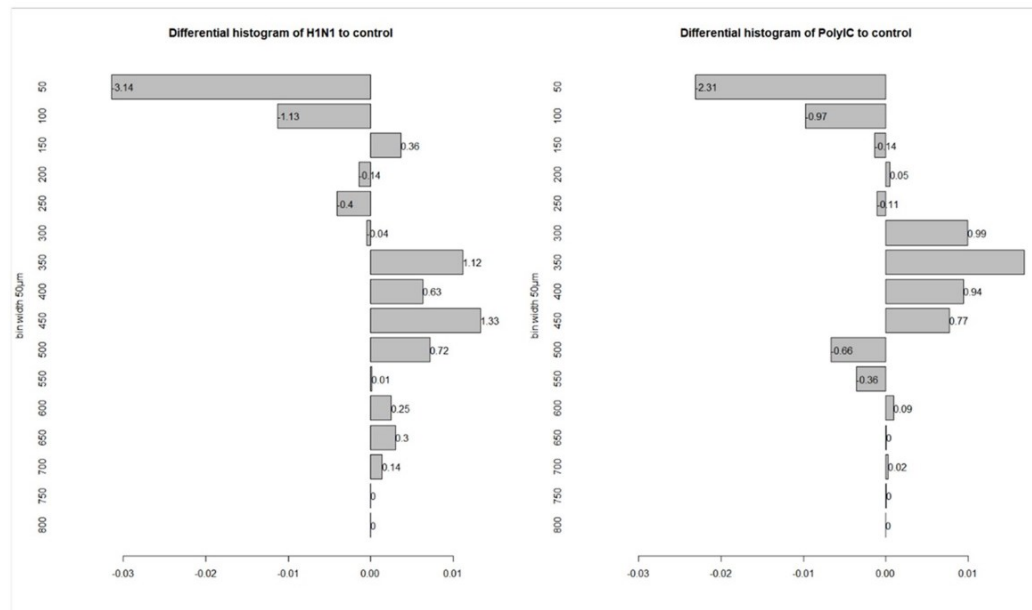
12.1.1.13 Supplementary Figure 13: Frequency distribution of *Ctip2* positive neurons.

The percental distribution of *ctip2* positive neurons is plotted in a, separated by the maternal treatment, and plotted in 50µm bins. In b, the difference for each bin between the maternally treated and untreated neurons is plotted with H1N1 infected mothers on the left and Poly(I:C) treated mothers on the right.

a



b



Supplementary Figure 14: Frequency distribution of *Satb2* positive neurons.

12.1.1.14 Supplementary Figure 14: Frequency distribution of *Satb2* positive neurons.

The percental distribution of *satb2* positive neurons is plotted in a, separated by the maternal treatment, and plotted in 50µm bins. In b, the difference for each bin between the maternally treated and untreated neurons is plotted with H1N1 infected mothers on the left and Poly(I:C) treated mothers on the right.

13 Literature

- Abu-Raya, B., Michalski, C., Sadarangani, M., & Lavoie, P. M. (2020). Maternal Immunological Adaptation During Normal Pregnancy. *Frontiers in Immunology*, *11*(October), 1–18. <https://doi.org/10.3389/fimmu.2020.575197>
- Acosta, J., Campolongo, M. A., Höcht, C., Depino, A. M., Golombek, D. A., & Agostino, P. V. (2018). Deficits in temporal processing in mice prenatally exposed to Valproic Acid. *European Journal of Neuroscience*, *47*(6), 619–630. <https://doi.org/10.1111/ejn.13621>
- Aguilera-Castrejon, A., Oldak, B., Shani, T., Ghanem, N., Itzkovich, C., Slomovich, S., Tarazi, S., Bayerl, J., Chugaeva, V., Ayyash, M., Ashouokhi, S., Sheban, D., Livnat, N., Lasman, L., Viukov, S., Zerbib, M., Addadi, Y., Rais, Y., Cheng, S., ... Hanna, J. H. (2021). Ex utero mouse embryogenesis from pre-gastrulation to late organogenesis. *Nature*, *593*(7857), 119–124. <https://doi.org/10.1038/s41586-021-03416-3>
- Aleman, S., Blok, E., Jansen, P. R., Muetzel, R. L., & White, T. (2021). Brain morphology, autistic traits, and polygenic risk for autism: A population-based neuroimaging study. *Autism Research*, *14*(10), 2085–2099. <https://doi.org/10.1002/aur.2576>
- Allen, N. J., & Lyons, D. A. (2018). Glia as architects of central nervous system formation and function. *Science*, *362*(6411), 181–185. <https://doi.org/10.1126/science.aat0473>
- Andoh, M., Shibata, K., Okamoto, K., Onodera, J., Morishita, K., Miura, Y., Ikegaya, Y., & Koyama, R. (2019). Exercise Reverses Behavioral and Synaptic Abnormalities after Maternal Inflammation. *Cell Reports*, *27*(10), 2817–2825.e5. <https://doi.org/10.1016/j.celrep.2019.05.015>
- Antonson, A. M., Lawson, M. A., Caputo, M. P., Matt, S. M., Leyshon, B. J., & Johnson, R. W. (2019). Maternal viral infection causes global alterations in porcine fetal microglia. *Proceedings of the National Academy of Sciences of the United States of America*, *116*(40), 20190–20200. <https://doi.org/10.1073/pnas.1817014116>
- Arai, Y., & Taverna, E. (2017). Neural progenitor cell polarity and cortical development. *Frontiers in Cellular Neuroscience*, *11*(December), 1–11. <https://doi.org/10.3389/fncel.2017.00384>
- Asperger, H. (1944). Die “Autistischen Psychopathen” im Kindesalter. Habilitationsschrift, eingereicht bei der medizinischen Fakultät der Wiener Universität. *Archiv Für Psychiatrie Und Nervenkrankheiten*, *117*(1), 76–136.
- Atladóttir, H. Ó., Pedersen, M. G., Thorsen, P., Mortensen, P. B., Deleuran, B., Eaton, W. W., & Parner, E. T. (2009). Association of family history of autoimmune diseases and autism spectrum disorders. *Pediatrics*, *124*(2), 687–694. <https://doi.org/10.1542/peds.2008-2445>
- Atladóttir, H. Ó., Thorsen, P., Østergaard, L., Schendel, D. E., Lemcke, S., Abdallah, M., & Parner, E. T. (2010). Maternal infection requiring hospitalization during pregnancy and autism spectrum disorders. *Journal of Autism and Developmental Disorders*, *40*(12), 1423–1430. <https://doi.org/10.1007/s10803-010-1006-y>
- Baghel, M. S., Singh, B., Dhuriya, Y. K., Shukla, R. K., Patro, N., Khanna, V. K., Patro, I. K., & Thakur, M. K. (2018). Postnatal exposure to poly (I:C) impairs learning and memory through changes in synaptic plasticity gene expression in developing rat brain. *Neurobiology of Learning and Memory*, *155*(December 2017), 379–389. <https://doi.org/10.1016/j.nlm.2018.09.005>
- Baines, K. J., Hillier, D. M., Haddad, F. L., Rajakumar, N., Schmid, S., & Renaud, S. J. (2020). Maternal Immune Activation Alters Fetal Brain Development and Enhances Proliferation of Neural Precursor Cells in Rats. *Frontiers in Immunology*, *11*(June). <https://doi.org/10.3389/fimmu.2020.01145>

- Banks, W. A. (2012). Brain meets body: The blood-brain barrier as an endocrine interface. *Endocrinology*, *153*(9), 4111–4119. <https://doi.org/10.1210/en.2012-1435>
- Bechmann, I., Kwidzinski, E., Kovac, A. D., Simbürger, E., Horvath, T., Gimsa, U., Dirnagl, U., Priller, J., & Nitsch, R. (2001). Turnover of rat brain perivascular cells. *Experimental Neurology*, *168*(2), 242–249. <https://doi.org/10.1006/exnr.2000.7618>
- Bergles, D. E., & Richardson, W. D. (2016). Oligodendrocyte Development and Plasticity. *Cold Spring Harbor Perspectives in Biology*, *8*(2), a020453. <https://doi.org/10.1101/cshperspect.a020453>
- Bertero, A., Liska, A., Pagani, M., Parolisi, R., Masferrer, M. E., Gritti, M., Pedrazzoli, M., Galbusera, A., Sarica, A., Cerasa, A., Buffelli, M., Tonini, R., Buffo, A., Gross, C., Pasqualetti, M., & Gozzi, A. (2018). Autism-associated 16p11.2 microdeletion impairs prefrontal functional connectivity in mouse and human. *Brain*, *141*(7), 2055–2065. <https://doi.org/10.1093/brain/awy111>
- Biever, A., Valjent, E., & Puighermanal, E. (2015). Ribosomal protein S6 phosphorylation in the nervous system: From regulation to function. *Frontiers in Molecular Neuroscience*, *8*(DEC), 1–14. <https://doi.org/10.3389/fnmol.2015.00075>
- Blizinsky, K. D., Diaz-Castro, B., Forrest, M. P., Schürmann, B., Bach, A. P., Martin-De-saavedra, M. D., Wang, L., Csernansky, J. G., Duan, J., & Penzes, P. (2016). Reversal of dendritic phenotypes in 16p11.2 microduplication mouse model neurons by pharmacological targeting of a network hub. *Proceedings of the National Academy of Sciences of the United States of America*, *113*(30), 8520–8525. <https://doi.org/10.1073/pnas.1607014113>
- Bölte, S., Girdler, S., & Marschik, P. B. (2019). The contribution of environmental exposure to the etiology of autism spectrum disorder. *Cellular and Molecular Life Sciences*, *76*(7), 1275–1297. <https://doi.org/10.1007/s00018-018-2988-4>
- Britanova, O., de Juan Romero, C., Cheung, A., Kwan, K. Y., Schwark, M., Gyorgy, A., Vogel, T., Akopov, S., Mitkovski, M., Agoston, D., Šestan, N., Molnár, Z., & Tarabykin, V. (2008). Satb2 Is a Postmitotic Determinant for Upper-Layer Neuron Specification in the Neocortex. *Neuron*, *57*(3), 378–392. <https://doi.org/10.1016/j.neuron.2007.12.028>
- Brucato, M., Ladd-Acosta, C., Li, M., Caruso, D., Hong, X., Kaczaniuk, J., Stuart, E. A., Fallin, M. D., & Wang, X. (2017). Prenatal exposure to fever is associated with autism spectrum disorder in the boston birth cohort. *Autism Research*, *10*(11), 1878–1890. <https://doi.org/10.1002/aur.1841>
- Cadwell, C. R., Bhaduri, A., Mostajo-Radji, M. A., Keefe, M. G., & Nowakowski, T. J. (2019). Development and Arealization of the Cerebral Cortex. *Neuron*, *103*(6), 980–1004. <https://doi.org/10.1016/j.neuron.2019.07.009>
- Calderon de Anda, F. (2013). Organotypic Slice Culture of Embryonic Brain Sections. *BIO-PROTOCOL*, *3*(3), 5–8. <https://doi.org/10.21769/BioProtoc.327>
- Calderon de Anda, F., & Gaertner, A. (2018). Editorial: Neuronal Polarity: Establishment and Maintenance. In *Frontiers in Cellular Neuroscience* (Vol. 12). <https://doi.org/10.3389/fncel.2018.00137>
- Canfield, R. L., Henderson, C. R., Cory-Slechta, D. A., Cox, C., Jusko, T. A., & Lanphear, B. P. (2003). Intellectual Impairment in Children with Blood Lead Concentrations below 10 µg per Deciliter. *New England Journal of Medicine*, *348*(16), 1517–1526. <https://doi.org/10.1056/NEJMoa022848>
- Carl Roth GmbH. (2021). *Safety data sheet Formaldehyde solution (Art. Nr. 4980)*. <https://www.carlroth.com/de/de/fixierung/formaldehydloesung-35-%25/p/4980.1>
- Carl Roth GmbH. (2022). *Safety data sheet Triton X 100 (Art. Nr. 3051)*. <https://www.carlroth.com/de/de/von-a-bis-z/triton-x-100/p/3051.2>

- Castelbaum, L., Sylvester, C. M., Zhang, Y., Yu, Q., & Constantino, J. N. (2020). On the Nature of Monozygotic Twin Concordance and Discordance for Autistic Trait Severity: A Quantitative Analysis. *Behavior Genetics*, *50*(4), 263–272. <https://doi.org/10.1007/s10519-019-09987-2>
- Caviness, V. S. (1982). Neocortical histogenesis in normal and reeler mice: A developmental study based upon [3H]thymidine autoradiography. *Developmental Brain Research*, *4*(3), 293–302. [https://doi.org/10.1016/0165-3806\(82\)90141-9](https://doi.org/10.1016/0165-3806(82)90141-9)
- Chao, M. W., Chen, C. P., Yang, Y. H., Chuang, Y. C., Chu, T. Y., & Tseng, C. Y. (2016). N-acetylcysteine attenuates lipopolysaccharide-induced impairment in lamination of Ctip2-and Tbr1-expressing cortical neurons in the developing rat fetal brain. *Scientific Reports*, *6*(March), 1–14. <https://doi.org/10.1038/srep32373>
- Chen, C., Lee, G. A., Pourmorady, A., Sock, E., & Donoghue, M. J. (2015). Orchestration of neuronal differentiation and progenitor pool expansion in the developing cortex by SoxC genes. *Journal of Neuroscience*, *35*(29), 10629–10642. <https://doi.org/10.1523/JNEUROSCI.1663-15.2015>
- Chen, V. S., Morrison, J. P., Southwell, M. F., Foley, J. F., Bolon, B., & Elmore, S. A. (2017). Histology Atlas of the Developing Prenatal and Postnatal Mouse Central Nervous System, with Emphasis on Prenatal Days E7.5 to E18.5. *Toxicologic Pathology*, *45*(6), 705–744. <https://doi.org/10.1177/0192623317728134>
- Chen, X., Liu, S., Goraya, M. U., Maarouf, M., Huang, S., & Chen, J. L. (2018). Host immune response to influenza A virus infection. *Frontiers in Immunology*, *9*(MAR), 1–13. <https://doi.org/10.3389/fimmu.2018.00320>
- Cheroni, C., Caporale, N., & Testa, G. (2020). Autism spectrum disorder at the crossroad between genes and environment: contributions, convergences, and interactions in ASD developmental pathophysiology. *Molecular Autism*, *11*(1), 69. <https://doi.org/10.1186/s13229-020-00370-1>
- Choi, G. B., Yim, Y. S., Wong, H., Kim, S., Kim, H., Kim, S. V., Hoeffler, C. A., Littman, D. R., & Huh, J. R. (2016). The maternal interleukin-17a pathway in mice promotes autism-like phenotypes in offspring. *Science*, *351*(6276), 933–939. <https://doi.org/10.1126/science.aad0314>
- Christensen, J., Grønberg, T. K., Sørensen, M. J., Schendel, D., Parner, E. T., Pedersen, L. H., & Vestergaard, M. (2013). Prenatal Valproate Exposure and Risk of Autism Spectrum Disorders and Childhood Autism. *JAMA*, *309*(16), 1696. <https://doi.org/10.1001/jama.2013.2270>
- Colombo, G., Cubero, R. J. A., Kanari, L., Venturino, A., Schulz, R., Scolamiero, M., Agerberg, J., Mathys, H., & Tsai, L. (2022). A tool for mapping microglial morphology, morphOMICs, reveals brain-region and sex-dependent phenotypes. *25*(October). <https://doi.org/10.1038/s41593-022-01167-6>
- Crawley, J. N. (2012). Translational animal models of autism and neurodevelopmental disorders. *Dialogues in Clinical Neuroscience*, *14*(3), 293–305. <https://doi.org/10.31887/dcns.2012.14.3/jcrawley>
- Crespo, Â. C., Mulik, S., Dotiwala, F., Ansara, J. A., Sen Santara, S., Ingersoll, K., Ovies, C., Junqueira, C., Tilburgs, T., Strominger, J. L., & Lieberman, J. (2020). Decidual NK Cells Transfer Granulysin to Selectively Kill Bacteria in Trophoblasts. *Cell*, *182*(5), 1125–1139.e18. <https://doi.org/10.1016/j.cell.2020.07.019>
- Cserép, C., Schwarcz, A. D., Pósfai, B., László, Z. I., Kellermayer, A., Környei, Z., Kisfali, M., Nyerges, M., Lele, Z., Katona, I., & Ádám Dénes. (2022). Microglial control of neuronal development via somatic purinergic junctions. *Cell Reports*, *40*(12), 111369. <https://doi.org/10.1016/j.celrep.2022.111369>
- Cunningham, C. L., Martínez-Cerdeño, V., & Noctor, S. C. (2013). Microglia regulate the number of neural precursor cells in the developing cerebral cortex. *Journal of Neuroscience*, *33*(10), 4216–

4233. <https://doi.org/10.1523/JNEUROSCI.3441-12.2013>

- Damisah, E. C., Hill, R. A., Rai, A., Chen, F., Rothlin, C. V., Ghosh, S., & Grutzendler, J. (2020). Astrocytes and microglia play orchestrated roles and respect phagocytic territories during neuronal corpse removal in vivo. *Science Advances*, *6*(26), 1–12. <https://doi.org/10.1126/sciadv.aba3239>
- Darnell, J. C., Van Driesche, S. J., Zhang, C., Hung, K. Y. S., Mele, A., Fraser, C. E., Stone, E. F., Chen, C., Fak, J. J., Chi, S. W., Licatalosi, D. D., Richter, J. D., & Darnell, R. B. (2011). FMRP stalls ribosomal translocation on mRNAs linked to synaptic function and autism. *Cell*, *146*(2), 247–261. <https://doi.org/10.1016/j.cell.2011.06.013>
- de Anda, F. C., Rosario, A. L., Durak, O., Tran, T., Gräff, J., Meletis, K., Rei, D., Soda, T., Madabhusi, R., Ginty, D. D., Kolodkin, A. L., & Tsai, L.-H. (2012). Autism spectrum disorder susceptibility gene TAOK2 affects basal dendrite formation in the neocortex. *Nature Neuroscience*, *15*(7), 1022–1031. <https://doi.org/10.1038/nn.3141>
- Delbridge, A. R. D., Huh, D., Brickelmaier, M., Burns, J. C., Roberts, C., Challa, R., Raymond, N., Cullen, P., Carlile, T. M., Ennis, K. A., Liu, M., Sun, C., Allaire, N. E., Foos, M., Tsai, H. H., Franchimont, N., Ransohoff, R. M., Butts, C., & Mingueneau, M. (2020). Organotypic Brain Slice Culture Microglia Exhibit Molecular Similarity to Acutely-Isolated Adult Microglia and Provide a Platform to Study Neuroinflammation. *Frontiers in Cellular Neuroscience*, *14*(December). <https://doi.org/10.3389/fncel.2020.592005>
- Delpech, J., Wei, L., Hao, J., Yu, X., Madore, C., Butovsky, O., & Kaffman, A. (2016). Early life stress perturbs the maturation of microglia in the developing hippocampus. *Brain, Behavior, and Immunity*, *57*, 79–93. <https://doi.org/10.1016/j.bbi.2016.06.006>
- Denny, K. J., Woodruff, T. M., Taylor, S. M., & Callaway, L. K. (2013). Complement in Pregnancy: A Delicate Balance. *American Journal of Reproductive Immunology*, *69*(1), 3–11. <https://doi.org/10.1111/aji.12000>
- Elgueta, D., Murgas, P., Riquelme, E., Yang, G., & Cancino, G. I. (2022). Consequences of Viral Infection and Cytokine Production During Pregnancy on Brain Development in Offspring. *Frontiers in Immunology*, *13*(April), 1–13. <https://doi.org/10.3389/fimmu.2022.816619>
- Ellul, P., Acquaviva, E., Peyre, H., Rosenzweig, M., Gressens, P., Klatzmann, D., & Delorme, R. (2022). Parental autoimmune and autoinflammatory disorders as multiple risk factors for common neurodevelopmental disorders in offspring: a systematic review and meta-analysis. *Translational Psychiatry*, *12*(1), 1–8. <https://doi.org/10.1038/s41398-022-01843-y>
- Estes, M. L., & McAllister, A. K. (2016). Maternal immune activation: Implications for neuropsychiatric disorders. *Science*, *353*(6301), 772–777. <https://doi.org/10.1126/science.aag3194>
- Etti, M., Calvert, A., Galiza, E., Lim, S., Khalil, A., Le Doare, K., & Heath, P. T. (2022). Maternal vaccination: a review of current evidence and recommendations. *American Journal of Obstetrics and Gynecology*, *226*(4), 459–474. <https://doi.org/10.1016/j.ajog.2021.10.041>
- Farhy-Tselnicker, I., & Allen, N. J. (2018). Astrocytes, neurons, synapses: A tripartite view on cortical circuit development. *Neural Development*, *13*(1), 1–12. <https://doi.org/10.1186/s13064-018-0104-y>
- Fernández de Cossío, L., Guzmán, A., van der Veldt, S., & Luheshi, G. N. (2017). Prenatal infection leads to ASD-like behavior and altered synaptic pruning in the mouse offspring. *Brain, Behavior, and Immunity*, *63*, 88–98. <https://doi.org/10.1016/j.bbi.2016.09.028>
- Fetit, R., Price, D. J., Lawrie, S. M., & Johnstone, M. (2020). Understanding the clinical manifestations of 16p11.2 deletion syndrome: a series of developmental case reports in children. *Psychiatric Genetics*, *30*(5), 136–140. <https://doi.org/10.1097/YPG.0000000000000259>

- Frazier, T. W., Thompson, L., Youngstrom, E. A., Law, P., Hardan, A. Y., Eng, C., & Morris, N. (2014). A twin study of heritable and shared environmental contributions to autism. *Journal of Autism and Developmental Disorders*, *44*(8), 2013–2025. <https://doi.org/10.1007/s10803-014-2081-2>
- Frotscher, M., Zhao, S., Wang, S., & Chai, X. (2017). Reelin signaling inactivates cofilin to stabilize the cytoskeleton of migrating cortical neurons. *Frontiers in Cellular Neuroscience*, *11*(May), 1–7. <https://doi.org/10.3389/fncel.2017.00148>
- Gallagher, D., Norman, A. A., Woodard, C. L., Yang, G., Gauthier-Fisher, A., Fujitani, M., Vessey, J. P., Cancino, G. I., Sachewsky, N., Woltjen, K., Fatt, M. P., Morshead, C. M., Kaplan, D. R., & Miller, F. D. (2013). Transient maternal IL-6 mediates long-lasting changes in neural stem cell pools by deregulating an endogenous self-renewal pathway. *Cell Stem Cell*, *13*(5), 564–576. <https://doi.org/10.1016/j.stem.2013.10.002>
- Garcez, P. P., Loiola, E. C., Da Costa, R. M., Higa, L. M., Trindade, P., Delvecchio, R., Nascimento, J. M., Brindeiro, R., Tanuri, A., & Rehen, S. K. (2016). Zika virus: Zika virus impairs growth in human neurospheres and brain organoids. *Science*, *352*(6287), 816–818. <https://doi.org/10.1126/science.aaf6116>
- Ge, W. P., Miyawaki, A., Gage, F. H., Jan, Y. N., & Jan, L. Y. (2012). Local generation of glia is a major astrocyte source in postnatal cortex. *Nature*, *484*(7394), 376–380. <https://doi.org/10.1038/nature10959>
- Ginhoux, F., Greter, M., Leboeuf, M., Nandi, S., See, P., Gokhan, S., Mehler, M. F., Conway, S. J., Ng, L. G., Stanley, E. R., Samokhvalov, I. M., & Merad, M. (2010). Fate mapping analysis reveals that adult microglia derive from primitive macrophages. *Science*, *330*(6005), 841–845. <https://doi.org/10.1126/science.1194637>
- Gładysz, D., Krzywdzińska, A., & Hozyasz, K. K. (2018). Immune Abnormalities in Autism Spectrum Disorder—Could They Hold Promise for Causative Treatment? *Molecular Neurobiology*, *55*(8), 6387–6435. <https://doi.org/10.1007/s12035-017-0822-x>
- Goasdoué, K., Miller, S. M., Colditz, P. B., & Björkman, S. T. (2017). Review: The blood-brain barrier; protecting the developing fetal brain. *Placenta*, *54*, 111–116. <https://doi.org/10.1016/j.placenta.2016.12.005>
- Gomes, A. K. S., Dantas, R. M., Yokota, B. Y., Silva, A. L. T. e., Griesi-Oliveira, K., Passos-Bueno, M. R., & Sertié, A. L. (2022). Interleukin-17a Induces Neuronal Differentiation of Induced-Pluripotent Stem Cell-Derived Neural Progenitors From Autistic and Control Subjects. *Frontiers in Neuroscience*, *16*(March), 1–10. <https://doi.org/10.3389/fnins.2022.828646>
- Gordon, A., & Geschwind, D. H. (2020). Human in vitro models for understanding mechanisms of autism spectrum disorder. *Molecular Autism*, *11*(1). <https://doi.org/10.1186/s13229-020-00332-7>
- GraphPad Software LLC. (2022). *GraphPad Prism* (GraphPad Prism 9 for Windows 64-bit).
- Griffiths, S. K., & Campbell, J. P. (2015). Placental structure, function and drug transfer. *Continuing Education in Anaesthesia, Critical Care and Pain*, *15*(2), 84–89. <https://doi.org/10.1093/bjaceaccp/mku013>
- Hansen, A. H., Duellberg, C., Mieck, C., Loose, M., & Hippenmeyer, S. (2017). Cell polarity in cerebral cortex development—cellular architecture shaped by biochemical networks. *Frontiers in Cellular Neuroscience*, *11*(June), 1–16. <https://doi.org/10.3389/fncel.2017.00176>
- Harb, K., Magrinelli, E., Nicolas, C. S., Lukianets, N., Frangeul, L., Pietri, M., Sun, T., Sandoz, G., Grammont, F., Jabaudon, D., Studer, M., & Alfano, C. (2016). Area-specific development of distinct projection neuron subclasses is regulated by postnatal epigenetic modifications. *ELife*,

- 5(JANUARY2016), 1–25. <https://doi.org/10.7554/eLife.09531>
- Harris, K. D., & Shepherd, G. M. G. (2015). The neocortical circuit: Themes and variations. *Nature Neuroscience*, *18*(2), 170–181. <https://doi.org/10.1038/nn.3917>
- Hattori, Y., & Miyata, T. (2018). Embryonic neocortical microglia express toll-like receptor 9 and respond to plasmid DNA injected into the ventricle: Technical considerations regarding microglial distribution in electroporated brain walls. *ENeuro*, *5*(6), 1–15. <https://doi.org/10.1523/ENEURO.0312-18.2018>
- Hattori, Y., Naito, Y., Tsugawa, Y., Nonaka, S., Wake, H., Nagasawa, T., Kawaguchi, A., & Miyata, T. (2020). Transient microglial absence assists postmigratory cortical neurons in proper differentiation. *Nature Communications*, *11*(1). <https://doi.org/10.1038/s41467-020-15409-3>
- Hayes, L. N., An, K., Carloni, E., Li, F., Vincent, E., Trippaers, C., Paranjpe, M., Dölen, G., Goff, L. A., & Ramos, A. (2022). *Prenatal immune stress blunts microglia reactivity , impairing neurocircuitry. May 2019.* <https://doi.org/10.1038/s41586-022-05274-z>
- Haynes, S. E., Hollopeter, G., Yang, G., Kurpius, D., Dailey, M. E., Gan, W. B., & Julius, D. (2006). The P2Y₁₂ receptor regulates microglial activation by extracellular nucleotides. *Nature Neuroscience*, *9*(12), 1512–1519. <https://doi.org/10.1038/nn1805>
- Holt, P. G., & Jones, C. A. (2000). The development of the immune system during pregnancy and early life. *Allergy: European Journal of Allergy and Clinical Immunology*, *55*(8), 688–697. <https://doi.org/10.1034/j.1398-9995.2000.00118.x>
- Holt, R., Barnby, G., Maestrini, E., Bacchelli, E., Brocklebank, D., Sousa, I., Mulder, E. J., Kantojärvi, K., Järvelä, I., Klauck, S. M., Poustka, F., Bailey, A. J., & Monaco, A. P. (2010). Linkage and candidate gene studies of autism spectrum disorders in European populations. *European Journal of Human Genetics*, *18*(9), 1013–1020. <https://doi.org/10.1038/ejhg.2010.69>
- Hossain, Z., Reza, A. H. M. M., Qasem, W. A., Friel, J. K., & Omri, A. (2022). Development of the immune system in the human embryo. *Pediatric Research, November 2021*, 1–5. <https://doi.org/10.1038/s41390-022-01940-0>
- Huang, Y., Li, G., An, L., Fan, Y., Cheng, X., Li, X., Yin, Y., Cong, R., Chen, S., & Zhao, S. (2017). Fyn regulates multipolar–bipolar transition and neurite morphogenesis of migrating neurons in the developing neocortex. *Neuroscience*, *352*, 39–51. <https://doi.org/10.1016/j.neuroscience.2017.03.032>
- Hughes, H. K., Mills Ko, E., Rose, D., & Ashwood, P. (2018). Immune Dysfunction and Autoimmunity as Pathological Mechanisms in Autism Spectrum Disorders. *Frontiers in Cellular Neuroscience*, *12*(November), 1–26. <https://doi.org/10.3389/fncel.2018.00405>
- Humann, J., Mann, B., Gao, G., Moresco, P., Ramahi, J., Loh, L. N., Farr, A., Hu, Y., Durick-Eder, K., Fillon, S. A., Smeyne, R. J., & Tuomanen, E. I. (2016). Bacterial Peptidoglycan Transverses the Placenta to Induce Fetal Neuroproliferation and Aberrant Postnatal Behavior. *Cell Host and Microbe*, *19*(3), 388–399. <https://doi.org/10.1016/j.chom.2016.02.009>
- Imai, Y., Iбата, I., Ito, D., Ohsawa, K., & Kohsaka, S. (1996). A novel gene *iba1* in the major histocompatibility complex class III region encoding an EF hand protein expressed in a monocytic lineage. *Biochemical and Biophysical Research Communications*, *224*(3), 855–862. <https://doi.org/10.1006/bbrc.1996.1112>
- Itoh, Y. (2016). A balancing Akt: How to fine-tune neuronal migration speed. *Neurogenesis*, *3*(1), 1–7. <https://doi.org/10.1080/23262133.2016.1256854>
- Jacobsen, H., Walendy-Gnirß, K., Tekin-Bubenheim, N., Kouassi, N. M., Ben-Batalla, I., Berenbrok, N.,

- Wolff, M., dos Reis, V. P., Zickler, M., Scholl, L., Gries, A., Jania, H., Kloetgen, A., Düsedau, A., Pilnitz-Stolze, G., Jeridi, A., Yildirim, A. Ö., Fuchs, H., Gailus-Durner, V., ... Gabriel, G. (2021). Offspring born to influenza A virus infected pregnant mice have increased susceptibility to viral and bacterial infections in early life. *Nature Communications*, *12*(1). <https://doi.org/10.1038/s41467-021-25220-3>
- Johansson, S., Bohman, S., Radesäter, A. C., Öberg, C., & Luthman, J. (2005). Salmonella lipopolysaccharide (LPS) mediated neurodegeneration in hippocampal slice cultures. *Neurotoxicity Research*, *8*(3–4), 207–220. <https://doi.org/10.1007/BF03033974>
- Jurga, A. M., Paleczna, M., & Kuter, K. Z. (2020). Overview of General and Discriminating Markers of Differential Microglia Phenotypes. *Frontiers in Cellular Neuroscience*, *14*(August), 1–18. <https://doi.org/10.3389/fncel.2020.00198>
- Kaiser, T., & Feng, G. (2019). Tmem119-EGFP and Tmem119-CreERT2 Transgenic Mice for Labeling and Manipulating Microglia. *Eneuro*, *6*(4), ENEURO.0448-18.2019. <https://doi.org/10.1523/eneuro.0448-18.2019>
- Kanner, L. (1943). Autistic Disturbances of affective contact. *Pathology*, 1–34. <file:///Users/MT/Dropbox/Library.papers3/Files/5E/5E14FA8B-E29C-4C26-AF6A-E49132B1F03E.pdf%5Cpapers3://publication/uuid/67CCEE9E-8FDD-48D1-B66A-892D550AC1B1>
- Kapfhamer, D., Taylor, S., Zou, M. E., Lim, J. P., Kharazia, V., & Heberlein, U. (2013). Taok2 controls behavioral response to ethanol in mice. *Genes, Brain and Behavior*, *12*(1), 87–97. <https://doi.org/10.1111/j.1601-183X.2012.00834.x>
- Kawauchi, T., Chihama, K., Nabeshima, Y. I., & Hoshino, M. (2003). The in vivo roles of STEF/Tiam1, Rac1 and JNK in cortical neuronal migration. *EMBO Journal*, *22*(16), 4190–4201. <https://doi.org/10.1093/emboj/cdg413>
- Kwan, K. Y., Šestan, N., & Anton, E. S. (2012). Transcriptional co-regulation of neuronal migration and laminar identity in the neocortex. *Development*, *139*(9), 1535–1546. <https://doi.org/10.1242/dev.069963>
- Lautarescu, A., Craig, M. C., & Glover, V. (2020). Prenatal stress: Effects on fetal and child brain development. In *International Review of Neurobiology* (1st ed., Vol. 150). Elsevier Inc. <https://doi.org/10.1016/bs.irn.2019.11.002>
- Lehnardt, S., Massillon, L., Follett, P., Jensen, F. E., Ratan, R., Rosenberg, P. A., Volpe, J. J., & Vartanian, T. (2003). Activation of innate immunity in the CNS triggers neurodegeneration through a Toll-like receptor 4-dependent pathway. *Proceedings of the National Academy of Sciences of the United States of America*, *100*(14), 8514–8519. <https://doi.org/10.1073/pnas.1432609100>
- Leow-Dyke, S., Allen, C., Denes, A., Nilsson, O., Maysami, S., Bowie, A. G., Rothwell, N. J., & Pinteaux, E. (2012). Neuronal toll-like receptor 4 signaling induces brain endothelial activation and neutrophil transmigration in vitro. *Journal of Neuroinflammation*, *9*, 1–11. <https://doi.org/10.1186/1742-2094-9-230>
- Lier, J., Streit, W. J., & Bechmann, I. (2021). Beyond activation: Characterizing microglial functional phenotypes. *Cells*, *10*(9), 1–13. <https://doi.org/10.3390/cells10092236>
- Lim, A. I., McFadden, T., Link, V. M., Han, S. J., Karlsson, R. M., Stacy, A., Farley, T. K., Lima-Junior, D. S., Harrison, O. J., Desai, J. V., Lionakis, M. S., Shih, H. Y., Cameron, H. A., & Belkaid, Y. (2021). Prenatal maternal infection promotes tissue-specific immunity and inflammation in offspring. *Science*, *373*(6558). <https://doi.org/10.1126/science.abf3002>
- Liong, S., Oseghale, O., To, E. E., Brassington, K., Erlich, J. R., Luong, R., Liong, F., Brooks, R., Martin, C.,

- O'Toole, S., Vinh, A., O'Neill, L. A. J., Bozinovski, S., Vlahos, R., Papagianis, P. C., O'Leary, J. J., Brooks, D. A., & Selemidis, S. (2020). Influenza A virus causes maternal and fetal pathology via innate and adaptive vascular inflammation in mice. *Proceedings of the National Academy of Sciences of the United States of America*, *117*(40), 24964–24973. <https://doi.org/10.1073/pnas.2006905117>
- Lossi, L., Castagna, C., Granato, A., & Merighi, A. (2019). The Reeler mouse: A translational model of human neurological conditions, or simply a good tool for better understanding neurodevelopment? *Journal of Clinical Medicine*, *8*(12). <https://doi.org/10.3390/jcm8122088>
- Lyall, K., Ashwood, P., Van De Water, J., & Hertz-Picciotto, I. (2014). Maternal immune-mediated conditions, autism spectrum disorders, and developmental delay. *Journal of Autism and Developmental Disorders*, *44*(7), 1546–1555. <https://doi.org/10.1007/s10803-013-2017-2>
- Ma, L., Wang, J., Ge, J., Wang, Y., Zhang, W., Du, Y., Luo, J., Li, Y., Wang, F., Fan, G., Chen, R., Yao, B., Zhao, Z., Guo, M., Kim, W., Chai, Y., & Chen, J. (2021). Reversing neural circuit and behavior deficit in mice exposed to maternal inflammation by Zika virus. *EMBO Reports*, *22*(8), 1–17. <https://doi.org/10.15252/embr.202051978>
- Marín, O., Valiente, M., Ge, X., & Tsai, L. H. (2010). Guiding neuronal cell migrations. *Cold Spring Harbor Perspectives in Biology*, *2*(2), 1–21. <https://doi.org/10.1101/cshperspect.a001834>
- Marques, V. de M., Santos, C. S., Santiago, I. G., Marques, S. M., Nunes Brasil, M. das G., Lima, T. T., & Costa, P. S. (2019). Neurological Complications of Congenital Zika Virus Infection. *Pediatric Neurology*, *91*, 3–10. <https://doi.org/10.1016/j.pediatrneurol.2018.11.003>
- McGann, J. P. (2017). Poor human olfaction is a nineteenth century myth. *Science*, *356*(6338), 1–17. <https://doi.org/10.1126/science.aam7263>
- Meyer, U. (2014). Prenatal Poly(I:C) exposure and other developmental immune activation models in rodent systems. *Biological Psychiatry*, *75*(4), 307–315. <https://doi.org/10.1016/j.biopsych.2013.07.011>
- Meyer, U., Nyffeler, M., Yee, B. K., Knuesel, I., & Feldon, J. (2008). Adult brain and behavioral pathological markers of prenatal immune challenge during early/middle and late fetal development in mice. *Brain, Behavior, and Immunity*, *22*(4), 469–486. <https://doi.org/10.1016/j.bbi.2007.09.012>
- Michetti, C., Romano, E., Altabella, L., Caruso, A., Castelluccio, P., Bedse, G., Gaetani, S., Canese, R., Laviola, G., & Scattoni, M. L. (2014). Mapping pathological phenotypes in reelin mutant mice. *Frontiers in Pediatrics*, *2*(SEP). <https://doi.org/10.3389/fped.2014.00095>
- Mildner, A., Huang, H., Radke, J., Stenzel, W., & Priller, J. (2017). P2Y12 receptor is expressed on human microglia under physiological conditions throughout development and is sensitive to neuroinflammatory diseases. *Glia*, *65*(2), 375–387. <https://doi.org/10.1002/glia.23097>
- Miyamoto, A., Wake, H., Ishikawa, A. W., Eto, K., Shibata, K., Murakoshi, H., Koizumi, S., Moorhouse, A. J., Yoshimura, Y., & Nabekura, J. (2016). Microglia contact induces synapse formation in developing somatosensory cortex. *Nature Communications*, *7*, 1–12. <https://doi.org/10.1038/ncomms12540>
- Mogensen, T. H. (2009). Pathogen recognition and inflammatory signaling in innate immune defenses. *Clinical Microbiology Reviews*, *22*(2), 240–273. <https://doi.org/10.1128/CMR.00046-08>
- Molho-Pessach, V., Ramot, Y., Mogilevsky, M., Cohen-Daniel, L., Eisenstein, E. M., Abu-Libdeh, A., Siam, I., Berger, M., Karni, R., & Zlotogorski, A. (2017). Generalized verrucosis and abnormal T cell activation due to homozygous TAOK2 mutation. *Journal of Dermatological Science*, *87*(2), 123–129. <https://doi.org/10.1016/j.jdermsci.2017.03.018>

- Molnár, Z., Clowry, G. J., Šestan, N., Alzu'bi, A., Bakken, T., Hevner, R. F., Hüppi, P. S., Kostović, I., Rakic, P., Anton, E. S., Edwards, D., Garcez, P., Hoerder-Suabedissen, A., & Kriegstein, A. (2019). New insights into the development of the human cerebral cortex. *Journal of Anatomy*, *235*(3), 432–451. <https://doi.org/10.1111/joa.13055>
- Morimoto, K., & Nakajima, K. (2019). Role of the Immune System in the Development of the Central Nervous System. *Frontiers in Neuroscience*, *13*(September). <https://doi.org/10.3389/fnins.2019.00916>
- Mrdjen, D., Pavlovic, A., Hartmann, F. J., Schreiner, B., Utz, S. G., Leung, B. P., Lelios, I., Heppner, F. L., Kipnis, J., Merkler, D., Greter, M., & Becher, B. (2018). High-Dimensional Single-Cell Mapping of Central Nervous System Immune Cells Reveals Distinct Myeloid Subsets in Health, Aging, and Disease. *Immunity*, *48*(2), 380-395.e6. <https://doi.org/10.1016/j.immuni.2018.01.011>
- Mukhtar, T., & Taylor, V. (2018). Untangling Cortical Complexity During Development. *Journal of Experimental Neuroscience*, *12*. <https://doi.org/10.1177/1179069518759332>
- Muraskas, J., Astrug, L., & Amin, S. (2020). FIRS: Neonatal considerations. *Seminars in Fetal and Neonatal Medicine*, *25*(4), 101142. <https://doi.org/10.1016/j.siny.2020.101142>
- Murphy, K., & Weaver, C. (2018). Janeway Immunologie. In *Janeway Immunologie*. Springer Berlin Heidelberg. <https://doi.org/10.1007/978-3-662-56004-4>
- Nadarajah, B., Brunstrom, J. E., Grutzendler, J., Wong, R. O. L., & Pearlman, A. L. (2001). Two modes of radial migration in early development of the cerebral cortex. *Nature Neuroscience*, *4*(2), 143–150. <https://doi.org/10.1038/83967>
- National center for the Replacement Refinement and Reduction of Animals in Research. (n.d.). *The 3Rs*. <https://nc3rs.org.uk/who-we-are/3rs>
- Noctor, S. C., Martínez-cerdeño, V., Ivic, L., & Kriegstein, A. R. (2004). Cortical neurons arise in symmetric and asymmetric division zones and migrate through specific phases. *Nature Neuroscience*, *7*(2), 136–144. <https://doi.org/10.1038/nn1172>
- Noctor, S. C., Penna, E., Shepherd, H., Chelson, C., Barger, N., Martínez-Cerdeño, V., & Tarantal, A. F. (2019). Periventricular microglial cells interact with dividing precursor cells in the nonhuman primate and rodent prenatal cerebral cortex. *Journal of Comparative Neurology*, *527*(10), 1598–1609. <https://doi.org/10.1002/cne.24604>
- Nomura, T., Yamashita, W., Gotoh, H., & Ono, K. (2018). Species-Specific Mechanisms of Neuron Subtype Specification Reveal Evolutionary Plasticity of Amniote Brain Development. *Cell Reports*, *22*(12), 3142–3151. <https://doi.org/10.1016/j.celrep.2018.02.086>
- O'Loughlin, E., Pakan, J. M. P., Yilmazer-Hanke, D., & McDermott, K. W. (2017). Acute in utero exposure to lipopolysaccharide induces inflammation in the pre- and postnatal brain and alters the glial cytoarchitecture in the developing amygdala. *Journal of Neuroinflammation*, *14*(1), 1–12. <https://doi.org/10.1186/s12974-017-0981-8>
- Ohsawa, K., Imai, Y., Kanazawa, H., Sasaki, Y., & Kohsaka, S. (2000). Involvement of Iba1 in membrane ruffling and phagocytosis of macrophages/microglia. *Journal of Cell Science*, *113*(17), 3073–3084. <https://doi.org/10.1242/jcs.113.17.3073>
- Ohsawa, K., Imai, Y., Sasaki, Y., & Kohsaka, S. (2004). Microglia/macrophage-specific protein Iba1 binds to fimbrin and enhances its actin-bundling activity. *Journal of Neurochemistry*, *88*(4), 844–856. <https://doi.org/10.1046/j.1471-4159.2003.02213.x>
- Onore, C. E., Schwartz, J. J., Careaga, M., Berman, R. F., & Ashwood, P. (2014). Maternal immune activation leads to activated inflammatory macrophages in offspring. *Brain, Behavior, and*

- Immunity*, 38(1), 220–226. <https://doi.org/10.1016/j.bbi.2014.02.007>
- Pan, Y. H., Wu, N., & Yuan, X. B. (2019). Toward a better understanding of neuronal migration deficits in autism spectrum disorders. *Frontiers in Cell and Developmental Biology*, 7(SEP), 1–8. <https://doi.org/10.3389/fcell.2019.00205>
- Papageorgiou, I. E., Lewen, A., Galow, L. V., Cesetti, T., Scheffel, J., Regen, T., Hanisch, U. K., & Kann, O. (2016). TLR4-activated microglia require IFN- γ to induce severe neuronal dysfunction and death in situ. *Proceedings of the National Academy of Sciences of the United States of America*, 113(1), 212–217. <https://doi.org/10.1073/pnas.1513853113>
- Paridaen, J. T., & Huttner, W. B. (2014). Neurogenesis during development of the vertebrate central nervous system. *EMBO Reports*, 15(4), 351–364. <https://doi.org/10.1002/embr.201438447>
- Park, J. E., Jardine, L., Gottgens, B., Teichmann, S. A., & Haniffa, M. (2020). Prenatal development of human immunity. *Science*, 368(6491), 600–603. <https://doi.org/10.1126/science.aaz9330>
- Piet, R., Vargová, L., Syková, E., Poulain, D. A., & Oliet, S. H. R. (2004). Physiological contribution of the astrocytic environment of neurons to intersynaptic crosstalk. *Proceedings of the National Academy of Sciences of the United States of America*, 101(7), 2151–2155. <https://doi.org/10.1073/pnas.0308408100>
- Pucilowska, J., Vithayathil, J., Tavares, E. J., Kelly, C., Karlo, J. C., & Landreth, G. E. (2015). The 16p11.2 Deletion Mouse Model of Autism Exhibits Altered Cortical Progenitor Proliferation and Brain Cytoarchitecture Linked to the ERK MAPK Pathway. *Journal of Neuroscience*, 35(7), 3190–3200. <https://doi.org/10.1523/jneurosci.4864-13.2015>
- Puntambekar, S. S., Davis, D. S., Hawel, L., Crane, J., Byus, C. V., & Carson, M. J. (2011). LPS-induced CCL2 expression and macrophage influx into the murine central nervous system is polyamine-dependent. *Brain, Behavior, and Immunity*, 25(4), 629–639. <https://doi.org/10.1016/j.bbi.2010.12.016>
- Purves, D., Augustine, G. J., Fitzpatrick, D., Hall, W. C., LaMantia, A.-S., Mooney, R. D., Platt, M. L., & White, L. E. (Eds.). (2018). *Neuroscience* (sixth). Sunderland, Massachusetts : Oxford University Press.
- Rasband, W. (2022). (*FIJI Is Just*) *ImageJ* (ImageJ 1.53r). National Institutes of Health, USA.
- Reemst, K., Noctor, S. C., Lucassen, P. J., & Hol, E. M. (2016). The indispensable roles of microglia and astrocytes during brain development. *Frontiers in Human Neuroscience*, 10(NOV2016), 1–28. <https://doi.org/10.3389/fnhum.2016.00566>
- Rezaie, P., & Male, D. (1999). Colonisation of the developing human brain and spinal cord by microglia: A review. *Microscopy Research and Technique*, 45(6), 359–382. [https://doi.org/10.1002/\(SICI\)1097-0029\(19990615\)45:6<359::AID-JEMT4>3.0.CO;2-D](https://doi.org/10.1002/(SICI)1097-0029(19990615)45:6<359::AID-JEMT4>3.0.CO;2-D)
- Richter, M., Murtaza, N., Scharrenberg, R., White, S. H., Johanns, O., Walker, S., Yuen, R. K. C., Schwanke, B., Bedürftig, B., Henis, M., Scharf, S., Kraus, V., Dörk, R., Hellmann, J., Lindenmaier, Z., Ellegood, J., Hartung, H., Kwan, V., Sedlacik, J., ... Calderon de Anda, F. (2018). Altered TAOK2 activity causes autism-related neurodevelopmental and cognitive abnormalities through RhoA signaling. *Molecular Psychiatry*. <https://doi.org/10.1038/s41380-018-0025-5>
- Ritchie, L., Tate, R., Chamberlain, L. H., Robertson, G., Zagnoni, M., Sposito, T., Wray, S., Wright, J. A., Bryant, C. E., Gay, N. J., & Bushnell, T. J. (2018). Toll-like receptor 3 activation impairs excitability and synaptic activity via TRIF signalling in immature rat and human neurons. *Neuropharmacology*, 135, 1–10. <https://doi.org/10.1016/j.neuropharm.2018.02.025>
- Rodgers, K. R., Lin, Y., Langan, T. J., Iwakura, Y., & Chou, R. C. (2020). Innate Immune Functions of

- Astrocytes are Dependent Upon Tumor Necrosis Factor-Alpha. *Scientific Reports*, 10(1), 1–15. <https://doi.org/10.1038/s41598-020-63766-2>
- Sacco, R., Gabriele, S., & Persico, A. M. (2015). Head circumference and brain size in autism spectrum disorder: A systematic review and meta-analysis. *Psychiatry Research - Neuroimaging*, 234(2), 239–251. <https://doi.org/10.1016/j.psychres.2015.08.016>
- Satoh, J. ichi, Kino, Y., Asahina, N., Takitani, M., Miyoshi, J., Ishida, T., & Saito, Y. (2016). TMEM119 marks a subset of microglia in the human brain. *Neuropathology*, 36(1), 39–49. <https://doi.org/10.1111/neup.12235>
- Satterstrom, F. K., Kosmicki, J. A., Wang, J., Breen, M. S., De Rubeis, S., An, J. Y., Peng, M., Collins, R., Grove, J., Klei, L., Stevens, C., Reichert, J., Mulhern, M. S., Artomov, M., Gerges, S., Sheppard, B., Xu, X., Bhaduri, A., Norman, U., ... Buxbaum, J. D. (2020). Large-Scale Exome Sequencing Study Implicates Both Developmental and Functional Changes in the Neurobiology of Autism. *Cell*, 180(3), 568-584.e23. <https://doi.org/10.1016/j.cell.2019.12.036>
- Scharrenberg, R., Richter, M., Johanns, O., Meka, D. P., Rücker, T., Murtaza, N., Lindenmaier, Z., Ellegood, J., Naumann, A., Zhao, B., Schwanke, B., Sedlacik, J., Fiehler, J., Hanganu-Opatz, I. L., Lerch, J. P., Singh, K. K., & de Anda, F. C. (2022). TAOK2 rescues autism-linked developmental deficits in a 16p11.2 microdeletion mouse model. *Molecular Psychiatry*, October 2021, 1–15. <https://doi.org/10.1038/s41380-022-01785-3>
- Sheppard, O., Coleman, M. P., & Durrant, C. S. (2019). Lipopolysaccharide-induced neuroinflammation induces presynaptic disruption through a direct action on brain tissue involving microglia-derived interleukin 1 beta. *Journal of Neuroinflammation*, 16(1), 1–13. <https://doi.org/10.1186/s12974-019-1490-8>
- Shi, L., Fatemi, S. H., Sidwell, R. W., & Patterson, P. H. (2003). Maternal influenza infection causes marked behavioral and pharmacological changes in the offspring. *Journal of Neuroscience*, 23(1), 297–302. <https://doi.org/10.1523/jneurosci.23-01-00297.2003>
- Shinawi, M., Liu, P., Kang, S. H. L., Shen, J., Belmont, J. W., Scott, D. A., Probst, F. J., Craigen, W. J., Graham, B. H., Pursley, A., Clark, G., Lee, J., Proud, M., Stocco, A., Rodriguez, D. L., Kozel, B. A., Sparagana, S., Roeder, E. R., McGrew, S. G., ... Lupski, J. R. (2010). Recurrent reciprocal 16p11.2 rearrangements associated with global developmental delay, behavioural problems, dysmorphism, epilepsy, and abnormal head size. *Journal of Medical Genetics*, 47(5), 332–341. <https://doi.org/10.1136/jmg.2009.073015>
- Silvin, A., & Ginhoux, F. (2018). Microglia heterogeneity along a spatio-temporal axis: More questions than answers. *Glia*, 66(10), 2045–2057. <https://doi.org/10.1002/glia.23458>
- Ślusarczyk, J., Trojan, E., Głombik, K., Budziszewska, B., Kubera, M., Lasoń, W., Popiołek-Barczyk, K., Mika, J., Wędzony, K., & Basta-Kaim, A. (2015). Prenatal stress is a vulnerability factor for altered morphology and biological activity of microglia cells. *Frontiers in Cellular Neuroscience*, 9(March), 1–14. <https://doi.org/10.3389/fncel.2015.00082>
- Smith, S. E. P., Li, J., Garbett, K., Mirnics, K., & Patterson, P. H. (2007). Maternal immune activation alters fetal brain development through interleukin-6. *Journal of Neuroscience*, 27(40), 10695–10702. <https://doi.org/10.1523/JNEUROSCI.2178-07.2007>
- Squarzoni, P., Oller, G., Hoeffel, G., Pont-Lezica, L., Rostaing, P., Low, D., Bessis, A., Ginhoux, F., & Garel, S. (2014). Microglia Modulate Wiring of the Embryonic Forebrain. *Cell Reports*, 8(5), 1271–1279. <https://doi.org/10.1016/j.celrep.2014.07.042>
- Stanelle-Bertram, S., Walendy-Gnirß, K., Speiseder, T., Thiele, S., Asante, I. A., Dreier, C., Kouassi, N. M., Preuß, A., Pilnitz-Stolze, G., Müller, U., Thanisch, S., Richter, M., Scharrenberg, R., Kraus, V.,

- Dörk, R., Schau, L., Herder, V., Gerhauser, I., Pfankuche, V. M., ... Gabriel, G. (2018). Male offspring born to mildly ZIKV-infected mice are at risk of developing neurocognitive disorders in adulthood. *Nature Microbiology*, *3*(10), 1161–1174. <https://doi.org/10.1038/s41564-018-0236-1>
- Stoner, R., Chow, M. L., Boyle, M. P., Sunkin, S. M., Mouton, P. R., Roy, S., Wynshaw-Boris, A., Colamarino, S. A., Lein, E. S., & Courchesne, E. (2014). Patches of disorganization in the neocortex of children with autism. *The New England Journal of Medicine*, *370*(13), 1209–1219. <https://doi.org/10.1056/NEJMoa1307491>
- Tan, Y. L., Yuan, Y., & Tian, L. (2019). Microglial regional heterogeneity and its role in the brain. *Molecular Psychiatry*, *351–367*. <https://doi.org/10.1038/s41380-019-0609-8>
- Tang, H., Hammack, C., Ogden, S. C., Wen, Z., Qian, X., Li, Y., Yao, B., Shin, J., Zhang, F., Lee, E. M., Christian, K. M., Didier, R. A., Jin, P., Song, H., & Ming, G. L. (2016). Zika virus infects human cortical neural progenitors and attenuates their growth. *Cell Stem Cell*, *18*(5), 587–590. <https://doi.org/10.1016/j.stem.2016.02.016>
- Teixeira, F. M. E., Pietrobon, A. J., Oliveira, L. de M., Oliveira, L. M. da S., & Sato, M. N. (2020). Maternal-Fetal Interplay in Zika Virus Infection and Adverse Perinatal Outcomes. *Frontiers in Immunology*, *11*(February), 1–15. <https://doi.org/10.3389/fimmu.2020.00175>
- Tetreault, N. A., Hakeem, A. Y., Jiang, S., Williams, B. A., Allman, E., Wold, B. J., & Allman, J. M. (2012). Microglia in the cerebral cortex in autism. *Journal of Autism and Developmental Disorders*, *42*(12), 2569–2584. <https://doi.org/10.1007/s10803-012-1513-0>
- The Simons Foundation. (2022). *SFARI Gene*. <https://gene.sfari.org/>
- Thion, M. S., Ginhoux, F., & Garel, S. (2018). Microglia and early brain development: An intimate journey. *Science*, *362*(6411), 185–189. <https://doi.org/10.1126/science.aat0474>
- Tilburgs, T., Crespo, Â. C., Van Der Zwan, A., Rybalov, B., Raj, T., Stranger, B., Gardner, L., Moffett, A., & Strominger, J. L. (2015). Human HLA-G+ extravillous trophoblasts: Immune-activating cells that interact with decidual leukocytes. *Proceedings of the National Academy of Sciences of the United States of America*, *112*(23), 7219–7224. <https://doi.org/10.1073/pnas.1507977112>
- Tilburgs, T., Scherjon, S. A., van der Mast, B. J., Haasnoot, G. W., Versteeg-v.d.Voort-Maarschalk, M., Roelen, D. L., van Rood, J. J., & Claas, F. H. J. (2009). Fetal-maternal HLA-C mismatch is associated with decidual T cell activation and induction of functional T regulatory cells. *Journal of Reproductive Immunology*, *82*(2), 148–157. <https://doi.org/10.1016/j.jri.2009.05.003>
- Tinevez, J. Y., Perry, N., Schindelin, J., Hoopes, G. M., Reynolds, G. D., Laplantine, E., Bednarek, S. Y., Shorte, S. L., & Eliceiri, K. W. (2017). TrackMate: An open and extensible platform for single-particle tracking. *Methods*, *115*(2017), 80–90. <https://doi.org/10.1016/j.ymeth.2016.09.016>
- Tioleco, N., Silberman, A. E., Stratigos, K., Banerjee-Basu, S., Spann, M. N., Whitaker, A. H., & Turner, J. B. (2021). Prenatal maternal infection and risk for autism in offspring: A meta-analysis. *Autism Research*, *14*(6), 1296–1316. <https://doi.org/10.1002/aur.2499>
- Urresti, J., Zhang, P., Moran-Losada, P., Yu, N.-K., Negraes, P., Trujillo, C., Antaki, D., Amar, M., Chau, K., Pramod, A. B., Diedrich, J., Tejwani, L., Romero, S., Sebat, J., Yates, J., Muotri, A., & Iakoucheva, L. (2020). Cortical Organoids Model Early Brain Development Disrupted by 16p11.2 Copy Number Variants in Autism. *Molecular Psychiatry*, *July*. <https://doi.org/10.1101/2020.06.25.172262>
- Vasistha, N. A., & Khodosevich, K. (2021). The impact of (ab)normal maternal environment on cortical development. *Progress in Neurobiology*, *202*(December 2020), 102054. <https://doi.org/10.1016/j.pneurobio.2021.102054>
- Volk, H. E., Lurmann, F., Penfold, B., Hertz-Picciotto, I., & McConnell, R. (2013). Traffic-related air

- pollution, particulate matter, and autism. *Archives of General Psychiatry*, 70(1), 71–77. <https://doi.org/10.1001/jamapsychiatry.2013.266>
- Vomund, S., De Souza Silva, M. A., Huston, J. P., & Korth, C. (2017). Behavioral resilience and sensitivity to locally restricted cortical migration deficits induced by in utero knockdown of disabled-1 in the adult rat. *Cerebral Cortex*, 27(3), 2052–2063. <https://doi.org/10.1093/cercor/bhw060>
- W.M.S. Russell, & Burch, R. L. (1960). The Principles of Humane Experimental Technique. *Medical Journal of Australia*, 1(13), 500–500. <https://doi.org/10.5694/j.1326-5377.1960.tb73127.x>
- Wang, X., Lu, J., Xie, W., Lu, X., Liang, Y., Li, M., Wang, Z., Huang, X., Tang, M., Pfaff, D. W., Tang, Y. P., & Yao, P. (2019). Maternal diabetes induces autism-like behavior by hyperglycemia-mediated persistent oxidative stress and suppression of superoxide dismutase 2. *Proceedings of the National Academy of Sciences of the United States of America*, 116(47), 23743–23752. <https://doi.org/10.1073/pnas.1912625116>
- Weiss, L. A., Shen, Y., Korn, J. M., & Daly, M. J. (2011). Association between Microdeletion and Microduplication at 16p11.2 and Autism. *The New England Journal of Medicine*, 358(7), 109–122. <https://doi.org/10.1056/NEJMoa1205361>
- Wickham, H. (2009). *ggplot2*. Springer New York. <https://doi.org/10.1007/978-0-387-98141-3>
- World Health Organization. (2022). *International Classification of Diseases Eleventh Revision (ICD-11)*. License: CC BY-ND 3.0 IGO.
- Wu, Y., Qi, F., Song, D., He, Z., Zuo, Z., Yang, Y., Liu, Q., Hu, S., Wang, X., Zheng, X., Yang, J., Yuan, Q., Zou, J., Guo, K., & Yao, Z. (2018). Prenatal influenza vaccination rescues impairments of social behavior and lamination in a mouse model of autism. *Journal of Neuroinflammation*, 15(1), 1–17. <https://doi.org/10.1186/s12974-018-1252-z>
- Xu, D., Cao, F., Sun, S., Liu, T., & Feng, S. (2016). Inhibition of the Ras/Raf/ERK1/2 Signaling Pathway Restores Cultured Spinal Cord-Injured Neuronal Migration, Adhesion, and Dendritic Spine Development. *Neurochemical Research*, 41(8), 2086–2096. <https://doi.org/10.1007/s11064-016-1921-1>
- Yang, K., Cao, F., Sheikh, A. M., Malik, M., Wen, G., Wei, H., Ted Brown, W., & Li, X. (2013). Up-regulation of Ras/Raf/ERK1/2 signaling impairs cultured neuronal cell migration, neurogenesis, synapse formation, and dendritic spine development. *Brain Structure and Function*, 218(3), 669–682. <https://doi.org/10.1007/s00429-012-0420-7>
- Yasumatsu, K., Nagao, J. I., Arita-Morioka, K. I., Narita, Y., Tasaki, S., Toyoda, K., Ito, S., Kido, H., & Tanaka, Y. (2020). Bacterial-induced maternal interleukin-17A pathway promotes autistic-like behaviors in mouse offspring. *Experimental Animals*, 69(2), 250–260. <https://doi.org/10.1538/expanim.19-0156>
- Yonk, L. J., Warren, R. P., Burger, R. A., Cole, P., Odell, J. D., Warren, W. L., White, E., & Singh, V. K. (1990). CD4+ helper T cell depression in autism. *Immunology Letters*, 25(4), 341–345. [https://doi.org/10.1016/0165-2478\(90\)90205-5](https://doi.org/10.1016/0165-2478(90)90205-5)
- Zeidan, J., Fombonne, E., Scora, J., Ibrahim, A., Durkin, M. S., Saxena, S., Yusuf, A., Shih, A., & Elsabbagh, M. (2022). Global prevalence of autism: A systematic review update. *Autism Research*, 15(5), 778–790. <https://doi.org/10.1002/aur.2696>
- Zerbo, O., Qian, Y., Yoshida, C., Grether, J. K., Van de Water, J., & Croen, L. A. (2015). Maternal Infection During Pregnancy and Autism Spectrum Disorders. *Journal of Autism and Developmental Disorders*, 45(12), 4015–4025. <https://doi.org/10.1007/s10803-013-2016-3>
- Zhang, D., Hu, X., Qian, L., O’Callaghan, J. P., & Hong, J. S. (2010). Astroglialosis in CNS pathologies: Is

there a role for microglia? *Molecular Neurobiology*, 41(2–3), 232–241.
<https://doi.org/10.1007/s12035-010-8098-4>

Zhang, F., Nance, E., Alnasser, Y., Kannan, R., & Kannan, S. (2016). Microglial migration and interactions with dendrimer nanoparticles are altered in the presence of neuroinflammation. *Journal of Neuroinflammation*, 13(1), 1–11. <https://doi.org/10.1186/s12974-016-0529-3>

Zhou, B., Zuo, Y. X., & Jiang, R. T. (2019). Astrocyte morphology: Diversity, plasticity, and role in neurological diseases. *CNS Neuroscience and Therapeutics*, 25(6), 665–673.
<https://doi.org/10.1111/cns.13123>

14 Appendix Material

14.1 Equipment

Equipment	Specification	Provider
Binocular	Stemi 2000	Zeiss
Microscope 1	EclipseTi2	Nikon
Microscope 1: Camera	ORCA-Flash4.0 V3 C13440-20CU	Hamamatsu
Microscope 1: LED	SPECTRA X Light Engine	Lumencor
Microscope 1: Software	NIS-Elements	Nikon
Microscope 2	Eclipse Ti	Nikon
Microscope 2: Camera	CoolSNAP HQ2	Roper Scientific
Microscope 2: Software	NIS-Elements	Nikon
Pipette	10 μ L, 50 μ L, 100 μ L, 1000 μ L	Eppendorf research plus
Pipette tips		Sarstedt
Cell culture Inserts	0.4 μ m, 30mm diameter	Millicell
Cryostat	CM3050 S	Leica
Vibratome	VT1000 S	Leica
Fluorescence Microscope	SZX16	Olympus
Fluorescence Laser	x-Cite Series 120 Q	EXFO

14.2 Material

Substance	Provider	LOT / Catalog number
Neurobasal	Invitrogen	21103049
B27	Invitrogen	17504044
N2 supplement	Gibco	17502048
Glucose	Sigma	G7021-1kg
Paraformaldehyde	Roth	0335.2
Triton x 100	Sigma	9036-19-5
Glycerol	Roth	3783.1
Mowiol 4-88	Roth	0713.2
Isofluorane	Baxter vet	21E06A35
Lectin	Vector laboratories	DL-1177 ZCO831
Donkey Serum	Sigma	D9663-10ML
Horse Serum	Capricon	DHS-1A-20
PBS	Invitrogen	14190094
Poly(I:C)	Sigma	P9582-5mg
LPS	Sigma	L3012-5mg

14.3 Software and Plugins

Software	Developer
NIS-Elements	Nikon
FIJI (Is Just ImageJ)	ImageJ 1.53u NIH, USA
Cellcounter Plugin	Kurt De Vos, University of Sheffield
Trackmate Plugin	(Tinevez et al., 2017)
PRISM	GraphPad Prism Version 9.3.1, GraphPad Software LLC
RStudio (posit.co)	RStudio 2022.02.1+461 "Prairie Trillium" Release for Windows
ggplot package	(Wickham, 2009)
openxlsx (R package)	Philipp Schaubberger et al., schaubberger.co.at
dplyr (R package)	Hadley Wickham et al., rstudio.com
rlist (R package)	Kun Ren, https://renkun-ken.github.io/rlist/
Rcpp (R package)	Dirk Eddelbuettel et al., edd at Debian.org
Word	Microsoft Office
Excel	Microsoft Office
Publisher	Microsoft Office
Mendeley	Mendeley 2008-2020 Glyph & Cog, LLC
Mendeley Word Plugin	Zotero / Center for History and New Media / George Mason University.

14.4 DNA

Plasmid	Provider
pCAGIG-EGFP-YFP	Calderon de Anda
TAOK2 α WT and variants	Calderon de Anda (Richter et al., 2018)
TAOK2 β WT and variants	Calderon de Anda (Richter et al., 2018)

14.5 GHS classification

Formaldehyde (Carl Roth GmbH, 2021)			
GHS	H	P	Amount used
GHS05 	H301+H311+H331 Toxic if swallowed, in contact with skin or if inhaled	P260 Do not breathe mist/vapours P280 Wear protective gloves/protective clothing/eye protection/face protection	450 mL 4% solution
GHS06 	H314 Causes severe skin burns and eye damage H317 May cause an allergic skin reaction H335 May cause respiratory irritation	P303+P361+P353 IF ON SKIN (or hair): Take off immediately all contaminated clothing. Rinse skin with water [or shower]	
GHS08	H341 Suspected of causing genetic defects H350 May cause cancer H370 Causes damage to organs (eye)	P304+P340 IF INHALED: Remove person to fresh air and keep comfortable for breathing	

		<p>P305+P351+P338 IF IN EYES: Rinse cautiously with water for several minutes. Remove contact lenses, if present and easy to do. Continue rinsing P308+P311 IF exposed or concerned: Call a POISON CENTER/doctor</p>	
Triton-X-100 (Carl Roth GmbH, 2022)			
GHS	H	P	Amount used
<p>GHS05</p>  <p>GHS07</p>  <p>GHS09</p> 	<p>H302 Harmful if swallowed H318 Causes serious eye damage H411 Toxic to aquatic life with long lasting effects</p>	<p>P270 Do not eat, drink or smoke when using this product P273 Avoid release to the environment P280 Wear protective gloves/eye protection P305+P351+P338 IF IN EYES: Rinse cautiously with water for several minutes. Remove contact lenses, if present and easy to do. Continue rinsing P310 Immediately call a POISON CENTER/doctor</p>	<p>750 mL 0.3% solution</p>

14.6 RStudio Script

- 1 Data import and distance calculations from ImageJ point selection tool
- 2 `install.packages("Rtools")`
- 3 `install.packages("openxlsx")`
- 4 `install.packages("rlist")`
- 5 `install.packages("dplyr")`

```

6  install.packages("Rcpp")
7  install.packages("tidyverse")
8  library(openxlsx)
9  library(dplyr)
10 library(rlist)
11 library(Rcpp)
12 options(warn = 10)
13 bin_low <- -1.1
14 bin_up <- 2.1
15 bin_stepsize <- 0.2
16 bin_width <- c(seq(bin_low,bin_up,bin_stepsize))
17 setwd("")
18 vector_zip <- list.files(path = ".", pattern = "*_neurons.zip", all.files = FALSE,
19                          full.names = FALSE, recursive = TRUE,
20                          ignore.case = TRUE, include.dirs = FALSE, no.. = FALSE)
21 list_zip <- as.data.frame(vector_zip)
22 list_zip
23 array_marg <- array(dim = c(3500,5,nrow(list_zip)))
24 number_list <- c(0)
25 ###
26 # loop through all zip files and add number of containing files into table column 2
27 # running through all experiments #####
28 for (i in (1:length(vector_zip))) {
29   vector_zip_cells_temp <- vector_zip[i]
30   list_zip[i,2] <- nrow(unzip(vector_zip_cells_temp,list = TRUE))
31   rois_list_temp = unzip(vector_zip_cells_temp, list = TRUE)
32   rois_table_temp = as.data.frame(rois_list_temp[,1])
33   print(vector_zip[i])
34   print(summary(nchar(as.character(rois_table_temp[,1]))))
35 }
36 for (i in (1:length(vector_zip))) {
37   vector_zip_cells_temp <- vector_zip[i]
38   list_zip[i,2] <- nrow(unzip(vector_zip_cells_temp,list = TRUE))
39   #####
40   rois_list_temp = unzip(vector_zip_cells_temp, list = TRUE)
41   rois_table_temp = as.data.frame(rois_list_temp[,1])
42   print(summary(nchar(as.character(rois_table_temp[,1]))))
43   rois_vector = rois_table_temp[,1]
44   by = gsub(".....$", "", rois_vector)
45   rois_ycoord = as.numeric(gsub("^.....", "", by))
46   bx = gsub("....$", "", rois_vector)
47   rois_xcoord = as.numeric(gsub("^.....", "", bx))
48   rois_table_temp[,2] = rois_xcoord
49   rois_table_temp[,3] = rois_ycoord
50   #slide nomenclature #####
51   slide_name_temp <- c(vector_zip[i])
52   slide_name_split_temp <- as.list(strsplit(slide_name_temp,"/"))
53   slide_name_table_temp <- as.data.frame(slide_name_split_temp)
54   slide_name_table_temp <- as.data.frame(slide_name_split_temp)
55   number <- paste(slide_name_table_temp[1:(nrow(slide_name_table_temp) - 1),1],sep = "_")
56   number <- paste(number, collapse = "_")
57   pattern_1 = paste("XY_MZ_",number, sep = "")
58   layer_list <- list.files(pattern = pattern_1,recursive = TRUE)
59   ##correlating rois with layers
60   cells_list = 0
61   cells_list <- rois_table_temp[,2:3]
62   cells_list <- cells_list[(order(cells_list[,1])),]
63   cells_list[,3] <- c(0)

```

```

64  ##transfer data into layer Marginal zone vector #####
65  frame_pattern <- slide_name_table_temp[nrow(slide_name_table_temp),]
66  frame_pattern_extr <- as.data.frame(strsplit(as.character(frame_pattern)[1],"_"))
67  frame_pattern_row <- grep(frame_pattern_extr[1,], layer_list)
68  number_list[i] <- paste(number,frame_pattern_extr[1,],frame_pattern_extr[2,],sep = "_")
69  pattern_2 <- paste(pattern_1,"csv",sep = ".")
70  raw_values <- read.csv2(layer_list[1],header = TRUE,sep = ",", dec = ".")
71  border_points <- c(0,0)
72  (for (m in 1:(nrow(raw_values) - 1)) {
73    border_points <- rbind(border_points, raw_values[m,])
74    raw_values_temp <- raw_values[(m:(m + 1)),]
75    raw_values_temp <- raw_values_temp[order(raw_values_temp[,1]),]
76    con_line_y <- (raw_values_temp[2,2] - raw_values_temp[1,2])
77    con_line_x <- (raw_values_temp[2,1] - raw_values_temp[1,1])
78    con_line <- 1*(con_line_y/con_line_x)
79    connect_seq <- (seq(raw_values_temp[1,1],raw_values_temp[2,1]))
80    k_x = raw_values_temp[2,1] - raw_values_temp[1,1]
81    k_y = raw_values_temp[2,2] - raw_values_temp[1,2]
82    p = k_x/k_y
83    (ifelse(p <= 0,(p <- -1),(p <- 1)))
84    for (k in 1:length(connect_seq)) {
85      con_point <- c(connect_seq[k],raw_values_temp[1,2] + (k*con_line))
86      border_points <- rbind(border_points, con_point)
87    }
88  })
89  layer_MZ <- 0
90  layer_MZ <- border_points[2:nrow(border_points),]
91  # visualize the correct assignment of UCP layer cells and positioning of marginal zone border #####
92  plot(cells_list[,2]~cells_list[,1],pty = "s",ylim = c(0,6000),xlim = c(0,6000),main = slide_name_temp)
93  # calculate distance from cells to MZ #####
94  for (r_num in 1:nrow(cells_list)) {
95    temp_dist <- layer_MZ
96    for (var_num in 1:nrow(temp_dist)) {
97      temp_dist[var_num,3] <- sqrt(((cells_list[r_num,2] - temp_dist[var_num,2])^2)
98        + ((cells_list[r_num,1] - temp_dist[var_num,1])^2))
99    }
100    dist_cells_mz <- subset(temp_dist,temp_dist[,3] == min(temp_dist[,3]))
101    cells_list[r_num,3:5] <- dist_cells_mz[1,]
102  }
103  plot(cells_list[,4]~cells_list[,3],ylim = c(0,6000),xlim = c(0,6000),main = slide_name_temp)
104  points(cells_list[,2]~cells_list[,1],pch = 3)
105  plot(sort(cells_list[,5]),main = slide_name_temp)
106  print(slide_name_temp)
107  print("this slice")
108  print(Sys.time() - slice_time)
109  print(Sys.time() - start_time)
110  slice_time <- Sys.time()
111  array_marg[(1:nrow(cells_list)),1,i] <- cells_list[,1]
112  array_marg[(1:nrow(cells_list)),2,i] <- cells_list[,2]
113  array_marg[(1:nrow(cells_list)),3,i] <- cells_list[,3]
114  array_marg[(1:nrow(cells_list)),4,i] <- cells_list[,4]
115  array_marg[(1:nrow(cells_list)),5,i] <- cells_list[,5]
116  }
117  array_marg_df <- as.data.frame(array_marg[,5,])
118  Scaling and uncoding of data in maternal immune activation
119  array_marg_df_scale <- array_marg_df*(0.2289618) #flu imaging
120  col_names_number_list <- sub("channel_1","Ctip2",number_list,ignore.case = TRUE)

```

```

121 col_names_number_list <- sub("channel_2","Satb2",col_names_number_list,ignore.case = TRUE)
122 col_names_number_list <- sub("channel_4","Satb2_clipped",col_names_number_list,ignore.case = TRUE)
123 colnames(array_marg_df_scale) <- (c(col_names_number_list))
124 write.xlsx(array_marg_df_scale, file = "distances_flu_ctip2_satb2.xlsx",colNames = TRUE)
125 # uncoding of flu data #####
126 sort(x = c((grep(pattern = "channel_1", x = number_list)),(grep(pattern = "channel_2", x =
127 number_list))),decreasing = FALSE)
128 ctip2_uncode <- c(grep(pattern = "Ctip2", x = col_names_number_list))
129 satb2_uncode <- c(grep(pattern = "channel_2", x = number_list))
130 H1N1_uncode <- c(32,9,18,24,29,6,3,12,15,21,35,27)
131 Polyic_uncode <- c(23,11,2,17,20,34,5,8,14,31,26)
132 PBS_uncode <- c(22,19,13,1,10,25,33,16,4,30,7,28)
133 # # binning into histogram #####
134 testmatrix <- array_marg_df_num
135 values_mean = array_marg_df_stat[,2]
136 boxplot(testmatrix,names = FALSE,varwidth = FALSE,plot = TRUE,notch = TRUE)
137 hist_breaks <- c(seq(-500,10000,50))
138 hist_matrix <- matrix(ncol = (length(hist_breaks) - 1),nrow = ncol(testmatrix))
139 rownames(hist_matrix) = number_list
140 colnames(hist_matrix) = c(hist_breaks[2:length(hist_breaks)])
141 for (his_t in 1:ncol(array_marg_df_num)) {
142   hist_matrix[his_t,] <- c(hist(testmatrix[,his_t],
143     breaks = hist_breaks,
144     plot = FALSE)$counts
145   )
146 }
147 hist_matrix_dif <- hist_matrix
148 hist_matrix_cumu <- hist_matrix_dif
149 for (his_cumu in 1:nrow(hist_matrix_dif)) {
150   hist_matrix_cumu[his_cumu,] <- as.numeric(cumsum(hist_matrix_dif[his_cumu,]))
151 }
152 trafo_hist_matrix_dif <- t(hist_matrix_dif)
153 trafo_hist_matrix_cumu <- t(hist_matrix_cumu)
154 })
155 Depiction of data in histograms and differential histograms
156 par.default <- par(no.readonly = TRUE)
157 h1n1_dataframe <- array_marg_df[,satb2_uncode][,H1N1_uncode]*(0.2289618)
158 h1n1_dataframe_200 <- h1n1_dataframe[(which(h1n1_dataframe >= 250,arr.ind = TRUE))]
159 h1n1_dataframe_200_400 <- h1n1_dataframe_200[(which(h1n1_dataframe_200 <= 350,arr.ind = TRUE))]
160 h1n1_dataframe_200_400 <- h1n1_dataframe[(which(h1n1_dataframe <= 350 & h1n1_dataframe >=
161 250,arr.ind = TRUE))]
162 pbs_dataframe <- array_marg_df[,satb2_uncode][,PBS_uncode]*(0.2289618)
163 polyic_dataframe <- array_marg_df[,satb2_uncode][,Polyic_uncode]*(0.2289618)
164 histogram_breaks <- c(seq(0,max(array_marg_df * (0.2289618),na.rm = TRUE) + 100,50))
165 h1n1_histogram <- hist(unlist(h1n1_dataframe),plot = FALSE,breaks = histogram_breaks)
166 pbs_histogram <- hist(unlist(pbs_dataframe),plot = FALSE,breaks = histogram_breaks)
167 polyic_histogram <- hist(unlist(polyic_dataframe),plot = FALSE,breaks = histogram_breaks)
168 plot(y = pbs_histogram$counts / sum(pbs_histogram$counts), x = pbs_histogram$mids,)
169 abline(points(y = polyic_histogram$counts / sum(polyic_histogram$counts),x = polyic_histogram$mids,col = 4)
170   ,points(y = h1n1_histogram$counts / sum(h1n1_histogram$counts),x = h1n1_histogram$mids,col = 8))
171 legend(max(pbs_histogram$mids) * 0.8,max(pbs_histogram$counts / sum(pbs_histogram$counts)),legend =
172 c("pbs","polyic","h1n1"), col = c(1,4,8),pch = 1,cex = 1)
173 dif_hist_density_h1n1_pbs <- (h1n1_histogram$counts / sum(h1n1_histogram$counts)) -
174 (pbs_histogram$counts / sum(pbs_histogram$counts))
175 dif_hist_density_polyic_pbs <- (polyic_histogram$counts / sum(polyic_histogram$counts)) -
176 (pbs_histogram$counts / sum(pbs_histogram$counts))
177 par(mfrow = c(1,2))

```

```

178 dif_hist_h1n1_bar <- barplot(rev(dif_hist_density_h1n1_pbs),
179   main = "Differential histogram of H1N1 to control",
180   names.arg = rev(histogram_breaks[2:length(histogram_breaks)]),
181   ylab = c("bin width 50µm"),
182   horiz = TRUE,
183   xlim = c((min(dif_hist_density_h1n1_pbs)*1.2),(max(dif_hist_density_h1n1_pbs)*1.2)),
184   )
185 text(dif_hist_h1n1_bar,
186   labels = c(round(rev(dif_hist_density_h1n1_pbs),digits = 4)*100),
187   x = c(rev(dif_hist_density_h1n1_pbs)),
188   adj = -0.5)
189 dif_hist_polyic_bar <- barplot(rev(dif_hist_density_polyic_pbs),
190   main = "Differential histogram of PolyIC to control",
191   names.arg = rev(histogram_breaks[2:length(histogram_breaks)]),
192   ylab = c("bin width 50µm"),
193   horiz = TRUE,
194   xlim = c((min(dif_hist_density_h1n1_pbs)*1.2),(max(dif_hist_density_h1n1_pbs)*1.2))
195   )
196 text(dif_hist_polyic_bar,
197   labels = c(round(rev(dif_hist_density_polyic_pbs),digits = 4)*100),
198   x = c(rev(dif_hist_density_polyic_pbs)),
199   adj = 0)
200 par(par.default)
201 sum(h1n1_histogram$counts / sum(h1n1_histogram$counts))
202 par(mfrow = c(1,2),pty = "s",xaxs = "i",yaxs = "i")
203 qqplot(y = (h1n1_histogram$counts / sum(h1n1_histogram$counts)),x = (pbs_histogram$counts /
204 sum(pbs_histogram$counts)))
205 abline(line(x = c(0,1),y = c(0,1)))
206 qqplot(y = (polyic_histogram$counts / sum(polyic_histogram$counts)),x = (pbs_histogram$counts /
207 sum(pbs_histogram$counts)))
208 abline(line(x = c(0,1),y = c(0,1)))
209 par(par.default)
210 par(mfrow = c(1,3))
211 h1n1_height <- round(rev(h1n1_histogram$counts / sum(h1n1_histogram$counts)),digits = 4)
212 h1n1_bar <- barplot(height = h1n1_height,
213   names.arg = rev(histogram_breaks[2:length(histogram_breaks)]),
214   ylab = c("bin width 50µm"),
215   horiz = TRUE,
216   xlim = c(0,0.4),
217   main = "Distribution of cells in H1N1")
218 text(h1n1_bar,
219   x = h1n1_height,
220   labels = h1n1_height*100,
221   adj = -1
222   )
223 pbs_height <- round(c(rev(pbs_histogram$counts / sum(pbs_histogram$counts))),digits = 4)
224 pbs_bar <- barplot(height = pbs_height,
225   names.arg = rev(histogram_breaks[2:length(histogram_breaks)]),
226   ylab = c("bin width 50µm"),
227   horiz = TRUE,
228   xlim = c(0,0.4),
229   main = "Distribution of cells in PBS")
230 text(pbs_bar,
231   x = (pbs_height),
232   labels = (pbs_height*100),
233   adj = -1
234   )
235 polyic_height <- round(rev(polyic_histogram$counts / sum(polyic_histogram$counts)), digits = 4)

```

```

236 polyic_bar <- barplot(height = polyic_height,
237     names.arg = rev(histogram_breaks[2:length(histogram_breaks)]),
238     ylab = c("bin width 50µm"),
239     horiz = TRUE,
240     xlim = c(0,0.4),
241     main = "Distribution of cells in Poly:IC")
242 text(polyic_bar,
243     x = polyic_height,
244     labels = polyic_height*100,
245     adj = -1
246 )
247 par(par.default)
248 Velocity of single neurons with coordinates from ImageJ tracking
249 # List all zip files in the folder
250 # create table to collect roi information with ZIP files as rownames
251 install.packages("ggplot2")
252 library(ggplot2)
253 options(warn = 2)
254 getwd()
255 setwd("")
256 getwd()
257 vector_zip <- list.files(path = ".", pattern = "*.zip", all.files = FALSE,
258     full.names = FALSE, recursive = TRUE,
259     ignore.case = FALSE, include.dirs = FALSE, no.. = FALSE)
260 list_zip <- as.data.frame(vector_zip)
261 list_zip[,2:8] <- c(NaN)
262 # loop through all zip files and add number of containing files into table
263 for (i in (1:length(vector_zip))) {
264     a <- vector_zip[i]
265     list_zip[i,2] <- nrow(unzip(a,list = TRUE))
266 }
267 for (i in (1:length(vector_zip))) {
268     coordinates_temp <- unzip(vector_zip[i], list = TRUE)
269     coordinates_temp <- coordinates_temp[,1:2]
270     #list_zip[i,2] <- nrow(unzip(vector_zip_cells_temp,list = TRUE))
271     reference_temp = vector_zip[i]
272     ref_list = unzip(reference_temp, list = TRUE)
273     ref_table = as.data.frame(ref_list[,1])
274     ref_vector = ref_table[,1]
275     ref_y = gsub(".....$", "", ref_vector)
276     ref_ycoord = as.numeric(gsub("^.....", "", ref_y))
277     ref_x = gsub("....$", "", ref_vector)
278     ref_xcoord = as.numeric(gsub("^.....", "", ref_x))
279     coordinates_temp[,1] = ref_xcoord
280     coordinates_temp[,2] = ref_ycoord
281     for (p in (1:(nrow(coordinates_temp) - 1))) {
282         z_dist = sqrt(((coordinates_temp[(p + 1),2] - coordinates_temp[(p),2])^2) + ((coordinates_temp[(p + 1),1] -
283 coordinates_temp[(p),1])^2))
284         coordinates_temp[p,3] = as.numeric(z_dist)
285         tt <- coordinates_temp[,3]
286         loc_max <- length(which(tt/(2*mean(tt,na.rm = TRUE))>1)) # local maximum speed more than 2 times the
287 average speed
288     }
289     list_zip[i,3] = sum(coordinates_temp[,3], na.rm = TRUE)
290     list_zip[i,4] = median(coordinates_temp[,3], na.rm = TRUE)
291     list_zip[i,8] = loc_max
292 }

```

```

293 Experiment1 <- grep("*Experiment 1", list_zip[,1])
294 Experiment13 <- grep("*Experiment 13", list_zip[,1])
295 Experiment14 <- grep("*Experiment 14", list_zip[,1])
296 Experiment15 <- grep("*Experiment 15", list_zip[,1])
297 Experiment16 <- grep("*Experiment 16", list_zip[,1])
298 Experiment18 <- grep("*Experiment 18", list_zip[,1])
299 Experiment20 <- grep("*Experiment 20", list_zip[,1])
300 Experiment21 <- grep("*Experiment 21", list_zip[,1])
301 Experiment22 <- grep("*Experiment 22", list_zip[,1])
302 Experiment23 <- grep("*Experiment 23", list_zip[,1])
303 Experiment24 <- grep("*Experiment 24", list_zip[,1])
304 polyIC_values <- grep("*polyIC",ignore.case = TRUE,list_zip[,1])
305 polyic_values <- grep("*polyic",list_zip[,1])
306 LPS_treated <- grep("*LPS",ignore.case = TRUE,list_zip[,1])
307 ctrl_values <- grep("*ctrl",list_zip[,1])
308 control_values <- grep("*control",list_zip[,1])
309 old_microscope <- grep("*old",list_zip[,1])
310 Nomenclature <- list_zip
311 Nomenclature[Experiment1,5] <- c("Exp.1")
312 Nomenclature[Experiment13,5] <- c("Exp.13")
313 Nomenclature[Experiment14,5] <- c("Exp.14")
314 Nomenclature[Experiment15,5] <- c("Exp.15")
315 Nomenclature[Experiment16,5] <- c("Exp.16")
316 Nomenclature[Experiment18,5] <- c("Exp.18")
317 Nomenclature[Experiment20,5] <- c("Exp.20")
318 Nomenclature[Experiment21,5] <- c("Exp.21")
319 Nomenclature[Experiment22,5] <- c("Exp.22")
320 Nomenclature[Experiment23,5] <- c("Exp.23")
321 Nomenclature[Experiment24,5] <- c("Exp.24")
322 Nomenclature[polyIC_values,6] <- c("polyIC")
323 Nomenclature[polyic_values,6] <- c("polyIC")
324 Nomenclature[LPS_treated,6] <- c("lps")
325 Nomenclature[ctrl_values,7] <- c("ctrl")
326 Nomenclature[control_values,7] <- c("ctrl")
327 Nomenclature[is.na(Nomenclature)] <- c("")
328 for (nom in (1:(nrow(list_zip)))) {
329   list_zip[nom,5] <- paste(Nomenclature[nom,(c(5:7))],collapse = "_")
330 }
331
332 Exp1_poly <- grep("*Exp.1_poly", list_zip[,5])
333 Exp1_lps <- grep("*Exp.1_lps", list_zip[,5])
334 Exp13_poly <- grep("*Exp.13_poly", list_zip[,5])
335 Exp14_poly <- grep("*Exp.14_poly", list_zip[,5])
336 Exp14_lps <- grep("*Exp.14_lps", list_zip[,5])
337 Exp15_poly <- grep("*Exp.15_poly", list_zip[,5])
338 Exp15_lps <- grep("*Exp.15_lps", list_zip[,5])
339 Exp16_poly <- grep("*Exp.16_poly", list_zip[,5])
340 Exp16_lps <- grep("*Exp.16_lps", list_zip[,5])
341 Exp18_poly <- grep("*Exp.18_poly", list_zip[,5])
342 Exp18_lps <- grep("*Exp.18_lps", list_zip[,5])
343 Exp20_poly <- grep("*Exp.20_poly", list_zip[,5])
344 Exp21_poly <- grep("*Exp.21_poly", list_zip[,5])
345 Exp22_lps <- grep("*Exp.22_lps", list_zip[,5])
346 Exp23_lps <- grep("*Exp.23_lps", list_zip[,5])
347 Exp24_lps <- grep("*Exp.24_lps", list_zip[,5])
348 list_zip[Exp1_poly,6] <- (list_zip[Exp1_poly,3]/48)*0.92
349 list_zip[Exp1_lps,6] <- (list_zip[Exp1_lps,3]/48)*0.92
350 list_zip[Exp13_poly,6] <- (list_zip[Exp13_poly,3]/36)*0.92

```

```

351 list_zip[Exp14_poly,6] <- (list_zip[Exp14_poly,3]/36)*0.92
352 list_zip[Exp14_lps,6] <- (list_zip[Exp14_lps,3]/36)*0.92
353 list_zip[Exp15_poly,6] <- (list_zip[Exp15_poly,3]/36)*0.92
354 list_zip[Exp15_lps,6] <- (list_zip[Exp15_lps,3]/36)*0.66
355 list_zip[Exp16_poly,6] <- (list_zip[Exp16_poly,3]/60)*0.66
356 list_zip[Exp16_lps,6] <- (list_zip[Exp16_lps,3]/60)*0.92
357 list_zip[Exp18_poly,6] <- (list_zip[Exp18_poly,3]/60)*0.66
358 list_zip[Exp18_lps,6] <- (list_zip[Exp18_lps,3]/60)*0.66
359 list_zip[Exp20_poly,6] <- (list_zip[Exp20_poly,3]/60)*0.66
360 list_zip[Exp21_poly,6] <- (list_zip[Exp21_poly,3]/60)*0.66
361 list_zip[Exp22_lps,6] <- (list_zip[Exp22_lps,3]/60)*0.66
362 list_zip[Exp23_lps,6] <- (list_zip[Exp23_lps,3]/60)*0.92
363 list_zip[Exp24_lps,6] <- (list_zip[Exp24_lps,3]/60)*0.66
364
365 list_zip[Exp1_poly,7] <- (list_zip[Exp1_poly,4]/3)*0.92
366 list_zip[Exp1_lps,7] <- (list_zip[Exp1_lps,4]/3)*0.92
367 list_zip[Exp13_poly,7] <- (list_zip[Exp13_poly,4]/2)*0.92
368 list_zip[Exp14_poly,7] <- (list_zip[Exp14_poly,4]/2)*0.92
369 list_zip[Exp14_lps,7] <- (list_zip[Exp14_lps,4]/2)*0.92
370 list_zip[Exp15_poly,7] <- (list_zip[Exp15_poly,4]/2)*0.92
371 list_zip[Exp15_lps,7] <- (list_zip[Exp15_lps,4]/3)*0.66
372 list_zip[Exp16_poly,7] <- (list_zip[Exp16_poly,4]/3)*0.66
373 list_zip[Exp16_lps,7] <- (list_zip[Exp16_lps,4]/2)*0.92
374 list_zip[Exp18_poly,7] <- (list_zip[Exp18_poly,4]/3)*0.66
375 list_zip[Exp18_lps,7] <- (list_zip[Exp18_lps,4]/3)*0.66
376 list_zip[Exp20_poly,7] <- (list_zip[Exp20_poly,4]/3)*0.66
377 list_zip[Exp21_poly,7] <- (list_zip[Exp21_poly,4]/3)*0.66
378 list_zip[Exp22_lps,7] <- (list_zip[Exp22_lps,4]/3)*0.66
379 list_zip[Exp23_lps,7] <- (list_zip[Exp23_lps,4]/3)*0.92
380 list_zip[Exp24_lps,7] <- (list_zip[Exp24_lps,4]/3)*0.66
381 colnames(list_zip) <- c("Experiment evctor","Number of frames",
382 "Distance moved pixel","Median distance per frame","Name sorting",
383 "Movement per 10 min in micron","Median movement per 10 min in micron",
384 "N local maxima > 2*mean")
385 viol <- ggplot(list_zip, aes(list_zip[,6],list_zip[,5])) + geom_violin(aes(group=list_zip[,5]))+ggtitle("mean")
386 viol + coord_flip()
387 ggplot(list_zip, aes(list_zip[,6],list_zip[,5])) + geom_boxplot(aes(group=list_zip[,5])) + ggtitle("mean")#+
388 coord_flip()
389 dots_mean <- qplot(x = list_zip[,6],y = list_zip[,5],data = list_zip, geom = "point") + ggtitle("mean")
390 dots_mean
391 dots_median <- qplot(x = list_zip[,7],y = list_zip[,5],data = list_zip, geom = "point") + ggtitle("median")
392 dots_median
393 # create filterable table of micron per 10 minutes time
394 speedtable_filter <- Nomenclature[,1:7]
395 speedtable_filter[,3] <- list_zip[,6]
396 speedtable_filter[,4] <- list_zip[,8]
397 colnames(speedtable_filter) <- c("filevector","N frames","micron per 10 minutes","N local maximum distance
398 moved >2*mean","Experiment","Treatment","Control")
399 write.csv(speedtable_filter, file = "Table velocity neurons.csv")
400 dots_jumps <- qplot(x = list_zip[,8],y = list_zip[,5],data = list_zip, geom = "point") + ggtitle("jumps")
401 dots_jumps
402 viol_jumps <- ggplot(list_zip, aes(list_zip[,8],list_zip[,5])) + geom_violin(aes(group=list_zip[,5]))+ggtitle("N
403 Jumps")
404 viol_jumps #+ coord_flip()
405 ggplot(list_zip, aes(list_zip[,8],list_zip[,5])) + geom_boxplot(aes(group=list_zip[,5])) + ggtitle("jumps")#+
406 coord_flip()

```

15 Acknowledgement

I want to express my thankfulness to Dr. Froylan Calderon de Anda and the Calderon research group I was allowed to work with for this thesis. Dr. Melanie Richter, Dr. Praveen Durga and Birgit Schwanke for the active support, the required mouse work and procedures. For the opportunity to work with you. For the help I received from you. For the work we have been doing together. For active discussions in times of decision making. For the guidance in times of aimlessness. For support in times of struggles. For trust in times of doubts.

I want to thank Prof. Dr. Matthias Kneussel and Prof. Dr. Hartmut Schlüter for supervision of this work.

I want to thank the group of Prof. Dr. Gülsah Gabriel from the *Leibniz-Institut für Virologie* for the collaboration in the MIA project.

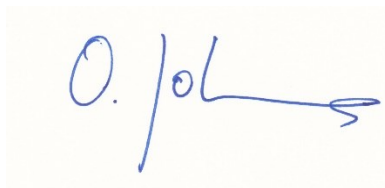
I want to thank Prof. Dr. Thomas Oertner for providing experience with microglia and the dye-coupled Tomato Lectin.

I want to express my thankfulness towards my family and beloved wife who stood by my side. For believing in me when I doubted. For lending me an ear to listen to ideas in the making. For putting things into perspective.

I want to express my thankfulness to my friends who I had to keep waiting far too often for far too long during the work associated with this thesis. Thank you for still being with me.

16 Eidesstattliche Versicherung

Hiermit versichere ich an Eides statt, die vorliegende Dissertation selbst verfasst und keine anderen als die angegebenen Hilfsmittel benutzt zu haben. Die eingereichte schriftliche Fassung entspricht der auf dem elektronischen Speichermedium. Ich versichere, dass diese Dissertation nicht in einem früheren Promotionsverfahren eingereicht wurde.



12.06.2023

Datum

Unterschrift